12-2021

Effects of Localized Oxygen Production by Electrolysis on the First-Generation Glucose Sensor Response

Nandita Halder
University of Arkansas, Fayetteville

Effects of Localized Oxygen Production by Electrolysis on the First-Generation Glucose Sensor Response

A dissertation submitted in partial fulfillment
of the requirements for the degree of
Doctor of Philosophy in Chemistry

by

Nandita Halder
Bangladesh University of Engineering and Technology
Bachelor of Science in Materials and Metallurgical Engineering, 2011

December 2021
University of Arkansas

This dissertation is approved for recommendation to the Graduate Council.

_____
David Paul, PhD
Dissertation Director

_____
Bill Durham, PhD
Committee Member

_____
Julie Stenken, PhD
Committee Member

_____
Ingrid Fritsch, PhD
Committee Member

Abstract

Glucose sensors are very important for detecting blood glucose both in vitro and in vivo. First-generation glucose biosensors were based on the glucose oxidase (GOx) enzyme using molecular oxygen as the electron acceptor and therefore oxygen dependent. Unfortunately for in-vivo work, oxygen in the body is variable and limited. Alternative approaches to overcome the oxygen dependency came with their own limitations. The widely used and commercially available ex-vivo glucose test strip uses a mediator in place of oxygen to free it from oxygen dependency. The mediator-based technology, in most cases cannot be transferred to in vivo applications due to the leaching-out of the toxic mediator. The present in vivo sensors use additional film coatings over the sensor to restrict glucose from reaching the sensor surface while allowing oxygen to pass. The technique succeeds in presenting oxygen in excess to the glucose at the sensor's surface but at a loss in sensitivity, and precision. This work investigates the construction and optimization of first-generation GOx sensors on both platinum and gold macro and microelectrodes. It addresses an alternative approach to the oxygen-dependency of first-generation sensors by supplying oxygen from an electrode within micro-range proximity to the glucose sensor. The additional oxygen is provided by water electrolysis by poising an oxygen generating electrode at a high positive potential. During this development, the stability of microband electrodes at such high positive potentials was discovered to depend upon the electrode materials and construction. This included gold and platinum MEAs fabrication, and effects of various adhesion metals (chromium, titanium) and contact metal (gold, platinum) properties on the sustainability towards oxygen evolution reaction (OER) voltage. Despite what appeared to be a straightforward approach, the action of the generator actually reduced the glucose signal (derived from the oxidation of enzymatically produced peroxide) at the sensor electrode. This led to numerous experiments and to the

conclusion that the action of the oxygen generator produced oxygen but also consumed the glucose signal derived from peroxide oxidation. Different solutions were proposed and demonstrated in this dissertation. The success of this work provides a highly sensitive glucose sensor superior to existing technology for in-vivo applications, and a solution to in vivo sensing by electrochemically supplying the natural and harmless mediator- oxygen. Areas of application of this technique include glucose monitoring under hypoxic conditions such as in tumors, brain, or areas where oxygen is insufficient compared to glucose concentrations.

Acknowledgments

I would like to give my sincere gratitude to the Director of Graduate Studies of the Chemistry department, Dr. Julie Stenken for showing confidence in me and allowing me to pursue the Ph.D. program in Chemistry.

I am grateful to my Advisor, Dr. David Paul for his wonderful mentorship and for helping ease the research stress with his positive attitude and his often-made Bengali tagline ‘chinta korbe na’ (meaning no worries). I am grateful to the other committee members- Dr. Bill Durham, Dr. Ingrid Fritsch, and Dr. Julie Stenken for their suggestions, guidance, and constant support along the way.

I am grateful to my parents, to my tiny world abroad with my daughter and husband away from my home, to my family and friends, and all the educators from the beginning of my academic learning till now for being the source of the driving force behind my journey this far.

I want to thank all my colleagues, lab mates for all the help and support, especially the undergraduate researchers: Maegan Weaver, Elizabeth Mace, Hunter Jones, Leah Ward, Jansen Reidler, and Aisha Soliman for actively participating and contributing to this project. I specifically want to thank my Advisor’s wife, Mrs. Annette Paul, for her emotional support and help with proofreading, to my husband, Atanu Dutta for his technical help and guidance with formatting, and my mother, Mrs. Lauxmi Rani Halder for taking of my daughter and everything else when I was busy writing the dissertation.

I want to acknowledge the cooperation and support in the project I got from the staff from the Chemistry department, the High Density Electronics Center (HiDEC), and the Nano and Biomaterials Characterization Facility at the University of Arkansas. I am thankful to the Chemistry department for providing me with an international student scholarship, graduate teaching assistantship, and my Advisor, Dr. David Paul for providing research assistantship during

my Ph.D. journey. All this financial assistance and the physical and mental health assistance offered by the university made my graduate school days much less stressful.

Finally, and most importantly, I am eternally grateful to God for granting me a better life with the capability to fulfill my dreams.

The research was financially supported through the Arkansas Biosciences Institute, the major research component of the Arkansas Tobacco Settlement Proceeds Act of 2000.

Dedication

I would like to dedicate this dissertation to the four most important people of my graduate life who have been the biggest source of my strength, support, and motivation behind this journey: my father, Ruhidas Halder, mother, Lauxmi Rani Halder -- whose biggest dream in life is to see their children achieve the highest academic degree, and to my advisor, Dr. David Paul, and his wife, Mrs. Annette Paul-- who have always been there in this journey for me whenever I needed.

Table of Contents

Table of Figures

1.1 Introduction

1.2 Introduction to electrochemical glucose sensors

Diabetes mellitus is one of the fastest growing global health challenges of the 21st century as it is increasing at an alarming rate.[1-3] According to the International Diabetes Federation report in 2019, the United States is one of three countries with largest number of adults with diabetes.[4] According to a 2020 report from National Diabetes Statistics, 34.2 million people or 10.5% of the total U.S. population have diabetes, of which 7.3 million people or 21.4% of people with diabetes are undiagnosed.[5] Diabetes has been reported as the seventh leading cause of death in the U.S in 2017. On average, medical expenditures for people diagnosed diabetes are about 2.3 times higher than those without the disease.[6] Worldwide direct healthcare expenditure on diabetes in 2019 was 760 billion USD and is forecasted to reach 845 billion USD by 2045.[7] According to the International Diabetes Federation report in 2019, 463 million people around the world have diabetes, and 1 in every 2 people with diabetes do not know they have it.[4] By 2045, the number of people with the disease is anticipated to reach 700 million.[4, 8] According to American Diabetes Association, diabetes is defined as 'a group of metabolic diseases characterized by hyperglycemia resulting from defects in insulin secretion, insulin action, or both'.[9] Due to defective insulin functioning, blood glucose cannot be metabolized in the cells and it rises in the body. In addition to chronic metabolic illness, other co-existing conditions and complications among diabetic patients include high blood pressure, heart disease and stroke, poor vision and blindness, kidney disease and failure, amputations, nerve diseases, periodontal (gum) diseases, complications of pregnancy, etc.[5, 10] Unhealthy modern sedentary lifestyle has been blamed for this chronic disease with its deadly consequences.[3, 10, 11] Table 1.1 gives the comparison of the blood glucose range for diabetic vs a healthy individual:[12]

Table 1.1: Blood glucose range comparison			
Test	Healthy	Prediabetes	Diabetes
A1C (percent)	<5.7	5.7-6.4	6.4 or higher
Fasting Plasma Glucose (mmol/L)	<5.6	5.6-6.94	6.94 or higher

A1C test reflects the homeostatic control of blood glucose levels over a 3-month period. A small percentage of hemoglobin is normally glycated with glucose. The A1C test measures the percentage of hemoglobin that is glycated. If this percentage becomes higher than the healthy range, it indicates higher levels of blood glucose than normal. Fasting plasma glucose (FPG) is a measure of glucose levels in the blood at the moment of performing the test. For those stricken with diabetes, higher levels of blood glucose results in the compromising health conditions listed above.

Blood glucose monitoring (BGM) fulfills four roles: [13]

(1) Provides data to the patient that can be used to adjust medication

(2) Provides average glucose concentration that gives the patient rough information about how well they are doing (both for avoiding hypoglycemia and in terms of blood glucose control)

(3) Reminds the person with diabetes that they have the disease to take necessary precautionary steps

(4) Used by the health care providers to evaluate and make changes in the diabetes treatment of the patient.

In 1962, Clark and Lyons introduced an amperometric method of glucose sensing by measuring the oxygen consumed during the enzymatic reaction of the glucose oxidase (GOx) enzyme with glucose.[14] The GOx enzyme was incorporated into the membrane of Clark's oxygen electrode, reacting with the glucose in blood plasma, and altering the oxygen sensed at the electrode. From this first biosensor, numerous electrochemically based biosensors have emerged based on using not only enzymes but also using affinity-based biosensors incorporating antibodies, deoxyribonucleic acids (DNAs), and aptamers.[15]

Glucose sensors evolved by focusing on the problems brought on by the need for oxygen to accept the electrons collected by the enzyme from glucose oxidation. Using the natural mediator is oxygen comprised the first generation of glucose sensors. Oxygen is variable and limited in most applications (discussed with examples in section 1.3), so synthetic mediators are used, and these are classified as second-generation sensors. The third generation does not require any mediator and electrons from the enzyme are taken by the electrode. Of the three, variants of the second generation are mature products and commercially successful. More details about these three types of sensors with their limitations will be discussed in this chapter.

1.3 Working Mechanism

The working mechanism of an electrochemical glucose sensor has been most simply described by George S. Wilson.[16-20] According to Wilson, the reactions at the electrode surface, which is known as the "ping-pong" mechanism are as follows:

$$S_R + E_O \rightarrow S_O + E_R$$

$$E_R + M_O \rightarrow E_O + M_R$$

Where S, M, and E define substrate, mediator, and enzyme, respectively, and the subscripts O and R define their oxidized and reduced state. Most glucose biosensors contain glucose oxidase (GOx)

enzyme, and it is considered as the gold standard of glucose sensing. GOx contains a flavin adenine dinucleotide (FAD) coenzyme molecule on its active site. This cofactor goes through reversible electrochemistry first by oxidizing glucose to gluconolactone (P1) producing $FADH_2$ (E_{red}), and then E_{red} oxidizes back to FAD (E_{ox}) reducing oxygen to peroxide.

Wilson's treatment describes second generation sensors. The replacing oxygen with excess synthetic mediator simplifies the theoretical description of enzyme activity. The limiting substrate becomes singularly glucose and the simple single substrate and simple Michaelis-Menten kinetics can be applied; resulting in an apparent Km describing the affinity the enzyme has for the substrate. In the case here, oxygen is limited, and two substrate enzyme kinetics must be considered. Two substrate enzyme kinetics will be introduced here and related to current in chapter 4.

First-generation glucose sensors:

As for kinetic details, in the presence of glucose oxidase, the reaction sequence with glucose is[21]-

$$E_{ox} + glu \underset{\rightarrow}{\overset{k_1}{}} E_{red}P1 \underset{\rightarrow}{\overset{k_2}{}} E_{red} + P1 \qquad (1)$$

$$E_{red} + O_2 \underset{\rightarrow}{\overset{k_3}{}} E_{ox}H_2O_2 \underset{\rightarrow}{\overset{k_4}{}} E_{0x} + H_2O_2 \qquad (2)$$

The enzyme oxidizes β-D-glucose (glu) to glucono-δ-lactone (P1), and O_2 re-oxidizes the enzyme, producing H_2O_2.

The reaction rate is

$$R = \frac{d[P1]}{dt} = \frac{d[H_2O_2]}{dt} = -\frac{d[O_2]}{dt}$$

At steady state, the rates of all steps are equal, so

$R = k_1[E_{ox}][glu] = k_2[E_{red}P1] = k_3[E_{red}][O_2] = k_4[E_{ox}H_2O_2]$ (3)

The rates will be equal, but the magnitude of rate will depend upon the slowest step or smallest term: which is k_1 or k_3 term. k_1 is estimated to be 32 $(mM\text{-}s)^{-1}$, k_3 ranges from 440 to 2400 $(mM\text{-}s)^{-1}$.[21]

Reaction rates have two factors- concentration and rate constant. The enzyme acts as a catalyst to increase the over rate constants k_1 and k_3, but concentration still plays a factor.

The Glucono–D-lactone (P1) produced in the reaction (1) gets hydrolyzed in presence of water producing gluconic acid:

Glucono–D-lactone + H_2O $\longrightarrow$ Gluconic acid (4)

The overall reaction for a first-generation sensor-

β-D-Glucose+ O_2 + H_2O $\longrightarrow$ Gluconic acid+ H_2O_2 (5)

To sense the glucose, H_2O_2 is oxidized at the working electrode to O_2 upon the application of peroxide oxidizing potential.

$H_2O_2 \longrightarrow O_2 + H^+ + 2e^-$ (6)

Oxidation current i_{ox} produced from H_2O_2 oxidation is proportional to rate of H_2O_2 production (reaction 5). However, the rate of peroxide production has two factors, glucose and oxygen and each of these factors contain concentration and rate constant. The mechanistic steps are sequential, so it is crucial that the rate of glucose oxidation (reaction 1) be rate limiting or:

$k_1[Glu] < k_3[O_2]$ (7)

The resulting limiting current will be dominated by the component containing glucose or the other containing oxygen. Fortunately, k_3 is much larger than k_1, so if the ratio of $\frac{[gluc]}{[O_2]}$ is less than one, the current will be glucose limited. Unfortunately, in vivo the concentrations of glucose are much larger than oxygen so the optimum ratio of glucose to oxygen in vivo is impossible to achieve. The implantable glucose monitoring system tried to overcome the limitation by incorporating glucose-

restrictive layers to the electrode, compromising the sensitivity of the glucose sensor though (discussed in 1.3).

Second-generation glucose sensors: For this type of glucose sensors an artificial mediator, denoted by M, replaces the naturally available oxygen (reaction 1, 7).[22] As before:

$$E_{ox} + glu \xrightarrow{k_1} E_{red}P1 \xrightarrow{k_2} E_{red} + P1 \qquad (1)$$

But,

$$E_{red} + M_{Ox} \xrightarrow{k_3} E_{ox}M_{red} \xrightarrow{k_4} E_{0x} + M_{red} \qquad (8)$$

The reduced species of mediator, M_{red} is oxidized back at the working electrode upon applying oxidation potential vs the reference electrode (reaction 9)

$$M_{red} + 2e^- \rightarrow M_{Ox} \qquad (9)$$

And reactions 1,8 ad 9 repeat.

The most common FDA approved mediators: hexaammineruthenium(III) chloride and potassium ferricyanide and are used in the commercially available finger-prick type glucose sensor strips.[23]

Third-generation glucose sensors: This type of sensor does not require any mediator as it can transfer the charge directly to the working electrode surface (reaction 1, 9)[22]-

$$E_{ox} + glu \rightarrow E_{red} + P1$$

$$E_{red} \xrightarrow{direct\ electron\ transfer\ to\ electrode} E_{Ox} + 2H^+ + 2e^-$$

Schematic of basic differences among the working mechanism of these three generation glucose sensors are shown in Figure 2.1

1.4 Limitations of the existing electrochemical glucose sensors

The optimum performance of a sensor depends on the glucose/mediator ratio. If the glucose/mediator ratio is less than one, optimum performance is achieved through the glucose-

limiting reaction. With insufficient oxygen, the response becomes dependent on oxygen or mediator concentration and independent of glucose. For optimum performance, the rate-limiting enzymatic reaction must be glucose (equation 1). The oxygen limitation was first observed in first-generation electrochemical sensors such as those based on the Clark oxygen electrode. The oxygen limitation results from the limited solubility of oxygen in biological fluids and the relatively high concentration of glucose. For example, in vivo or implantable type glucose monitoring system is crucial for diabetic patients; specially those who need intensive insulin therapy or in the risk of having frequent high or low blood glucose. Implantable continuous glucose monitors currently available are implanted into subcutaneous tissue where interstitial fluid (ISF) glucose is correlated to plasma levels.[24] The ratio of glucose to oxygen less than one is found nowhere in the body. For example, oxygen in brain ECF is 50 μM by contrast, ECF glucose is 5 mM.[25] Tumor hypoxia has been well studied and remains an interest in relationship to tumor metabolism.[26] To meet the optimum glucose/oxygen ratio and eliminate oxygen dependence, several techniques have been adopted.

One of the alternative approaches initiated the second-generation glucose sensors. These use an artificial redox mediator to perform the same role as oxygen. Since the artificial mediator is not found in the body, its concentration can be made large and independent of respiration. Generally in commercially available finger-prick type glucose sensors, two carbon-based electrodes both are coated with mediator, but the enzyme is applied only one electrode, and the signals subtracted in order to compensate for background interferences.[27] Unlike first-generation sensors, the oxidized form of the synthetic mediator takes the electrons from the reduced form of the enzyme and shuttles them to the electrode where the mediator is re-oxidized, and the cycle continues (equations 1, 8 & 9). This has two advantages, it is oxygen-independent, and the mediator oxidizes at a less positive

potential than hydrogen peroxide. The less positive potential will find fewer electroactive species to add to the background. Even so, there is a possible interference from freely diffusing oxygen oxidizing the enzyme instead of the mediator, resulting in a reduced sensor response.[25] There is also a serious potential health hazard by leaching out of the harmful toxic mediator. For this reason, the second-generation technology is limited to ex-vivo finger-prick type disposable glucose sensors. These glucose test strips have enjoyed commercial success, but the technology cannot be transferred to in vivo use due to safety concerns. These glucose test strips have enjoyed commercial success, but the technology cannot be transferred to in vivo use due to safety concerns, such as- potential leaching due to leaching and loss of stability over time. However, Abbott Diabetes Care Inc. (Alameda, CA) addressed these limitations by introducing wired enzyme technology where enzyme is connected to the electrode surface through crosslinked redox-conductive polymeric "wires".[28, 29]

An alternated approach first proposed by Wilson was to lower the glucose sensitivity in order to lower the rate of oxygen consumption, there by maintaining a lower glucose/oxygen ratio.[30] This can be achieved by modification of the first-generation type sensor film with the application of multiple membrane layers during sensor film fabrication having 100% permeability to oxygen but limited permeability to glucose.[22, 31-37] Generally the sensors are coated with multiple layers of membranes where the outer layer limits the diffusion of glucose molecules as well as restricts any interferences, but oxygen is fully permeable to all the layers of the sensor film thereby keeping glucose concentration less than that of oxygen at the enzymatic reaction site.

However, lowering of sensitivity limits precision, making it difficult to resolve small differences in glucose concentrations. This is illustrated in **Error! Reference source not found.** where for

the same step, increase in the glucose a low-sensitivity sensor records one-fifteenth the current of the high-sensitivity sensor. Such lack of precision in glucose reading can be detrimental, especially in tissues where higher precision is needed, such as brain tissues. Oxygen content in brain extracellular fluid by microdialysis has been reported to be 0.03 – 0.08 mM,[38] and varies throughout the brain.[39] Glucose brain ECF levels also determined by microdialysis is 1.57±0.76 mM but levels can vary up to about 2 mM.[40]

The third-generation enzyme electrodes are based on direct electron transfer eliminating the need for oxy gen or a mediator. The development of these types of sensors are still at early stages, and none are commercially available.[25]

1.5 Proposed scheme and its significance

Among the three types of electrochemical sensors discussed above, the first-generation principle is still the most researched. Despite its limitations, it is still considered the gold standard for all glucose-sensing methods.[20, 25, 41] Commercially available minimally invasive continuous-glucose-monitoring-system (CGMS) such as- CGMS products by Medtronic, Dexcom, Abbott Diabetes Care, Senseonics, etc are based on the first-generation working principle using GOx enzyme and glucose diffusion barrier creating polymer membrane/s.[42-50] An optimum glucose sensor for in vivo use would be a first-generation but without compromised sensitivity nor the dependence on endogenous oxygen.

This project proposes a solution to the existing limitations of first-generation glucose sensors for in vivo applications. The placement of an oxygen generating electrode at micro-range proximity (25-500 µm) to the glucose sensor could provide the additional oxygen needed for glucose-limited operation. Producing the natural media via water electrolysis would supply oxygen to the sensor via diffusion. A schematic of the proposed solution is shown in Figure 2.3. A rough estimation

of oxygen production from the generator is 100X what is needed to achieve excess oxygen for this amount of glucose. The detailed calculation is shown in chapter 3. Assuming the demand for oxygen is linear the maximum amount of glucose measured with excess oxygen from the generator is predicted to be 200 mM. This estimate assumes that oxygen/peroxide delivery/consumption is not limited by diffusion through electrode films.

Upon successful implementation the following impacts on glucose-sensing can be expected:

● A highly sensitive first-generation glucose sensor

● A micro array for in vivo use providing precise in vivo glucose monitoring under ischemic conditions

1.6 Overview of studies discussed in the dissertation

Chapter 1 of this dissertation introduces the types of electrochemical glucose sensors focusing on the first-generation type. The accurate response of the first generation depends on the glucose/oxygen ratio which is difficult to achieve in vivo. Second-generation sensors were developed to overcome the dependence on oxygen but introduced new limitations. The chapter concludes with a proposed plan for optimum performance of first-generation sensors maintaining the required glucose/oxygen ratio by introducing an oxygen generating electrode. Chapter 2 explores first-generation glucose sensor membrane construction using macro 2 mm Pt disk electrodes. A method of construction detecting glucose successfully with optimized performance was eventually found, but many of the methods found in the literature could not be reproduced. It was assumed the method of construction world carry-over to micro-band electrodes. Chapter 3 discusses the detailed fabrication procedures to produce a stable oxygen generating microband electrode. Microelectrode arrays (MEA) composed of sixteen interdigitated micro-bands (each with 25 µm width x 2 mm length x 25 µm inter-band gap) were constructed using combinations

of adhesion and conduction metals: Cr/ Au, Ti/ Au, and Ti/ Pt. Selected microband surfaces were electroplated with Pt black or Pt and then subjected to oxygen evolution reaction (OER) voltage. From the oxygen generate-detect experiment, a rough idea about the oxygen concentration was obtained by developing back of the envelope calculation. The electrodes' ability to withstand the oxygen evolution reaction potential of +1.4 V vs. Ag/AgCl at neutral pH was determined, and the chemical and morphological changes of the constituent metals were evaluated. Chapter 4 explores the unique methods of glucose sensor film construction on microband electrodes with glucose oxidase enzyme entrapment with poly o-phenylenediamine (PoPD) polymer as well as cross-linking with glutaraldehyde/BSA. All work on GOx immobilization with macro electrodes in chapter 2 was assumed to be directly transferrable to microband electrodes. However, this assumption proved false and a new enzyme immobilization procedure was developed for micro band electrodes. Chapter 4 also reports the construction of the complete glucose sensing system with the inclusion of the oxygen-generating micro band. The initial results are that the additional oxygen did not provide the anticipated results, i.e. the action of oxygen generation actually reduced the glucose signal when the electrodes were 25 µm apart. A reasonable explanation for the ineffective results was proposed, and additional experiments increasing the distance between two eleectrodes to 500 µm proved that the method could be made to work if the enzyme generated peroxide could be sequestered at the sensor electrode. Chapter 5 sums up the research with conclusions and further investigations proposed.

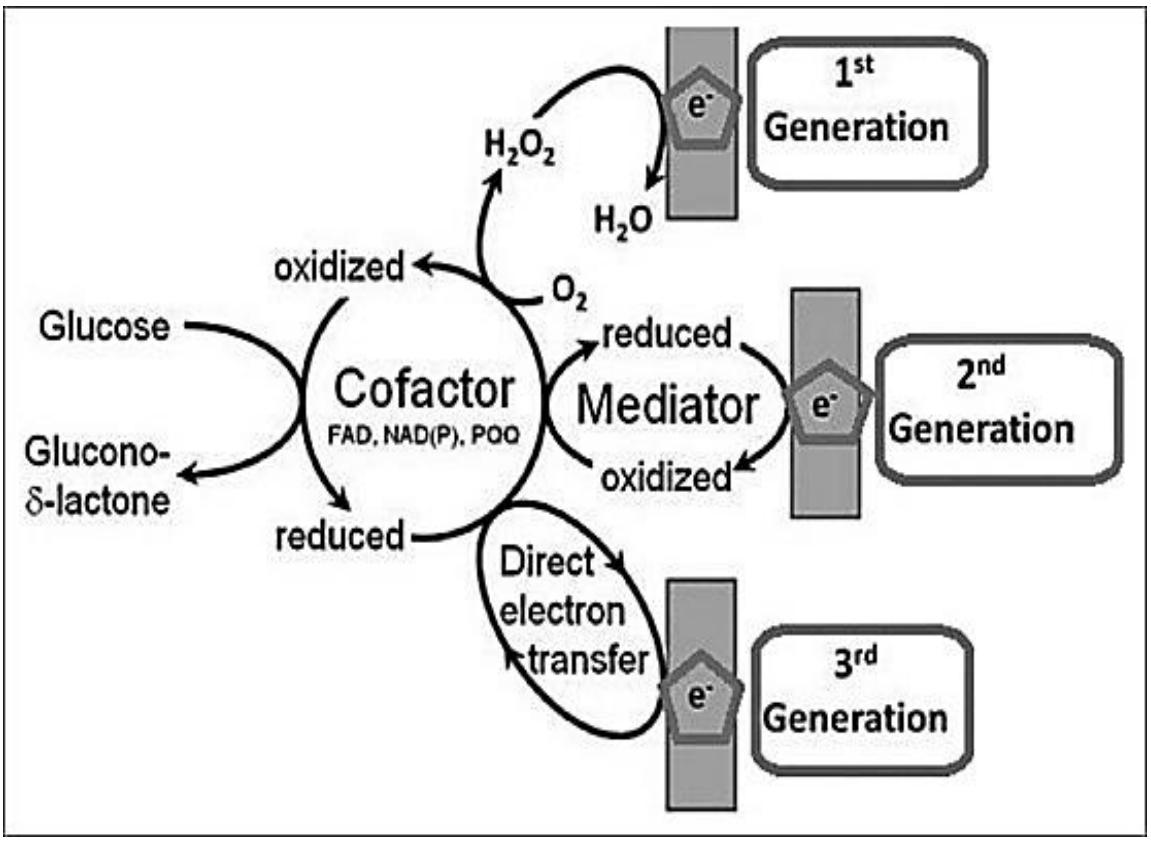

Figure 2.1 Working principle of three generations of electrochemical glucose sensors: first two generation type use oxygen or artificial species as charge transferring mediator, and third type is mediator-less mechanism. Picture obtained with permission from S. Ferri, K. Kojima and K. Sode, Journal of diabetes science and technology, 2011, 5, 1068-1076.[20]

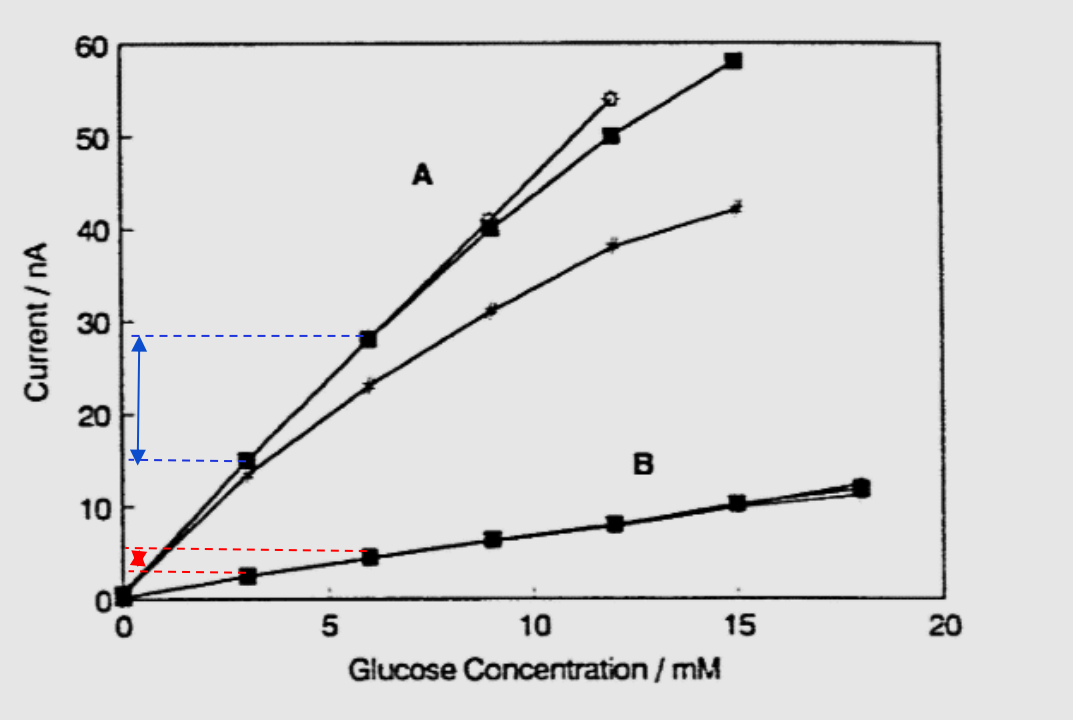

Figure 2.2 In vitro oxygen effect on high (A) and low (B) sensitivity sensors. (○) PO2= 150 mmHg; (■)PO2= 40 mmHg; (#) PO2= 7.6 mmHg. The effect of oxygen between two glucose readings (3 and 6 mM) are highlighted for A, blue vs. B, red glucose sensor at 40 mmHg for reference. Between two glucose readings, A detects more than 5 times higher current value than B. Picture obtained with permission from Y. Zhang and G. S. Wilson, Analytica chimica acta, 1993, 281, 513-520.[30]

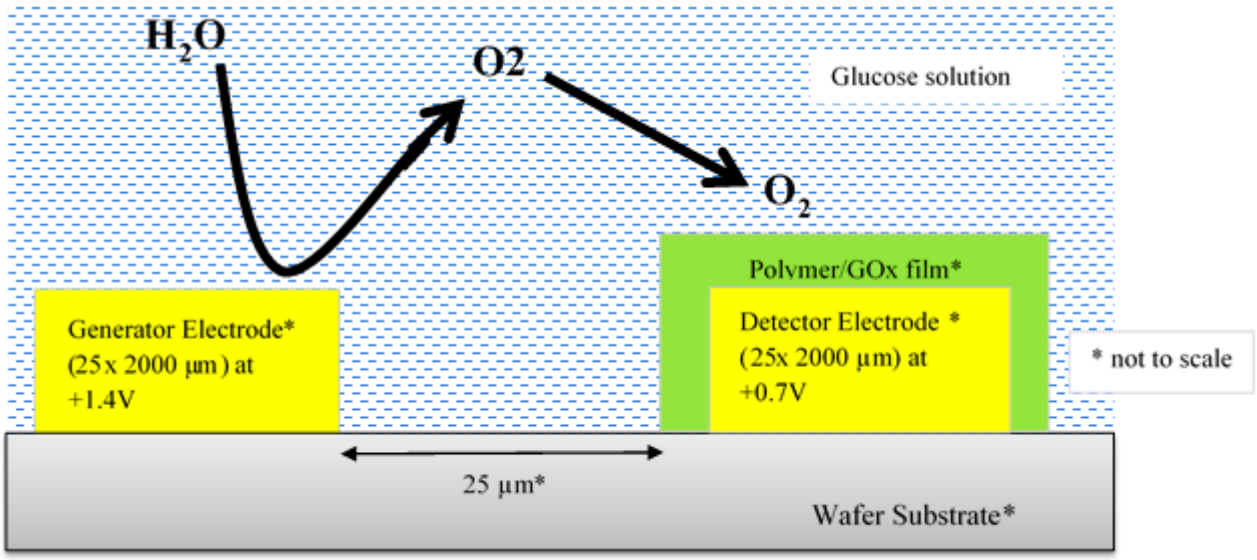

Figure 2.3 Proposed solution to eliminate oxygen dependence of first Generation GOx enzyme sensor electrode for in-vivo application (schematic cross-section): generation of oxygen from water electrolysis by the generator electrode (platinized gold or platinum microelectrode at +1.4 V vs Ag/AgCl) and supply to the detector or sensor electrode (platinized gold or platinum microelectrode at +0.7 V vs Ag/AgCl) located at micro-range proximity from the generator.

1.7 References

1. E. E. Partridge, E. J. Mayer-Davis, R. L. Sacco and A. J. Balch, *Circulation*, 2011, **123**, 3012-3014.

2. G. Roglic, *Global report on diabetes*, World Health Organization, 2016.

3. O. World Health, *Global report on diabetes: executive summary*, World Health Organization, 2016.

4. I. D. Federation, *Dunia: IDF*, 2019.

5. P. Centers for Disease Control and, *Atlanta, GA: Centers for Disease Control and Prevention, US Department of Health and Human Services*, 2020, 12-15.

6. A. American Diabetes, *Diabetes care*, 2018, **41**, 917-928.

7. R. Williams, S. Karuranga, B. Malanda, P. Saeedi, A. Basit, S. Besançon, C. Bommer, A. Esteghamati, K. Ogurtsova and P. Zhang, *Diabetes research and clinical practice*, 2020, **162**, 108072.

8. P. Saeedi, I. Petersohn, P. Salpea, B. Malanda, S. Karuranga, N. Unwin, S. Colagiuri, L. Guariguata, A. A. Motala and K. Ogurtsova, *Diabetes research and clinical practice*, 2019, **157**, 107843.

9. A. American Diabetes, *Diabetes care*, 2014, **37**, S81-S90.

10. E. Standl, K. Khunti, T. B. Hansen and O. Schnell, *European journal of preventive cardiology*, 2019, **26**, 7-14.

11. S. Lone, K. Lone, S. Khan and R. A. Pampori, *Journal of epidemiology and global health*, 2017, **7**, 235-239.

12. A. American Diabetes, *Diabetes care*, 2020, **43**, S14-S31.

13. B. H. Ginsberg, *Journal*, 2007.

14. L. C. Clark Jr and C. Lyons, *Annals of the New York Academy of sciences*, 1962, **102**, 29-45.

15. A. Sanati, M. Jalali, K. Raeissi, F. Karimzadeh, M. Kharaziha, S. S. Mahshid and S. Mahshid, *Microchimica Acta*, 2019, **186**, 1-22.

16. A. Harper and M. R. Anderson, *Sensors*, 2010, **10**, 8248-8274.

17. E. Wilkins and P. Atanasov, *Medical engineering & physics*, 1996, **18**, 273-288.

18. D. M. Fraser, *Biosensors in the Body: Continuous in vivo Monitoring*, John Wiley & Sons Incorporated, 1997.

19. S. Borgmann, A. Schulte, S. Neugebauer and W. Schuhmann, *Advances in Electrochemical Science and Engineering*, 2011, **2**.

20. S. Ferri, K. Kojima and K. Sode, *Journal of diabetes science and technology*, 2011, **5**, 1068-1076.

21. Z. Tao, R. A. Raffel, A.-K. Souid and J. Goodisman, *Biophysical journal*, 2009, **96**, 2977-2988.

22. S. Vaddiraju, D. J. Burgess, I. Tomazos, F. C. Jain and F. Papadimitrakopoulos, *Journal of diabetes science and technology*, 2010, **4**, 1540-1562.

23. N. Loew, W. Tsugawa, D. Nagae, K. Kojima and K. Sode, *Sensors*, 2017, **17**, 2636.

24. S. C. Kanick, P. A. Schneider, B. Klitzman, N. A. Wisniewski and K. Rebrin, *Microvascular research*, 2019, **124**, 6-18.

25. B. M. Dixon, J. P. Lowry and R. D O'Neill, *Journal of Neuroscience Methods*, 2002, **119**, 135-142.

26. T. Ishida, T. Shimamoto, N. Ozaki, S. Takaki, T. Kuchimaru, S. Kizaka-Kondoh and T. Omata, *Micromachines*, 2016, **7**, 155.

27. D. C. Harris, *Quantitative chemical analysis*, Macmillan, 2010.

28. A. Heller and B. Feldman, *Chemical reviews*, 2008, **108**, 2482-2505.

29. H. Teymourian, A. Barfidokht and J. Wang, *Chemical Society Reviews*, 2020.

30. Y. Zhang and G. S. Wilson, *Analytica chimica acta*, 1993, **281**, 513-520.

31. R. Tipnis, S. Vaddiraju, F. Jain, D. J. Burgess and F. Papadimitrakopoulos, *Journal of diabetes science and technology*, 2007, **1**, 193-200.

32. S. Vaddiraju, D. J. Burgess, F. C. Jain and F. Papadimitrakopoulos, *Biosensors and Bioelectronics*, 2009, **24**, 1557-1562.

33. S. Vaddiraju, H. Singh, D. J. Burgess, F. C. Jain and F. Papadimitrakopoulos, *Journal of diabetes science and technology*, 2009, **3**, 863-874.

34. S. Vaddiraju, A. Legassey, Y. Wang, L. Qiang, D. J. Burgess, F. Jain and F. Papadimitrakopoulos, *Journal*, 2011.

35. R. A. Croce, S. Vaddiraju, F. Papadimitrakopoulos and F. C. Jain, *Sensors*, 2012, **12**, 13402-13416.

36. R. A. Croce, S. Vaddiraju, J. Kondo, Y. Wang, L. Zuo, K. Zhu, S. K. Islam, D. J. Burgess, F. Papadimitrakopoulos and F. C. Jain, *Biomedical microdevices*, 2013, **15**, 151-160.

37. Y. Wang, S. Vaddiraju, B. Gu, F. Papadimitrakopoulos and D. J. Burgess, *Journal of diabetes science and technology*, 2015, **9**, 966-977.

38. P. K. Nair, D. G. Buerk and J. H. Halsey, Jr., *Stroke*, 1987, **18**, 616-622.

39. L. Wang, Y. Li, H. Han, G. Liu and P. G. Osborne, *Neuroscience letters*, 2003, **344**, 91-94.

40. W. M. Abi-Saab, D. G. Maggs, T. Jones, R. Jacob, V. Srihari, J. Thompson, D. Kerr, P. Leone, J. H. Krystal and D. D. Spencer, *Journal of Cerebral Blood Flow & Metabolism*, 2002, **22**, 271-279.

41. J. Okuda-Shimazaki, H. Yoshida and K. Sode, *Bioelectrochemistry*, 2020, **132**, 107414.

42. G. McGarraugh, *Diabetes technology & therapeutics*, 2009, **11**, S-17.

43. J. Wang, *Chemical reviews*, 2008, **108**, 814-825.

44. B. C. Gilligan, M. Shults, R. K. Rhodes, P. G. Jacobs, J. H. Brauker, T. J. Pintar and S. J. Updike, *Diabetes Technology & Therapeutics*, 2004, **6**, 378-386.

45. G. Sparacino, A. Facchinetti and C. Cobelli, *Sensors*, 2010, **10**, 6751-6772.

46. G. Acciaroli, M. Vettoretti, A. Facchinetti and G. Sparacino, *Biosensors*, 2018, **8**, 24.

47. D. Olczuk and R. Priefer, *Diabetes & Metabolic Syndrome: Clinical Research & Reviews*, 2018, **12**, 181-187.

48. O. Didyuk, N. Econom, A. Guardia, K. Livingston and U. Klueh, *Journal of Diabetes Science and Technology*, 2020, 1932296819899394.

49. G. Cappon, M. Vettoretti, G. Sparacino and A. Facchinetti, *Diabetes & metabolism journal*, 2019, **43**, 383.

50. A. Facchinetti, *Sensors*, 2016, **16**, 2093.

2. Construction of a Glucose Oxidase Enzyme Sensor on a Macro-electrode

2.1 Abstract

This work investigated polypyrrole (Ppy), glutaraldehyde (Glut), and poly-o-phenylenediamine (PoPD) polymers, and a suitable technique for the construction of glucose oxidase (GOx) based glucose sensor film on a 2 mm platinum macroelectrode surface. Several parameters in the construction were adjusted to optimize the response to glucose and stability: the amount of the enzyme, pH of the buffer used during enzyme immobilization, and the concentration of the buffer used during the glucose determination. The preliminary data showed PoPD as an effective polymer for the purpose, 500 U/ml GOx loading and pH 5.2 acetate buffer optimized the sensor film construction method, and 10 mM PBS optimize the sensor film's glucose response. The effect of oxygen on the constructed glucose sensors and glucose sensitivity over time were investigated. It was assumed that these proof of concept studies would carry over to construction onto microband electrodes.

2.2 Introduction

For a first-generation glucose sensor to operate accurately, the concentration of oxygen must exceed that of the glucose present. For in vivo applications in tissues this condition is never the case. Oxygen content in brain extracellular fluid (ECF) is reported by microdialysis to be 0.03 – 0.08 mM and varies throughout the brain.[1] Brain ECF glucose levels also determined by microdialysis are 1.57±0.76 mM, but levels can vary up to about 2 mM (glucose/O_2 ratio ≅ 28).[2, 3] In the subcutaneous tissue, the concentration of oxygen is reported to be only 0.18 mM, whereas the physiological glucose concentration is 5.6 mM (glucose/O_2 ratio ≅ 30) for a healthy person.[4, 5] By any estimation, oxygen is in short supply. In both cases, the ratio of glucose to oxygen is higher than one, whereas a ratio less than one is required for optimum performance of the sensor. For an in-vivo glucose sensor to work in such oxygen-deficient conditions, without sacrificing its sensitivity, a source of additional oxygen must be provided. The ultimate goal is to form a glucose sensor onto one member of a microelectrode array. The additional oxygen is provided by water electrolysis at an oxygen-generating electrode at another member of the microarray.

As the construction of a glucose sensor onto a microband electrode is the primary goal, and since there was no collective experience in glucose sensor fabrication in the lab, sensor construction was first done on macro electrodes, reproducing the methods found in the literature in many cases. Numerous procedures can be found in the literature relating to the construction of glucose sensors, and many thousands of references can be found concerning glucose sensors in general. Once the sensor construction was perfected on macro electrodes, it was believed the method would be directly transferable to microband electrodes. This was a naive assumption as will be explained in a later chapter.

The polymers investigated in this study as possible enzyme hosts for glucose oxidase enzyme immobilization on platinum macroelectrodes were polypyrrole, glutaraldehyde, and poly o-phenylenediamine. Electropolymerization and drop-casting techniques were applied in attempts to construct an enzyme-polymer film on the electrode surface. The successful construction of the glucose sensor was verified by a glucose response test. The parameters contributing to the sensor construction procedure such as the amount of enzyme, electropolymerizing buffer concentration, and pH were modified in order to achieve optimization towards a more sensitive and responsive GOx based sensor. Later, the effect of oxygen on the sensor's responses to glucose was investigated. The sensitivity of the sensor over time was also conducted to have a preliminary idea about the sensor's lifetime.

All the reported methods of glucose sensor construction involve the immobilization of the enzyme on the electrode surface. This has been done by entrapment of the enzyme by electropolymerization or mechanical cross-linking. Polypyrrole (Ppy) is the polymeric form of pyrrole monomer. Ppy is electrically conducting and serves as an excellent enzyme host immobilizing the enzyme via electropolymerization. Immobilization of the enzyme by Ppy is also an inexpensive and effective technique. It is one of the few polymers that exhibit electrical conductivity upon oxidative polymerization. Its conductive nature is due to the presence of a conjugated double bond where rearrangement of loosely bound electrons along with the backbone of the ring structure results in electron flow.[6-11] In fact, it is the first polymer to show such a high conductivity.[12] The chemical structure of Ppy is shown in Figure 2.1. Ppy has been used in many applications such as sensors, batteries, microactuators, and biomedical devices. Its main application is in biosensors and immunosensors due to its excellent in vitro and in vivo biocompatibility, thermal stability, and relative ease of its synthesis and immobilization.[6, 8, 10, 12]

Serious limitations to the Ppy polymer include difficulties in polymerization reproducibility, loss of glucose response when using high electropolymerization time, and degradation of Ppy at the potential for H_2O_2 detection.

Glutaraldehyde (Glut) plays the role of an effective crosslinking agent and co-crosslinking with bovine serum albumin permits a high loading of the enzyme.[13] Glutaraldehyde is a linear 5-carbon dialdehyde (Figure 2.2) and is widely used as an enzyme immobilization technique. [13-15] Glut has a multi-component nature due to the presence of several forms in equilibrium.[14]

Poly o-phenylenediamine (PoPD) is a conducting polymer obtained from oxidative polymerization of the o-phenylenediamine monomer (Figure 2.3).[16] Studies have shown PoPD to have excellent properties for enzyme immobilization as well as producing highly reproducible and strongly adherent films.[17, 18] In their studies Trojanwicz et. al. showed that both Ppy and PoPD had the best sensitivities to glucose among all the electrodeposited conductive polymers they studied, but maximum glucose sensitivity and minimum background current was observed for PoPD/GOx film.[19] It has been observed that the structure and properties of PoPD vary depending on the type of inorganic acid medium used during electro polymerization.[20] Applications of PoPD include preparation of photovoltaic cells, anticorrosion coatings, pH measurements, fuel cell, and biosensors.[21, 22] PoPD is extensively used in fast-response and interference-free biosensor fabrication due to its built-in permselectivity.[13, 17] The advantages of PoPD for GOx sensor construction include abatement of interferences, ease of miniaturization, and the possibility of oxygen interference-free applications in the case of additionally applied overlayers. [17, 23, 24]

2.3 Instruments and reagents

Pyrrole (Accron LP), 25% Glutaraldehyde(Alfa Aesar), oPD (Sigma-Aldrich), KCl (EMD), calcium chloride (Amresco Chemical), bovine serum albumin (BSA) (Amresco Chemical), D-

glucose (Alfa Aesar), glucose oxidase from *Aspergillus niger* type VII (110 KIU/g of enzyme from Amresco, or 100 KIU/g from Sigma Aldrich), phenol (VWR), 4-amino antipyrine (Sigma Aldrich), NaH_2PO_4 and Na_2HPO_4 (Sigma-Aldrich), and horseradish peroxidase (Amresco Chemical) were obtained and used in the experimental studies. PBS tablets were obtained from Alfa Aesar and dissolved in a calculated volume of analytical HPLC grade distilled water (VWR) to obtain desired PBS concentration. A 0.8 M stock glucose solution of D-glucose in 10 mM PBS buffer was prepared and kept overnight before the experiments were performed to ensure mutarotation of the glucose to the β form.[25] Required concentrations of glucose were made by dilution of this concentrated stock solution. Pyrrole was freshly distilled at close to 130 ^oC, and KCl solution was degassed by heating it close to the boiling point at 102 ^oC for a few minutes before use. The 70 mM phosphate buffer silane solution contained 135 mM sodium chloride, 2.7 mM potassium chloride (KCl), 4.3 mM disodium phosphate (Na_2HPO_4), 1.4 mM monosodium phosphate (NaH_2PO_4). The colorimetric assay reagent was prepared with 70mM phosphate buffer solution, 0.1% bovine serum albumin, 0.5 mM 4-amino antipyrine, 500U/L horseradish peroxidase, and 15mM phenol.

Potentiostats used were CHI 830A, 1030A, or 750A (CH Instruments, Austin, TX, USA). Reference electrodes were either an Ag/AgCl in saturated KCl or a standard calomel electrode (SCE) with a Pt flag electrode as the counter electrode. A YSI 500 (YSI, Yellow Springs Ohio, USA) oxygen meter was calibrated and used for measuring the dissolved oxygen concentration. The pH of the buffers was verified by the Schott Instruments pH meter (SI analytics).

2.4 Experimental

2.4.1 GOx sensor construction

Three different methods were used for enzyme immobilization: cross-linking with Glut, or electrochemical polymerization/entrapment with either Ppy or PoPD onto a 2mm platinum disc electrode. Before enzyme entrapment, the bare electrode was polished with a series of progressively smaller grits, starting with a 1µm diamond slurry, followed by 0.3 µm, and then 0.05 µm alumina. The electrode surface was rinsed with distilled water between each polishing slurry and rinsed thoroughly after the last polishing. After the enzyme immobilization, the glucose sensors were stored overnight in 10 mM PBS at 4^{o}C before use.

2.4.1.1 With Polypyrrole

Four different GOx sensor fabrication procedures by electropolymerization using polypyrrole as shown in table 2.1 were reproduced from literature.

The reslts of these experiments have been dicussed in section 2.5.1.1

Table 2.1: Various Pt/Ppy/GOx electrode fabrication techniques reproduced in lab from the literature			
Literature resource	Procedure	Time	Other factors
1.By Fortier et. al.[26]	Freshly distilled pyrrol- 1mmol (70µl); Degassed KCl- 10mM (2ml) GOx- 500 U +v0.65 V vs SCE	20 min	Avg charge =400mC/cm^2
2. By Sadik et. al.[27]	Freshly distilled pyrrole- 0.5M; Degassed KCl- 100mM GOx- 150 U/ml +0.65 V vs SCE	5-10 min	~10µm thick film
3.By Lowe et. al.[28]	Freshly distilled pyrrole- 0.2M; 0.1 KCl GOx- 1mg/ml 0.8V vs Ag/AgCl in sat'd KCl	2.5 hrs	-
4.By Guerrieri et. al.[13]	Step1: Pt/Ppy film grown from 0.4M pyrrole, 0.1M KCl Step2: overoxidation in Phosphate buffer for at least 6 hrs Step3: pipetting Glut-bovine serum albumin-phosphate buffer- GOx solution on overoxidized electrode	Step1: deposit time- ~33.5 min (by back-calculation for 0.67µm)	Step1: 0.67µm thick film; 300mC/cm^2 charge Step2: until stable background current obtained

2.4.1.2 With Glutaraldehyde

GOx sensor fabrication was is similar to that described by Guirrieri et. al., adopting only the physical adsorption step (step 3 of the fourth method in Table 1).[13] The GOx coating solution was prepared by mixing 300 µl of 70 mM PBS with 8 mg bovine serum albumin (BSA), 0.1 g GOx, and 30 µl of 2.5% glutaraldehyde. A 2mm electrode was polished and the enzyme solution was

drop cast by pipetting 2-3 µl on the electrode surface then air-dried for 30 minutes. The GOx electrode was then stored in 70 mM PBS at 4^{o} C when not in use.

The glucose response of the GOx drop-cast films was performed to verify successful sensor fabrication and to discover the sensitivity, linearity, and calibration stability of the sensors. Sensor optimization was determined by amperometric i-t curves obtained from oxidation of the enzyme generated hydrogen peroxide at +0.7 V vs. Ag/AgCl in saturated KCl. For the Glut-BSA-GOx sensor film, glucose concentrations were increased by increments of 2 mM from 0 to 8 mM by pipetting the concentrated glucose stock every 20 minutes. The solution was stirred continuously by a magnetic stir bar while i-t responses were recorded. Glucose calibration curves were constructed by plotting the absolute values of stable oxidation current readings against respective glucose concentrations.

2.4.1.3 With PoPD

Enzyme entrapment with PoPD electropolymerization was adopted from the sensor construction procedure described by Malitesta et. al..[17] The polished Pt electrode was electrochemically pretreated in 0.5 M H_2SO_4 by cyclic voltammetry between -0.21V and +1.19V vs. standard calomel electrode until a steady-state CV was obtained. The electropolymerizing solution was 5 mM in oPD and 500 U/ml in GOx contained in acetate buffer at pH 5.2 (ionic strength of 0.2 M). This solution was sonicated for 15 minutes or until homogeneous. The pH of the acetate buffer was verified by a Schott Instrument pH meter. The enzyme film was grown for 15 minutes at +0.65V vs. SCE while the solution remained unstirred. The enzyme that was loosely attached to the electropolymerized film was removed by stirring in 10mM PBS for 3 minutes. The electrode was stored in 10mM PBS at 4^{o}C overnight before its first use and stored the same way when not in use.

Glucose response tests were performed by recording amperometric i-t curves with the sensor electrode at +0.7 V vs. Ag/AgCl in saturated KCl. The current from the oxidation of the enzyme-generated peroxide was recorded for glucose concentrations between 0 and 8mM increasing in 1mM increments every 5 minutes. Glucose calibration curves were constructed by plotting the absolute values of stable oxidation current readings against respective glucose concentrations.

2.4.2 Effect of enzyme concentration

The effect of GOx concentration on the sensor response involved four different Pt electrodes of equal diameter (2 mm), and PoPD/GOx coatings on the electrodes' surface were obtained from the sensor fabrication procedure according to what was described by Malitesta et. al,[17] except with four different GOx concentrations- Original GOx =500 U/ml[17], 25% less than original GOx, 50% less than original GOx, 25% more than original GOx, and 50% more than original GOx. Glucose response for 0 to 8 mM glucose was performed in a similar manner as described in section 2.4.1.3 on each sample sensor electrode.

2.4.3 Effect of buffer concentration

One parameter for the GOx sensor to study was the effect of the buffer concentration in the solution of glucose in which the measurement was taking place. The current response from 0 to 4 mM glucose was measured twice with other parameters and ingredients remaining constant except for the ionic strength of phosphate buffer, 10 mM PBS and 70 mM PBS.

2.4.4 Effect of electropolymerizing buffer pH

oPD was electropolymerized onto 2 mm Pt electrodes from buffers of different pH. A 0.5 M sulfate buffer at pH 1 was made by adding H_2SO_4 to 0.5M Na_2SO_4. Other electropolymerizing buffers included A 0.2 M acetate buffer at pH 5.2 and a 0.01 M phosphate buffer at pH 7.4. Each electropolymerizing buffer solution was made 5mM in oPD and 500 U/ml in GOx.

Electropolymerization at pH 5.2 and 7.4 was done by performing amperometric i-t at +0.65V vs. SCE for 15 minutes while the solution remained unstirred. Electropolymerization at pH 1 was accomplished by CV between 0V and +0.8 V (vs. Ag/AgCl in satd. KCl) for 15 cycles at 50mV/s scan rate. Glucose responses at each pH were recorded for 0 to 8 mM glucose, and a respective glucose calibration curve was constructed for each enzyme sensor.

2.4.5 Effect of oxygen on the glucose responses of the sensor

Oxygen-stress experiments indicated how the glucose response i-t curve changes with dissolved oxygen concentration for a constant glucose concentration. Amperometric i-t responses for the oPD/GOx sensor were recorded for 3mM glucose in10 mM PBS at +0.7 V vs the SCE as the reference electrode. After calibration, the oxygen meter recorded the changes in the dissolved oxygen concentration simultaneously with the amperometric i-t responses from the sensor. After the glucose signal reached a stable value, the oxygen was purged by bubbling nitrogen through the solution. The oxygen-stress procedure was repeated for 3, 4, and 5 mM glucose. The glucose solution was stirred constantly at a moderate rate with a magnetic stir bar, and the cell was covered with parafilm to keep oxygen from the air from redissolving in the purged solution.

A second method determined the sensor's response with oxygen concentrations greater than what would dissolve under atmospheric conditions. Oxygen was added externally into the glucose from the oxygen gas cylinder by gently bubbling oxygen through the solution. The dissolved oxygen concentration was measured with a YSI 500 oxygen meter. I-t responses were recorded twice with glucose ranging from 0 to 12 mM once for atmospheric or endogenous oxygen, and again with externally added oxygen. Such range of glucose concentrations was selected to observe the dynamic range or the deviation from glucose linearity.

2.4.6 Sensitivity over time

The sensitivity of the GOx sensor over time was measured by repeatedly constructing calibration curves for glucose between 0 to 8 mM from day 1, and then every few days until day 63. Sensitivities from the calibration curves were extracted and plotted over time.

2.5 Results and Discussion

2.5.1 GOx sensor construction

The results of attempts to construct GOx sensor on 2 mm Pt electrodes with various construction methods are discussed below.

2.5.1.1 With Polypyrrole

The different construction methods for immobilizing GOx onto the electrode with polypyrrole are described in table 2.1. The construction parameters: time durations, the concentration of materials, and pre/post-treatment were variable, but the procedure for construction was constant. None of these construction methods produced sensors that could amperometrically detect glucose in solution. To verify if enzyme inactivity was a cause of failure, a colorimetric enzyme activity test was performed using a slightly modified glucose detection colorimetric test (Figure 2.4).[28, 29] [26] In one vial, a reference solution was prepared by adding 5 mg of GOx (resulting in 5000 U/L GOx enzyme) to 100 μL of 10 mM glucose with 1000 μL of colorimetric assay solution. In a second vial, the electropolymerized electrode with hopefully entrapped GOx was combined with glucose and assay solution. The presence of an active enzyme was confirmed by the appearance of bright pink color in the reference solution within a few seconds of the enzyme addition. The vial with the enzyme electrode, on the other hand, did not show any remarkable color change. Referring to Table 2.1, enzyme concentrations and electropolymerization times resulted in films of various thicknesses. After several hours a pale pink color finally appeared in the solution containing the

GOx/Ppy electrode indicating the presence of either insufficient or almost inactive immobilized enzyme. Too thick a polypyrrole coating has been reported to reduce enzyme activity, and too short a deposition time would cause entrapment of insufficient enzyme.[17, 26] An optimum deposition time or optimum thickness could help overcome this problem. Trojanwicz et. al. reported in their Ppy/GOx sensor studies that the responses to glucose initially increased with an increase in deposition time. However after 1.5 minutes, higher deposition time caused loss of the sensor's sensitivity, and for deposition time longer than 10 minutes, glucose response was completely lost.[18] Also, the study reported difficulties in reproducibility of the Ppy/GOx using a one-step process. In addition, conflicting values for optimum film deposition time and thickness estimations were found in the literature. For example, to obtain 0.67μm film (Table 2.1), 33.5 minutes was needed according to Fortier's report, while 1.5 min was needed according to Guirrieri's. These differences in construction parameters made for a confusing set of instructions when attempting to repeat what was found in the literature. Moreover, electrodes with Ppy films were reported to degrade in presence of H_2O_2 at the potential applied to oxidize H_2O_2.[17] For these reasons construction of a GOx enzyme electrode based on Ppy immobilization was abandoned.

2.5.1.2 With Glutaraldehyde

The Glut-BSA-GOx sensor electrode successfully detected the presence of glucose. As normal human blood glucose range is between 4 to 7.8 mM, a calibration curve between 0 to 8 mM glucose was constructed using amperometric i-t data (Figure 2.5a). The H_2O_2 oxidation current increased with increasing glucose concentration. Additional glucose results in increased production of H_2O_2, increasing the oxidation current magnitude. The calibration curve appeared linear (R^2=0.99)with the sensitivity of 13.85 (±0.32) μA/mM-cm^2 (Figure 2.5b)

Constructing GOx sensors by cross-linking with glutaraldehyde was convenient and successful, but the life of the coating was found to be between seven to ten days, with a gradual decrease in the linearity of calibration over time. Glut-BSA-GOx sensor fabrication was done by a drop-casting technique for enzyme immobilization. Since the ultimate goal is to construct a glucose sensor over micro band electrodes, electropolymerization entrapment of GOx on a single band would still need to be developed.

2.5.1.3 With PoPD

The Pt/PoPD/GOx sensor successfully detected the presence of glucose, and the i-t curve showed a sharp increase in oxidative current at the moment of glucose addition which gradually leveled off during the glucose response test (Figure 2.6a). The figure shows the glucose responses of the bare electrode and PoPD/BSA coated electrode lacking the enzyme as controls. Only the Pt/PoPD/GOx enzyme sensor electrode responded to glucose. The noise in the response was possibly due to the stirring and striking of the magnetic bar against the glass beaker wall. The calibration curve obtained had a sensitivity of 17. 00(±0.54) μA/ mM-cm^2 per electrode surface area (Figure 2.6b) The sensitivity of the PoPD incorporated sensor was slightly higher than the sensitivity obtained from the Glut incorporated sensor 13.85(±0.32) μA/mM-cm^2, (figure 2.5b). This comparison may not be statistically valid as sensitivities vary between electrodes constructed in the same way.

2.5.2 Effect of enzyme concentration

The glucose calibration curves obtained from sensors made with different GOx loadings showed a huge variation in sensitivities to glucose. Sensitivities obtained from 500 U/ml, 625 U/ml, 750 U/ml, 375 U/ml, and 250 U/ml GOx loading were 17.85(± 0.64) μA/mM-cm^2, 8.57(± 0.96) μA/mM-cm^2, 4.81(± 0.32) μA/mM-cm^2, 12.44(± 0.96) μA/mM-cm^2, and 7.67(± 0.96) μA/mM-

cm^2 respectively. The calibration curve for the 500U/ml GOx loaded enzyme electrode showed maximum sensitivity and linearity over the range of 0 to 8 mM glucose compared to the other loadings. Glucose sensitivity per unit of electrode surface area of the 2 mm diameter electrode vs. enzyme loading in Figure 2.7 indicates a peak response for the 500 U/ml GOx loading.[26] At lower concentrations of GOx, H_2O_2 production takes place uniformly throughout the polymer film. The result is that there is an optimum amount of GOx that will provide maximum sensitivity. The reason for low sensitivity at higher enzyme loading was explained for polypyrrole immobilization as this results in the consumption of the glucose analyte in an outer layer of the film.[30, 31] This, in turn, favored the diffusion of the product H_2O_2 back to the bulk solution instead of advancing to the electrode surface. Another possible reason could be GOx enzyme inhibition from the electropolymerization step which resulted in poor glucose sensitivity.[31, 32]

2.5.3 Effect of buffer concentration

Figure 2.8 shows comparative glucose calibration curves for a sensor calibrated in glucose solutions in either 10 mM or 70 mM PBS. Though both the calibration curves obtained deviated from linearity at higher glucose concentrations, the lower ionic strength buffer (10 mM) resulted in a sensitivity of 50.0± 4.5 μA/ mM-cm^2 and linearity of R^2 = 0.98, while the more concentrated one (70 mM) showed 35% lower sensitivity at 32.2± 4.5 μA/ mM-cm^2 and less linearity with R^2 = 0.95. Hence, 10mM PBS was selected for the subsequent experiments.

These results are confirmed by the literature as enzyme activity has been reported to be inhibited at higher pH and higher ionic strength (>0.5 M).[33, 34] The use of phosphate buffer solution (PBS) was reported to result in a maximum glucose response at 2.5 mM buffer strength and gradually decreasing at higher concentrations.[35] GOx has shown some exceptions to this convention depending on the buffer used. For example, the activity of glucose oxidase in sodium perchlorate

increases with an increase in sodium perchlorate concentration. It is believed that perchlorate changes in the conformational state of the protein enzyme which in turn makes the oxygen more accessible, leading to higher enzyme activity. Electrostatics dictates that ions which are more dispersed have weaker interactions than those crowded together.[33, 35] This basic principle is why higher ionic strength inhibits enzyme activity. Still, the more biologically relevant PBS was used in all experiments.

2.5.4 Effect of electropolymerizing buffer pH

Figure 2.9 shows how the pH of the electropolymerization solution affects the sensitivity of the resulting sensor to glucose. It is observed that the GOx sensor constructed by electropolymerization at pH 5.2 results in about nine times higher sensitivity than those constructed at electropolymerization at pH 7.4. Another observation, which is one of the themes of this work, is that the calibration curve for the more sensitive sensor shows a deviation from linearity beyond 6 mM glucose. The less sensitive sensor shows linearity over the entire glucose concentration range. This can be attributed to an oxygen limitation due to higher oxygen demand with increasing sensitivity to glucose.

Compared to other enzymes GOx is robust with and can function between pH 2-8, but film thickness is set by the conductivity of the film which decreases with increasing film thickness.[36] Not shown are the results of glucose responses from other sensors constructed by electropolymerization at other pHs. The GOx sensor constructed by electropolymerization at pH 1 showed no response to glucose, The relation between sensor film thickness and pH of the electropolymerizing solution was explained by Long et. al. Electropolymerization at lower pH (around 1) values produces thick (>1 μm) conducting PoPD films. Electropolymerization at higher pH (around pH 10) produces thin (<10 nm) nonconducting films.[37] According to Losito et. al.,

the conversion from a conducting polymer to a non-conducting one occurs around pH 5.[38] At higher pH (~pH 7), self-limiting thickness slows the growth due to a shut-down of current through non-conducting polymer film.

Film thickness calculations reported from Holdcroft and Funt indicate 0.178 μm films at pH 5.2 electropolymerization, and 0.133 μm films at pH 7.4.[39] For data in figure 2.9, the thinner film formed by electropolymerization at pH 7.4 probably entrapped less GOx, resulting in a lower sensitivity to glucose that the one constructed at pH 5.2. Electropolymerization at pH 5.2 provides for thicker film entrapping more GOx resulting in a higher sensitivity to glucose.

2.5.5 Effect of oxygen on the glucose responses of the sensor

"Oxygen-stress tests" were performed to determine the minimum oxygen concentration needed to ensure glucose-limited reactions at the enzyme site. The current from peroxide oxidation was measured as oxygen concentration was adjusted in a glucose solution over time. The oxygen stress test in Figure 2.10 shows an increase in the oxidation current to -2.0 μA at 3 minutes by increasing glucose concentration from 0 to3 mM glucose. Oxygen purging starting at 10 minutes resulted in a decrease in oxygen and oxidation current for peroxide. When oxygen was dropped to 3.5 ppm, the anodic current from peroxide oxidation started to fall (11 min). This means for this particular sensor's age and enzyme loading, 3.5 ppm oxygen is the minimum oxygen concentration required for 3 mM glucose, to be glucose-limited. As the oxygen concentration continued to fall, so did the peroxide oxidation current, reaching a minimum at 25 min. At this minimum oxygen value, the oxidation current was very close to the level where it was with 0 mM glucose, erroneously indicating that there is no glucose in the solution, when in fact it is known to be 3 mM. The salient point is that the current readings between 10 to 25 minutes would indicate less glucose than is actually present. When the enzymatic demand for oxygen is not met, the peroxide generated

becomes limited by oxygen, not glucose. At the 25th minute, the nitrogen purge was ended, and ambient oxygen was allowed to re-enter the solution. Between 25th and 60th minute, the oxidation current again increased with increase in oxygen concentration.

Figure 2.11 shows a comparison of the glucose responses of the same Pt/PoPD/GOx- sensor at ambient oxygen vs. over oxygen saturation from the air vs. additional oxygen from a tank respectively. With added oxygen, the linearity of the calibration curve was found between 0 to 8 mM. With only ambient oxygen present, the linearity was cut short to 4 mM, but additional oxygen increases the linear range to 8 mM. In addition, an increase in the sensitivity at the higher oxygen concentration was evident (5.10±0.32 from 3.57±0.01 μA/ mM-cm^2).

2.5.6 Sensitivity Changes over time

To determine changes in sensitivity, calibration curves were constructed over a period of 70 days, and when not in use the sensor was stored in 10 mM PBS at 4^o C. Changes in sensor's sensitivity over 70 days period is shown in Figure 2.12. The initial sensitivity of a Pt/PoPD/GOx after construction was 17.85± 0.64 μA/mM-cm^2 on day one. A 20% decrease in sensitivity was seen in the first fourteen days. Between day fourteen and day fifty-two the sensitivity was variable but shows a decrease by 33% from day 1. The sensitivity finally decreased by 60% after 52 days of storage. The Pt/PoPD/GOx sensors constructed showed to be moderately stable unlike those reported in the literature: Corcuera et. al. reported a decrease of about 60% in glucose response after 18 days.[31] Malitesta et. al. reported at least 10 days of shelf life.[17] Jing-Juan and Hong-Yuan reported their GOx sensor stability over 2 months.[40] FDA approved commercial CGM systems such as Medtronic, Dexcom, and Abott Navigator have the useful life ranging from 6 to 14 days with Eversense, manufactured by Senseonics Inc. ranging up to 90 days respectively when in use.[41, 42]

2.6 Conclusion

Out of the three construction techniques for glucose sensing using a GOx enzyme film on Pt electrodes, polypyrrole led to failed attempts in detecting glucose. Glutaraldehyde and poly o-phenylenediamine both detected glucose successfully. The poly o-phenylenediamine polymer and its associated sensor construction procedure were applied for further experiments. This was considered the preferential sensor construction technique providing longer operational life and higher sensitivities to glucose.

The sensor performance was optimized by using 500 U/ml of GOx enzyme, pH 5.2 acetate buffer during electropolymerization step, and use of 10 mM PBS during glucose response tests. Externally added oxygen to glucose solutions under ambient conditions, provided 1.5 times increase in sensitivity and a doubling of the linear dynamic range. Sensor stability studies showed a 20% decrease in sensitivity over the first fourteen days, a 33% decrease at fifty-two days, and a 60% decrease in sensitivity after 52 days of storage. These results are not unlike those found in the literature.

Perhaps the most complicated parameter in the enzymatic generation of hydrogen peroxide is the amount of oxygen available. The oxygen stress tests performed on the sensor electrode showed that if oxygen is limited with respect to glucose, false conclusions about the glucose concentration are made. GOx constructed sensors with high sensitivity to glucose have a much higher demand for oxygen than less sensitive ones. The sensitivity of the constructed sensor to glucose decreases over time, making the oxygen demand a variable.

2.7 Acknowledgments

The authors acknowledge financial support from the Arkansas Biosciences Institute, the major research component of the Arkansas Tobacco Settlement Proceeds Act of 2000. The authors are

also grateful to Dr. Julie Stenken's research group at the University of Arkansas for the 4-amino antipyrine used in this study.

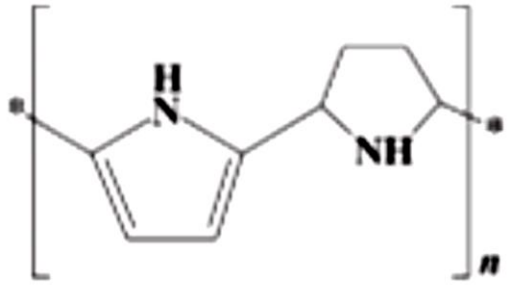

Figure 2.1 Molecular structure of polypyrrole. Picture obtained with permission from K. Deshmukh, M. B. Ahamed, R. Deshmukh, S. K. Pasha, P. Bhagat and K. Chidambaram, in Biopolymer composites in electronics, Elsevier, 2017, pp. 27-128. [43]

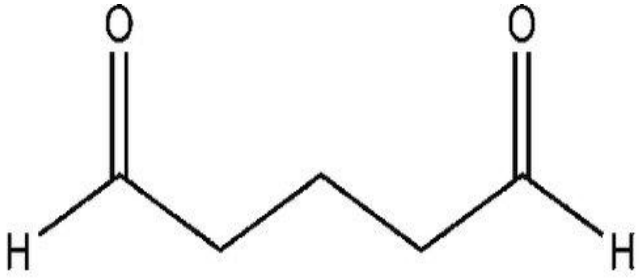

Figure 2.2 Molecular structure of glutaraldehyde. Picture obtained with permission from S. K. Sehmi, E. Allan, A. J. MacRobert and I. Parkin, Microbiologyopen, 2016, 5, 891-897.[44]

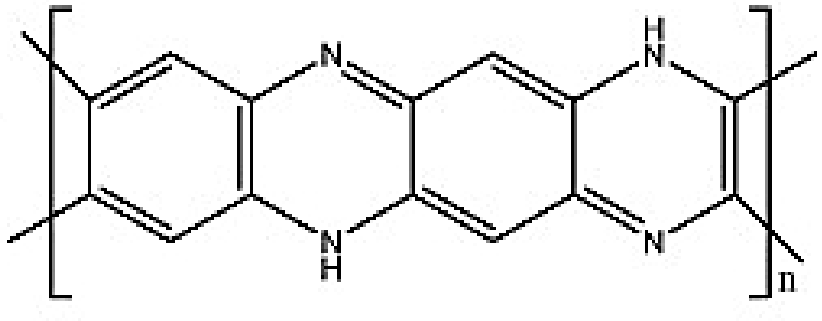

Figure 2.3 Molecular structure of poly o-phenylenediamine. Picture obtained with permission from P. Muthirulan, N. Kannan and M. Meenakshisundaram, Journal of advanced research, 2013, 4, 385-392 [45]

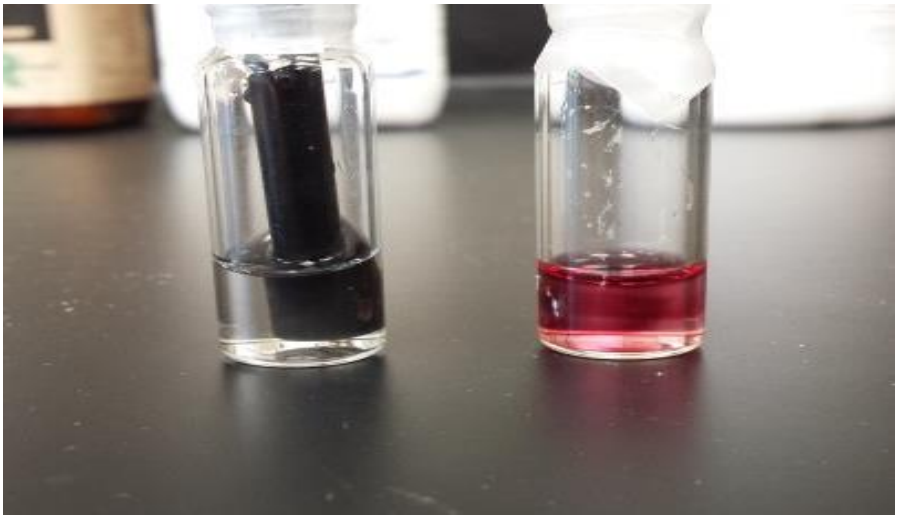

Figure 2.4 Colorimetric test results right after adding glucose: left vial- Ppy/GOx coated Pt electrode, right vial- known GOx solution.

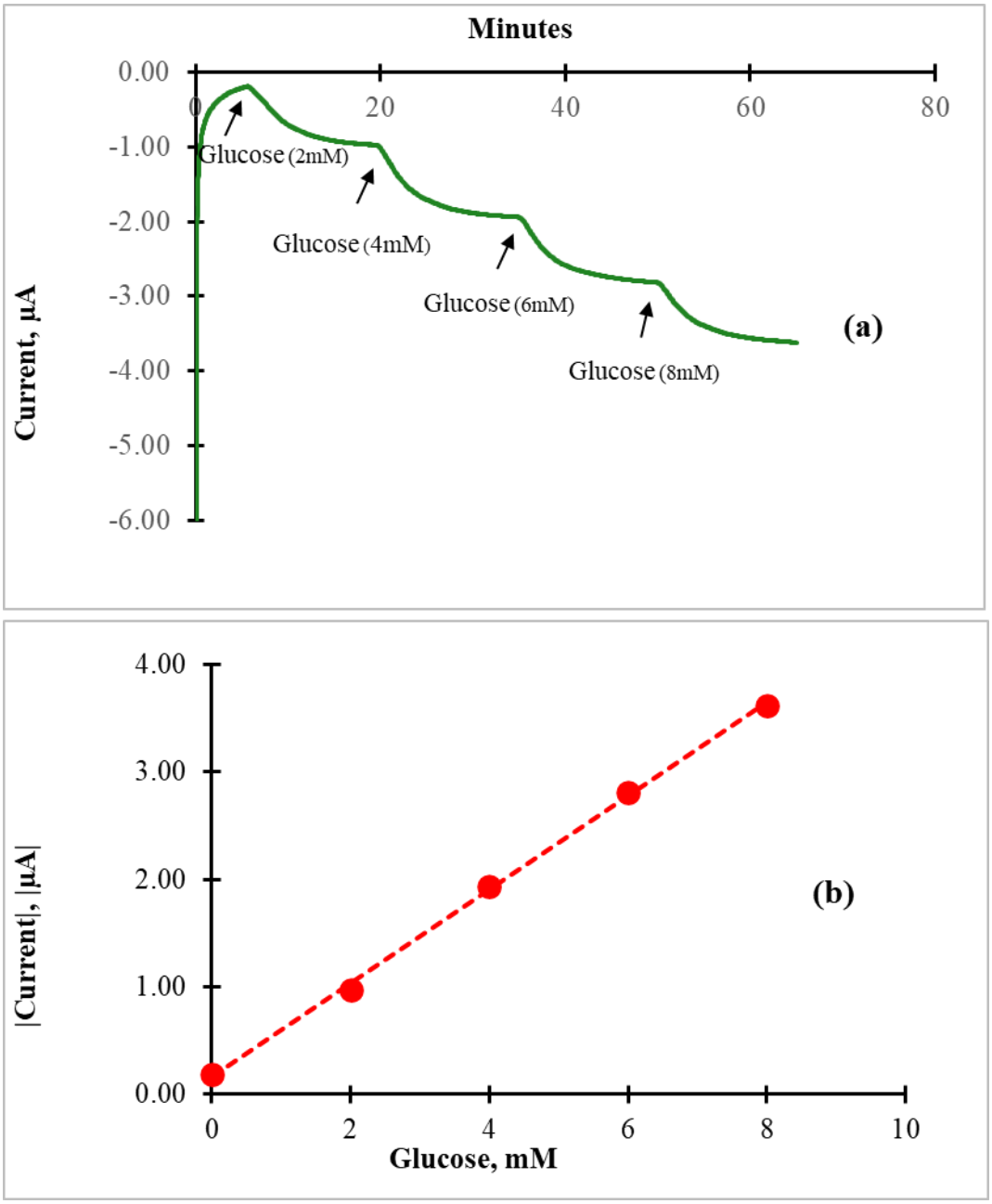

Figure 2.5 (a) 0-8 mM Glucose response and (b) corresponding glucose calibration curve where it leveled off for Glut-BSA-GOx coated platinum electrode taking current readings for each glucose concentration where it leveled off, just before adding the next one, n= 1. Sensitivity of the sensor electrode = 13.85±0.32 µA/mM-cm^2, R^2 (linearity)= 0.99 via line statistics function.

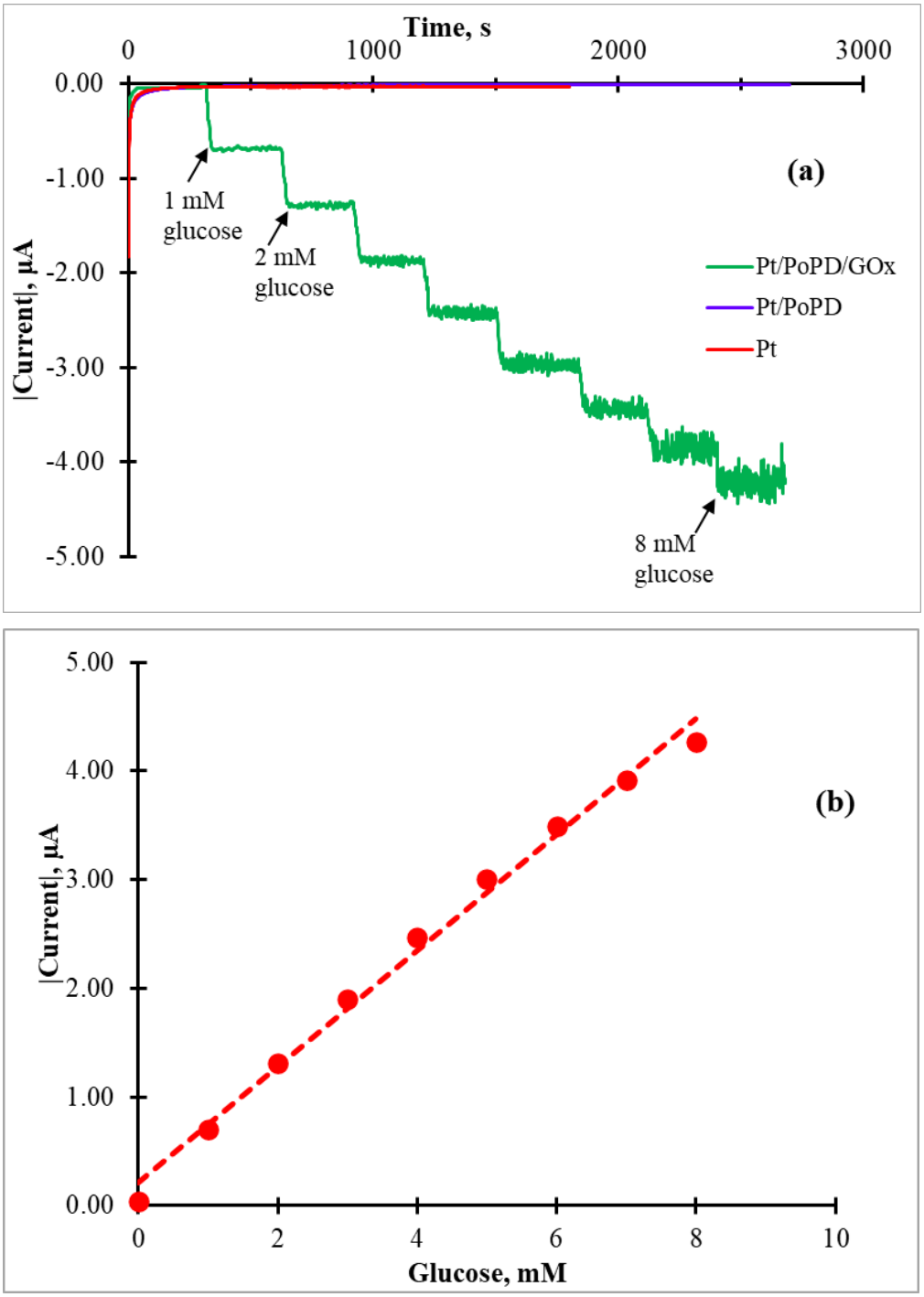

Figure 2.6 (a) 0-8 mM Glucose response for bare Pt electrode (red), Control PoPD coated electrode (blue) and PoPD/GOx electrode (green) and (b) corresponding glucose calibration curve for PoPD/GOx coated platinum electrode taking current readings for each glucose concentration where it leveled off, just before adding the next one, n= 1. Sensitivity of the sensor electrode= 17.00±0.54 µA/mM-cm^2, R^2 (linearity)= 0.99 via line statistics function.

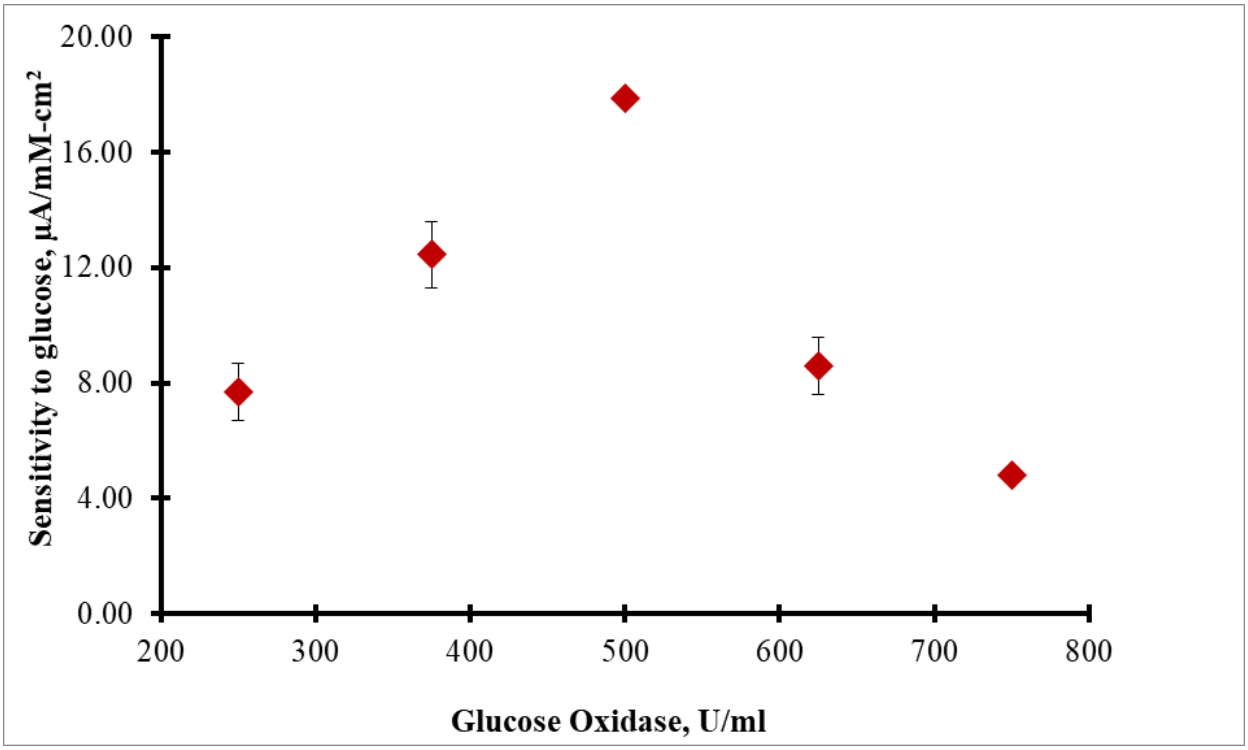

Figure 2.7 Glucose sensitivity of GOx enzyme electrodes Vs. GOx loading plot for 500 U/ml 625 U/ml, 750 U/ml, 375 U/ml, and 250 U/ml GOx showed sensitivity as 17.85± 0.64 µA/mM-cm^2 , 8.57± 0.96 µA/mM-cm^2, 4.81± 0.32 µA/mM-cm^2, 12.44± 0.96 µA/mM-cm^2, and 7.67± 0.96 µA/mM-cm^2 respectively. The plot shows gradual increase in sensitivity until 500 U/ml loading, peak at 500U/ml then decrease in sensitivity on higher GOx loading. Glucose sensitivities were taken as the slopes of glucose calibration curves for each enzyme loading.

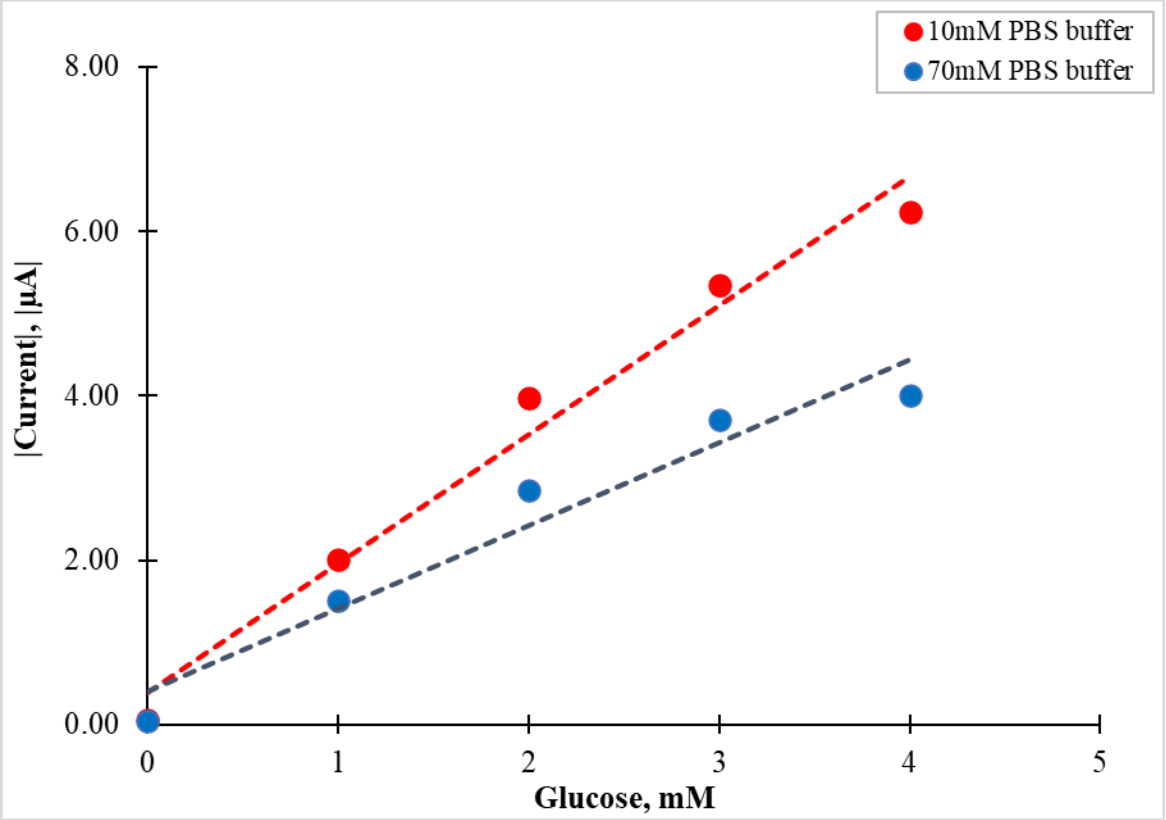

Figure 2.8 GOx enzyme calibration curves comparison for 0-4mM glucose solution in 10mM vs 70mM PBS. 10 mM PBS showed higher sensitivity (50 ± 4.5 µA/mM-cm^2) and linearity (0.98) for 0-4 mM glucose than the values obtained for 70 mM PBS (32.2± 4.5 µA/mM-cm^2 sensitivity and 0.95 linearity).

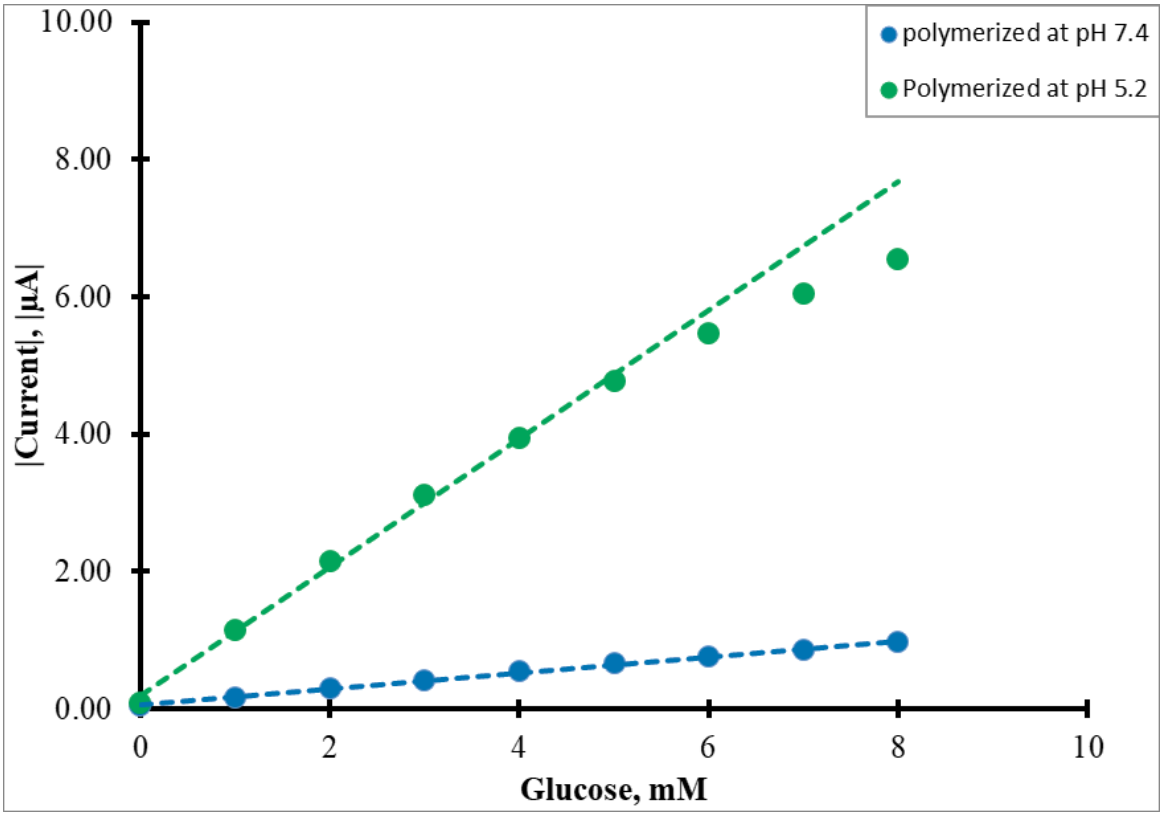

Figure 2.9 0-8mM glucose calibration curves obtained from Pt/PoPD/GOx electrode electropolymerized in pH 5.2 (green) vs. pH 7.4 (blue) buffer showed sensitivity as 29.81± 0.64 µA/mM-cm^2 and 3.71± 0.01 µA/mM-cm^2. pH 5.2 curve shows about 9 times higher sensitivity than pH 7.4 curve.

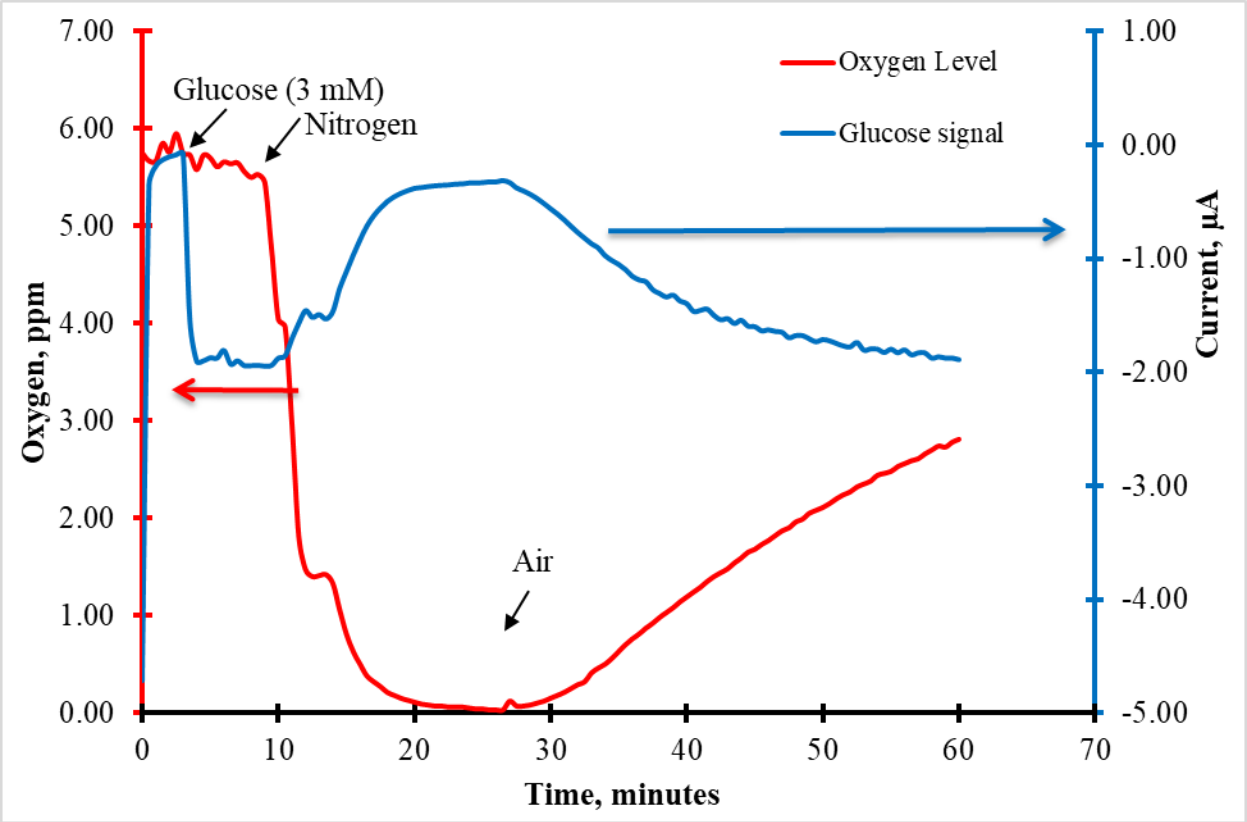

Figure 2.10 Oxygen stress experiment for 3 mM glucose showed oxygen limited signal at atmospheric condition by deviating from stable values the moment nitrogen flow started.

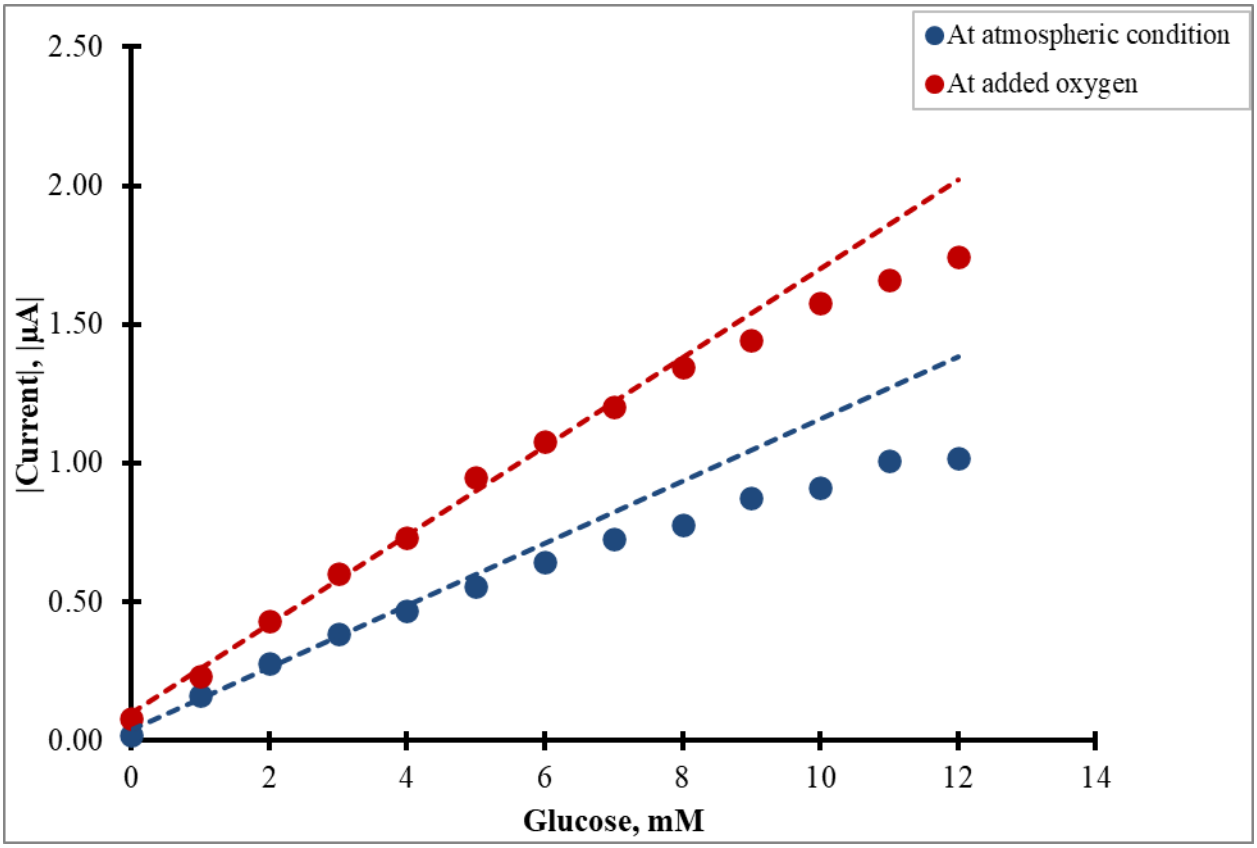

Figure 2.11 Calibration curves of GOx sensors for 0-12 mM glucose (a) at atmospheric condition (no added oxygen) showing lower sensitivity (5.10±0.32 µA/mM-cm^2)and linearity (0.99) only up to 4 mM glucose and (b) at the atmospheric condition and added oxygen flow during the experiment showing ~1.5 times higher sensitivity (3.57±0.01 µA/mM-cm^2) and linearity (0.99) up to 8 mM glucose.

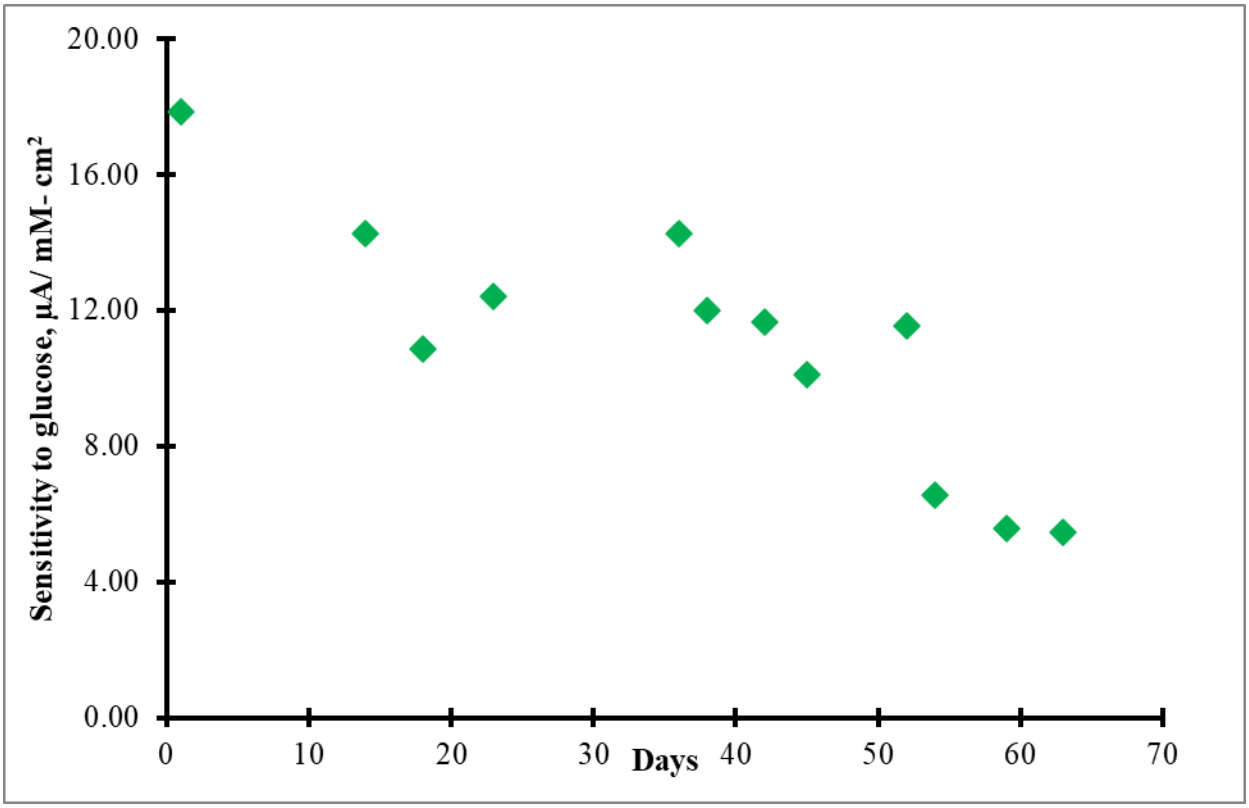

Figure 2.12 Sensitivity over time for a Pt/PoPD/GOx electrode. Sensitivity to glucose was observed to be 17.85±0.64 µA/mM-cm^2 on day one. About 20% decrease in the first fourteen days, and 33% decrease up to day fifty-two, resulting in a stable value over a long period of time, and finally 60% decrease after fifty-second day of storage. The sensor was stored in 10 mM PBS at 4ºC.

2.8 References

1. P. K. Nair, D. G. Buerk and J. H. Halsey Jr, *Stroke*, 1987, **18**, 616-622.

2. L. Wang, Y. Li, H. Han, G. Liu and P. G. Osborne, *Neuroscience letters*, 2003, **344**, 91-94.

3. W. M. Abi-Saab, D. G. Maggs, T. Jones, R. Jacob, V. Srihari, J. Thompson, D. Kerr, P. Leone, J. H. Krystal and D. D. Spencer, *Journal of Cerebral Blood Flow & Metabolism*, 2002, **22**, 271-279.

4. S. Vaddiraju, I. Tomazos, D. J. Burgess, F. C. Jain and F. Papadimitrakopoulos, *Biosensors and Bioelectronics*, 2010, **25**, 1553-1565.

5. R. A. Croce, S. Vaddiraju, F. Papadimitrakopoulos and F. C. Jain, *Sensors*, 2012, **12**, 13402-13416.

6. K. Arshak, V. Velusamy, O. Korostynska, K. Oliwa-Stasiak and C. Adley, *IEEE Sensors journal*, 2009, **9**, 1942-1951.

7. R. Ansari, *Journal of Chemistry*, 2006, **3**, 186-201.

8. A. Yussuf, M. Al-Saleh, S. Al-Enezi and G. Abraham, *International Journal of Polymer Science*, 2018, **2018**.

9. G. B. Street, S. E. Lindsey, A. I. Nazzal and K. J. Wynne, *Molecular Crystals and Liquid Crystals*, 1985, **118**, 137-148.

10. A. F. Diaz, J. I. Castillo, J. A. Logan and W.-Y. Lee, *Journal of electroanalytical Chemistry and Interfacial electrochemistry*, 1981, **129**, 115-132.

11. T. Zaharescu and S. Jipa, *e-Polymers*, 2008, **8**.

12. R. Balint, N. J. Cassidy and S. H. Cartmell, *Acta biomaterialia*, 2014, **10**, 2341-2353.

13. A. Guerrieri, G. E. De Benedetto, F. Palmisano and P. G. Zambonin, *Biosensors and Bioelectronics*, 1998, **13**, 103-112.

14. I. Migneault, C. Dartiguenave, M. J. Bertrand and K. C. Waldron, *Biotechniques*, 2004, **37**, 790-802.

15. O. Barbosa, C. Ortiz, Á. Berenguer-Murcia, R. Torres, R. C. Rodrigues and R. Fernandez-Lafuente, *Rsc Advances*, 2014, **4**, 1583-1600.

16. U. Olgun and M. Gülfen, *Reactive and Functional Polymers*, 2014, **77**, 23-29.

17. C. Malitesta, F. Palmisano, L. Torsi and P. G. Zambonin, *Analytical chemistry*, 1990, **62**, 2735-2740.

18. M. Trojanowicz, O. Geschke, T. K. vel Krawczyk and K. Cammann, *Sensors and Actuators B: Chemical*, 1995, **28**, 191-199.

19. K. Kojima, T. Yamauchi, M. Shimomura and S. Miyauchi, *Polymer*, 1998, **39**, 2079-2082.

20. S. Samanta, P. Roy and P. Kar, *Macromolecular Research*, 2016, **24**, 342-349.

21. Z. A. Jarjes, M. R. Samian and S. Ab Ghani, *Arabian Journal of Chemistry*, 2015, **8**, 726-731.

22. I. Losito, F. Palmisano and P. G. Zambonin, *Analytical Chemistry*, 2003, **75**, 4988-4995.

23. B. M. Dixon, J. P. Lowry and R. D O'Neill, *Journal of Neuroscience Methods*, 2002, **119**, 135-142.

24. G. S. Wilson and R. Gifford, *Biosensors and Bioelectronics*, 2005, **20**, 2388-2403.

25. Z. Tao, R. A. Raffel, A.-K. Souid and J. Goodisman, *Biophysical journal*, 2009, **96**, 2977-2988.

26. G. Fortier, E. Brassard and D. Belanger, *Biosensors and Bioelectronics*, 1990, **5**, 473-490.

27. O. A. Sadik, S. Brenda, P. Joasil and J. Lord, *Journal of chemical education*, 1999, **76**, 967.

28. N. C. Foulds and C. R. Lowe, *Journal of the Chemical Society, Faraday Transactions 1: Physical Chemistry in Condensed Phases*, 1986, **82**, 1259-1264.

29. S. Mamoru and H. Kazuyuki, *Clinica Chimica Acta*, 1977, **75**, 387-391.

30. J. R. Anusha, C. J. Raj, B.-B. Cho, A. T. Fleming, K.-H. Yu and B. C. Kim, *Sensors and Actuators B: Chemical*, 2015, **215**, 536-543.

31. J. I. R. De Corcuera, R. P. Cavalieri and J. R. Powers, *Journal of Electroanalytical Chemistry*, 2005, **575**, 229-241.

32. W. Schuhmann, *Sensors and Actuators B: Chemical*, 1991, **4**, 41-49.

33. R. K. Scopes, *e LS*, 2001.

34. G. A. El-Sherbeny, A. A. Shindia and Y. Sheriff, *Int J Agric Biol*, 2005, **7**, 953-958.

35. N. W. Barton, V. Lipovac and A. Rosenberg, *Journal of Biological Chemistry*, 1975, **250**, 8462-8466.

36. K. E. Toghill and R. G. Compton, *Int. J. Electrochem. Sci*, 2010, **5**, 1246-1301.

37. J. W. Long, C. P. Rhodes, A. L. Young and D. R. Rolison, *Nano Letters*, 2003, **3**, 1155-1161.

38. I. Losito, E. De Giglio, N. Cioffi and C. Malitesta, *Journal of Materials Chemistry*, 2001, **11**, 1812-1817.

39. S. Holdcroft and B. L. Funt, *Journal of electroanalytical chemistry and interfacial electrochemistry*, 1988, **240**, 89-103.

40. X. Jing-Juan and C. Hong-Yuan, *Analytical biochemistry*, 2000, **280**, 221-226.

41. A. P. F. Turner and R. Gifford, in *Autonomous Sensor Networks*, Springer, 2012, pp. 159-189.

42. J. I. Joseph, *Journal of diabetes science and technology*, 2021, **15**, 167-173.

43. K. Deshmukh, M. B. Ahamed, R. Deshmukh, S. K. Pasha, P. Bhagat and K. Chidambaram, in *Biopolymer composites in electronics*, Elsevier, 2017, pp. 27-128.

44. S. K. Sehmi, E. Allan, A. J. MacRobert and I. Parkin, *Microbiologyopen*, 2016, **5**, 891-897.

45. P. Muthirulan, N. Kannan and M. Meenakshisundaram, *Journal of advanced research*, 2013, **4**, 385-392.

3. Microelectrode Arrays Fabrication and Investigating Constituent Metal Property Effects on Microelectrode's Sustainability Towards OER Potential

3.1 Abstract

Single electrodes used for in-vivo implantation are held at electrical potentials that can change their morphological and electrochemical characteristics. Microfabricated electrodes are now being used for such purposes, and this work describes the durability and surface changes undergone when exposed to positive electrical potentials. Microelectrode arrays (MEA) composed of sixteen interdigitated micro-bands (25 µm width x 2 mm length each with 25 µm inter-band gap) were constructed using combinations of adhesion/conduction metals: Cr/ Au, Ti/ Au, and Ti/ Pt. Selected microband surfaces were plated with Pt black or Pt and then subjected to oxygen evolution reaction (OER) voltage. The electrodes' ability to withstand the oxygen evolution reaction potential at neutral pH was determined, and the chemical and morphological changes of the constituent metals were evaluated. The Cr/Au electrodes failed after 40 seconds at OER voltage +1.4 V (vs Ag/AgCl), whereas Ti/Pt metallization showed no sign of failure after 1200 seconds. The other metal combination failed at times between these two extremes. The results revealed that the adhesion layer plays a substantial role in performance at OER voltage largely depending upon diffusion of the adhesion layer into the conduction metal.

3.2 Introduction

Clark electrodes are calibrated using oxygenated solutions of known concentration and measuring the resulting current. The electrode becomes uncalibrated when the membrane covering the electrode, becomes fouled by components in the environment. In a previous work possibility of using two working electrodes to calibrate an oxygen sensor in situ has been demonstrated.[1] One of the electrodes is poised to a sufficient positive potential to electrolyze water to oxygen-- the generator electrode (GE)-

$O_2 + 4H^+ + 4e \rightarrow 2H_2O$, $E^o = +1.23V$ vs NHE (1)

A second electrode in close proximity acts as a Clark-type oxygen sensor determining oxygen amperometrically-- the oxygen detector electrode (DE). The advantage of in situ calibration is that the electrode does not have to be removed for calibration. This would be especially important in applications where oxygen was being determined in hazardous environments, or in vivo such as sensing brain oxygen.[2-11] All that is needed for calibration is a known change in concentration and the change in response that results. The two electrodes work together to accomplish this using two modes of operation: calibration and sensing. In sensing-mode, the GE is left open-circuit and the DE records the oxygen concentration i.e. no different than standard use. In calibration-mode, the GE poised at OER voltage to generate oxygen for several seconds, generating a known flux of oxygen. The increase in oxygen is seen as an increase in current at the DE. From these data changes in the sensor, sensitivity can be determined and tracked.

The previous work was done using bulky macroelectrodes, a polymer-covered 2 mm diameter gold electrode for the oxygen sensor, and a glassy carbon or Pt for the oxygen generator placed 0.5 mm away.[1] The advantages of transferring the method to a microelectrode array (MEA) are manifold. Less time is needed for oxygen to diffuse from the oxygen-generating to the detecting

microelectode due to the micrometer distances between the electrodes. The generated oxygen concentration increase at the sensor quickly reaches a steady-state, meaning that the generator could have a shorter duty cycle, causing less wear on the electrode and minimizing the generation of possibly unwanted oxidation products. This would be especially advantageous for in vivo applications. Unlike macroelectrodes, the small size of the MEAs with low background and charging currents provide high current densities.[12-14] Smaller currents result in lower iR drop, and steady-state diffusion currents making the microelectrode a favorable choice for in vivo analytical and physiological applications. In addition, the members of the electrode array can be made individually addressable, which is a requirement for the in situ calibration method.[15-19]

Oxygen evolution reaction (OER) occurs at high positive potentials and plays a crucial role in the above applications, as well as in fuel cells, metal-air batteries, and water splitting.[20-24] From a thermodynamic standpoint under standard conditions at applied voltages positive of E^o, water will split into oxygen (equation 1); negative of E^o, oxygen will be reduced to water. In practice the OER mechanism is complicated and the magnitude of the resulting current depends upon the applied potential, the pH of the solution, the electron-transfer kinetics, and the history of the electrode. The OER has been well studied in extreme acidic and alkaline solutions, but little studied at physiological pH. The stepwise mechanism of the OER changes with the composition of the electrode material. Gencoglu and Minerick studied the changes in morphology and compositional changes for single micro platinum electrodes after prolonged exposure to both AC and DC potentials between 1 to 6 volts.[23] As for the MEA, Pt has been electrodeposited over chromium/gold thin films coated onto a polyimide substrate and subjected to square wave galvanic pulses from +(-) 0.5 mA, but no chemical or microscopic analysis was done.[25] In the case of photolithographically fabricated microelectrodes, the situation is quite different. Instead of dealing

with a single substrate, microlithographic fabrication in most cases requires at least one adhesion layer and one overcoating metal to serve as the electrode. Due to their availability, microelectrode arrays are now starting to be used in neurological applications.[26] Our first attempts to transfer the oxygen in situ calibration method to microband electrodes met with complete oxidation of the generating electrode. The construction of the generator electrode was platinum electroplated over a microfabricated gold electrode. This led us to a more complete study of microfabricated electrode degradation at a high positive potential. Most previous studies focused on bulk electrodes determining how, and possibly why chemical and physical changes occur under various chemical and electrochemical conditions.[27-31] The corrosion of bulk titanium has been extensively studied as this material is used in prosthetic implants.[32] These studies also point out that it is nearly impossible to study metallic corrosion in vivo, but in vitro studies can still be valid and worthwhile, as corrosion and repassivation rates can be determined. In fact, all of the corrosion studies of in vivo electrodes have been done on the bench-top under physiological pH, as in the case of tungsten microelectrodes.[33] Historically, platinum needles are the most commonly used electrodes for neuro-stimulation, in electrokinetic and microdevice applications, and as such, they are exposed to high voltage. To the authors' knowledge, no reports on the topology and chemical composition of MEA micro-band electrodes after exposure to potentials within the range of OER potentials have appeared.

The point of this paper is to report the changes in microelectrode materials at applied potentials in the OER range. MEAs were fabricated via microphotolithography and three different electrode constructions: chromium/gold (Cr/Au), titanium/ gold (Ti/Au), and titanium/platinum (Ti/Pt) were used. The first metal in the combo serves as an adhesion layer to the silicon wafer; the second as the conduction material. As an option, the fabricated bands were also electroplated with Pt or Pt-

black to test the performance of these coatings at OER potential for up to 1200 s time. The reason behind selecting 1200 s time duration was to observe if the electrodes when applied as self-calibrating oxygen sensors, can successfully generate oxygen up to the duration of the average life of in vivo implantable oxygen sensor which is limited due to the body's response.[34] The action of the generator electrode can produce a steady-state level of oxygen at the adjacent sensing electrode in about 1 second. Generating oxygen once every 15 min and for 1 second or on for 96 s/day, thus a total of at 1200 s for up to at least 12 days of operational life. Changes to the metals during the electrode's OER operational life and performance were evaluated by cyclic voltammetry (CV) and chronoamperometry. Microscopy, scanning electron microscopy (SEM), energy-dispersive X-ray spectroscopy (EDX), and optical LASER surface profiling examined the morphological changes.

3.3 Materials and methods

3.3.1 Instruments and reagents

Fabrication of the electrode arrays was completed in the cleanroom at the University of Arkansas High Density Electronics Center (HiDEC) facilities. The fabricated microband electrodes were platinum plated with either YSI 3140 platinizing solution (Yellow Springs Instruments, OH, USA), a mixture that includes lead acetate, or a solution of chloroplatinic acid solution (Sigma Aldrich, USA) containing only platinum. Cyclic voltammetry, linear sweep voltammetry (LSV), and chronoamperometry were performed using CHI potentiostat 1030A or CHI 750A (CH Instruments, Austin TX, USA). All applied potentials are referenced to an Ag/AgCl in saturated KCl electrode, with a platinum counter electrode. Electrochemical experiments were performed in 10mM phosphate buffer saline (pH= 7.4) (PBS) prepared by dissolving one PBS tablet (EMD Millipore Corp., Massachusetts, USA) into one liter of HPLC grade water (EMD Millipore Corp) at room temperature. The pH of the buffers was verified by

the Schott Instruments pH meter (SI analytics). A Leica DM 2500M microscope was used to check the microband electrodes for imperfections. Surface analysis was done using an FEI Nova Nanolab 200 FIB/SEM (FEI, Oregon. USA) enabled with EDX using a 5keV electron beam on the Ti/Au electrodes, and 15 keV on the Ti/Pt electrodes. Microband electrode images and thickness profiles were captured using a Keyence VK Viewer V2.8 VK-H1XV2E (Keyence Corporation of America, Illinois, USA) with Analysis Application V1.2 VK-H1XME. Imaging processing was accomplished using the Keyence Multi-File software.

3.3.2 Fabrication of MEAs

The substrate, P-type (Boron) prime grade silicon wafers (125 mm diameter, <1-0-0> orientation, 1-5 Ω-cm resistivity, 600-650 µm thickness, front side polished, and backside etched, 2 µm ±5% thermal oxide on both sides), were purchased from Silicon Quest International (San Jose, CA). The microelectrode array (MEA) consisted of 16 interdigitated microband electrodes 2mm long, 25 µm wide with a 25 µm gap between adjacent bands (Figure 3.1). The electrode array pattern with the associated leads to an edge connector was drawn using AutoCAD software such that twelve 2.5 cm x 2.5 cm MEA chips could be patterned onto a single wafer. The pattern was imprinted on Mylar masks by Fine Line Imaging (Colorado Springs, CO). A visual inspection was done under a microscope to verify both completeness and clean, sharp edges with no contacts between two adjacent electrodes. Dicing of the wafer was followed, providing twelve microelectrode arrays. The MEAs were O_2-plasma cleaned using a PDC-32G Harrick plasma cleaner (Harrick Scientific, Ithaca, New York, USA) before use. 24 Cr/Au, 12 Ti/Au, and 12 Ti/Pt MEAs were fabricated in total, of which one MEA of each type was selected for experimental studies after passing the microscopic observation and connection test. The MEA, connection wires, and edge connector (Sullins RBB20DHHN) are

shown in figure 3.1. The wafer is thinner than the standard thickness of a circuit card, so a shim was placed behind the chip to ensure contact. Details concerning the materials and fabrication of MEAs are discussed in the appendix section of the dissertation.

3.3.3 Microelectrode samples preparation

In addition to unmodified microband electrodes, two types of platinum-coated electrodes: Pt black coated (Pt_b), and Pt coated (Pt) microelectrodes were prepared on each of the three types of MEA. Nine different microelectrode samples were prepared for experiments: three unmodified bands with designations given as Cr/Au, Ti/Au, and Ti/Pt, and six coated bands designated as Cr/Au/Pt_b, Cr/Au/Pt, Ti/Au/Pt_b, Ti/Au/Pt, Ti/Pt/Pt_b, and Ti/Pt/Pt. The Pt_b was electrochemically plated from YSI 3140 platinizing solution amperometrically at −1.0 V vs. satd. Ag/AgCl for 60 seconds and then repeated to ensure uniform coating. Microscopic observation verified the uniformness of the coating. Platinization with Pt was completed from chloroplatinic acid solution by applying −0.1V vs. Ag/AgCl for 5 seconds repeating two additional times. The chloroplatinic acid solution was prepared in the lab from 20 mM potassium tetrachloroplatinate(II) in 1M perchloric acid.[35] The Pt_b and Pt coated bands appeared as black and gray color respectively under the microscope. A schematic of the coated electrodes over the gold MEA is shown in Figure 3.2.

3.4 Experimental

3.4.1 Cyclic voltammetry experiments

Functionality test

To confirm electrical continuity between the potentiostat and the microelectrode as well as the functionality of the platinized microelectrode, cyclic voltammetry of the ferricyanide/ferrocyanide redox couple was performed between 0.5V and -0.2V (vs. Ag/AgCl) at 50mV/s scan rate using 5mM potassium ferricyanide in 0.1 M KCl in (Fisher Scientific Company, New Jersey, USA).

Oxygen generate-detect Experiment

To verify oxygen generation from water at unmodified platinum or modified (both Pt_b and Pt modified) gold and platinum microelectrodes, addressed as generator microelectrode (GME), linear sweep voltammetry (LSV) was performed between 0V to −1 V vs. Ag/AgCl at 100 mV/s scan rate at an adjacent unmodified band electrode 25 µm away from the GME, addressed as the detector microelectrode (DME), once when the GME was at open circuit potential and again when GME was at +1.4 V (vs Ag/AgCl).

3.5 OER potential sustainability

To test the sustainability of the different GMEs for continuous OER, the electrodes were subjected to a total of 150 potential steps of 8 seconds each (three sets of 50 cycles each) from 0 V to 1.4 V in 0.01M PBS (pH 7.4, unstirred) for a total of 1200 seconds.

3.5.1 SEM/EDX

SEM provided high-resolution images of the electrode's surface (Figure 3.10), while EDX (Figure 3.11) provided quantitative information about the composition of the constituent elements in terms of unnormalized concentration in weight percentage of the elements, normalized concentration in weight percentage of the elements (to make a sum of unity), and atomic weight percentage, and error in the weight percent concentration. SEM images of the Cr/Au MEA bands were taken before and after being subjected to OER potentials. Due to the failure of the Cr/Au during oxygen generate-detect experiments, the possibility of their compositional analysis was negated. The Ti/Au and Ti/Pt electrodes survived OER potential exposures and were subjected to SEM/EDX analysis before and after chronoamperometric sustainability tests.

3.5.2 Surface profiling by 3D LASER scanning microscopy

3D LASER surface profiling was performed to observe the changes in the surface morphology of the microband electrodes (thickness and surface roughness) as a result of OER potential exposures. The thickness measurements were performed at 50x magnification and the surface roughness measurements were performed at 150x magnification.

3.6 Results and Discussion

3.6.1 Cyclic voltammetric experiments

Functionality test

Figure 3.3 shows ferricyanide/ferrocyanide redox CV of a functioning and a non-functioning Ti/Pt microband electrode verifying the electrical continuity between the potentiostat and the microelectrode. For the functioning CV, reduction and oxidation peak potentials were seen at 0.22V and 0.33V respectively, whereas no such response was seen for the non-functioning CV due to non-conductivity. The presence of non-functioning bands can be due to discontinuity in the bands caused during the microfabrication procedure, or due to edge connector connection problem. These functionality tests were done first before proceeding to any experiments.

Oxygen generate-detect experiment

Figure 3.4 shows two linear sweep voltammetric traces at the Cr/Au DME with the Cr/Au/Pt_b GME once at open circuit potential, and then at a fixed potential of +1.4 V vs satd. Ag/AgCl. The solution was not purged, so the oxygen reduction wave with the generator open circuit is the result of the endogenous oxygen found in the solution. When the generator is energized, the oxygen reduction current increased 2.5 times higher than when the generator was at an open circuit. This increase in reduction current provided the evidence that OER was occurring at the Cr/Au/Pt-black band. Oxygen reduction was observed to peak at ~ −0.60 V for a DME on Cr/Au or Ti/Au

microband, and ~ −0.4V for Ti/Pt DME, in 0.01M PBS buffer (pH= 7.4). It was during these experiments that the failure of some of the GMEs was noticed while being exposed to OER potential. This led to the more in-depth study of the stability of microband electrodes held at oxidizing potentials.

Production of O_2 is given by:

$2H_2O \rightarrow O_2 + 4H^+ + 4e^-$

From Figure 3.4 the dotted line shows the reduction of oxygen at -0.6V (vs Ag/AgCl) at a microband 25 μm away from the action of the generator poised at +1.4 V. The action of the generator results in an increase in oxygen reduction at the adjacent electrode by 2 μA, which would include the collection efficiency for oxygen. The rate of arrival of oxygen at the neighboring electrode can be calculated from the current seen and Faraday's law.

$$\frac{1\ mole\ O_2}{4\ eq}\frac{1\ eq}{96500\ coul}\frac{2\ X\ 10^{-6}\ coul}{s} = 5\ \frac{pmol\ O_2}{s}$$

The rate of oxygen consumption can be estimated from the linear portion of the enzyme electrode which occurs at low glucose concentrations where oxygen is known to be in excess. From figure 4.5B, 100 nA is a typical current, for 2 mM oxygen.

$H_2O_2 + 2\ e^- \rightarrow 2H_2O$

$$\frac{1\ mole\ O_2}{2\ eq}\frac{1\ eq}{96500\ coul}\frac{100\ X\ 10^{-9}\ coul}{s} = 0.05\ \frac{pmol\ O_2}{s}$$

This calculation was made for 2 mM glucose. Oxygen production from the generator is 100X what is needed to achieve excess oxygen for this amount of glucose. Assuming the demand for oxygen is linear the maximum amount of glucose measured with excess oxygen from the generator is predicted to be 200 mM. This estimate assumes that oxygen/peroxide delivery/consumption is

not limited by diffusion through electrode films. Rates of diffusion through films did prove to be a factor as will be pointed out later in chapter 4.

3.6.2 Sustainability Studies

Cr/Au GMEs

The oxygen generating microelectrodes electroplated with Pt black or Pt constructed over the Cr/Au MEAs proved to be short-lived; less than 40 seconds upon application of the OER potential. Microscopy revealed partial disappearance of the Pt-black coated band, Figure 3.5(b), and complete disappearance of the Pt coated Cr/Au band, Figure 3.5(d) when poised at the OER potential (+1.4V vs. Ag/AgCl). No further testing could be done on the electrodes made with Cr/Au combination of metals. One obvious problem is gold dissolution due to oxidation occurring negative of +1.5 V vs. NHE.[36, 37] Also, it has been reported in the literature that the Cr adhesion layer can diffuse through the gold over-layer, where it is more easily oxidized than the noble metal.[38, 39] Leaching of the chromium to the surface provides openings for electrolyte solution to penetrate through the pores or pinholes which accelerates dissolution. Loss of the chromium adhesion layer would account for the disappearance of the whole microband. This was found to be due to Cr diffusion into the Au resulting in surface cracks.[40-43] Others have also reported the same that at anodic potentials (+1.6V vs. SCE) Cr/Au failed due to the anodic dissolution of Cr diffusing through gold and arriving at the surface of the electrode.[44] The coating of platinization layer provides some protection but has minimal effect on the diffusion of Cr through gold.

Ti/Au GMEs

Unlike the Cr/Au MEA, the construction of the Ti/Au MEAs remained undamaged and fully functional after 100 seconds at the OER potential (data not shown). Unlike the platinum-coated Cr/Au generator electrodes, no visible change was observed at the platinum-coated Ti/Au

generator electrodes after a minimum of five scans at OER potential (Figure 3.6). The superiority of the titanium under-layer at OER potential was previously noted by Hoogvilet and Van Bennekom performing electrochemical quartz crystal microbalance (EQCM) studies that allowed them to determine the mass loss of both types of adhesion layers.[44] Rigorous testing of the microbands continued with repetitive potential step chronoamperometry to the OER potential. The results in Figure 3.7 (a-c) show that the Ti/Au/Pt_b electrode failed after 960 seconds (120 steps), the OER current dropping to near zero (Figure 3.7c). The Ti/Au/Pt electrode sustained longer at OER potential than the Pt_b microband (Figure 3.7d-f), completing all 150 cycles (1200 seconds). Pt_b deposition was found to be weakly bonded to the gold compared to the Pt because most of the Pt_b coated layer could be removed easily by light scraping, but the Pt coatings could not. Although Ti/Au couple outperforms the Cr/Au couple, it is possible that the Ti/Au would eventually fail since the passivated Ti adhesion layer eventually degrades.[38, 40] The platinizing solution used for the Pt black platinization contains lead (Pb) as one of the ingredients. Platinization is most widely applied on platinum electrodes whereas in this case Platinization on a gold surface was applied.[41] Adsorption of Pb at the Pt black coated electrode was confirmed by SEM/EDX analysis data (Table 3.1). The presence of Pb promotes the Pt_b coating, but its oxidation (+0.13V vs. SHE) may cause the Pt_b to fail earlier than the Pt coated band. It has been reported that Pb creates a "sink" for gold, gold diffusing to the Pb to form an Au-Pb intermetallic compound.[39] Thus, Pb and its interaction with Au might also be responsible for the early failure of the Pt_b electrode at OER potential.

Ti/Pt GMEs

Ti/Pt MEAs showed the highest sustainability, lasting longer at OER potential than either the Cr/Au or Ti/Au electrodes regardless of additional overlayers. Bare (unmodified surface) Ti/Pt or modified (coated with Pt_b or Pt) completed all 150 potential steps to the OER potential with no

decrease in the OER current level. (Figure 3.8). Of the three, the Pt_b coated generator showed the highest anodic and cathodic current responses, which was probably due to its higher surface area. As pointed out previously, Ti is better adhesion metal than Cr, at least in this application. The combination of titanium and platinum is much more durable at high anodic potential compared to Cr/Au or the Ti/Au combination. The results show that unlike the Ti/Au/Pt-black at OER potential, the Ti/Pt/Pt-black generator was not affected by the presence of Pb. Pb is known to diffuse through the Pt metallization layer, but unlike with Au, it does not form an intermetallic with Pt, only ends-up at the Si-SiO_2 surface of the wafer.[45]

3.6.3 SEM/EDX

The SEM images of the Cr/Au generator electrodes before and after being subjected to OER potential are shown in Figure 3.9. Figure 3.9(b) shows that no traces of Au or the underlying Cr metal layer after applying the OER potential. A few fragments of the displaced microbands can be observed, adhering to the insulating layer of the MEA (middle and bottom inset of figure 3.9(b)). The existence of the displaced fragments indicates that only portions of the underlayer underwent dissolution during this experiment. Because the Cr/Au bands were destroyed, surface analysis comparison of before and after voltage application was impossible. Unlike Cr/Au MEA samples, the Ti/Au and Ti/Pt constructions were able to withstand the OER sustainability testing. SEM images of these two MEA electrode samples were shown in Figure 3.10. The uncoated electrodes (Figure 3.10(a) and (d)) were used for comparison. The torn edges of the Ti/Pt band were caused by the undercutting during the etching process in fabrication.

SEM of the Pt-black coated electrodes showed heavy and thick deposition of granular Pt_b (Figure 3.10(b) and (e)), whereas the chloroplatinic acid produced a flat and smooth Pt deposition. Pt_b and Pt deposition on the Au surface (Figure 3.10(b) and (c)) appeared to be denser than deposition on

the Pt surface (Figure 3.10(e) and (f)). This observation was supported later by the surface profiling measurement. No visible differences were seen in the SEM images of the Ti/Pt and Ti/Au constructions before and after (not shown) exposure to the OER potential for 1200 s (Figure 3.10(b),(c), (e), and (f)).

A representative EDX of a microband electrode after OER potentials is shown in Figure 3.11. It provides quantitative information about the composition of the constituent elements in terms of unnormalized concentration in weight percentage of the elements, normalized concentration in weight percentage of the elements (to make a sum of unity), atomic weight percentage, and error in the weight percent concentration. The normalized wt% of the elements obtained by EDX before and after exposure to OER potential can be found in Table 3.1. The percentages do not add up to 100% because wt% C, Si, and O are not included. Electrodes with a Pt_b coating showed a Pb peak, (Pb detection was not done for the Ti/Au/Pt_b generator after exposure to the OER potential). There was a decrease in the normalized wt% of Ti of the Pt or Pt black coated Ti/Au electrodes by a factor of more than two, after exposure to OER potential. Whereas the Ti% remained unchanged in the Ti/Pt electrodes, coated or not. Although Ti diffuses through both Pt and Au along grain boundaries, the diffusion through gold works differently at oxidizing potentials than diffusion through Pt.[46-48] In oxygen-rich conditions, Ti diffuses through the Au layer to the free surface, oxidizing in a channel for further interdiffusion until all the Ti source is consumed. In the Ti/Pt couple, multiple diffusion and reaction processes compete together: interdiffusion of Ti and Pt, diffusion of oxygen through Pt, and oxidation of Ti near Ti-Pt interface. Due to a faster rate of Ti oxidation than the Ti-Pt reaction, a continuous layer of titanium oxide forms near the Ti-Pt interface which restricts further oxidation of Ti and provides an unreacted Pt layer on top. Thus,

the oxygen-rich condition at the OER potential increases diffusion in the Ti/Au couple resulting in a decrease in the normalized Ti%, but it limits diffusion in the Ti/Pt couple resulting in no significant change in the normalized Ti%.

Table 3.1: EDX data showing Normalized wt% of the elements present at the generators before and after the longevity test (Only metallic elements are shown)

Generator electrode	Normalized wt% before OER potential application	Normalized wt% after OER potential application
Ti/Au/Pt black	Ti= 12.81 Au= 7.70 Pt = 54.79 Pb= 1.61	Ti=3.78 Au=10.20 Pt=75.74 Pb= x
Ti/Au/Pt	Ti= 11.98 Au= 8.83 Pt= 69.72	Ti= 5.39 Au= 11.51 Pt= 71.21
Ti/Pt	Ti= 0.85 Pt= 72.79	Ti= 0.89 Pt= 7 2.67
Ti/Pt/Pt black	Ti= 0.09 Pt= 79.98 Pb= 1.28	Ti= 0.08 Pt= 79.93 Pb= 1.42
Ti/Pt/Pt	Ti= 0.12 Pt= 78.14	Ti= 0.16 Pt= 76.76

3.7 Surface Morphology Studies

Thickness profiling of the microband electrodes was performed using 50x magnification and surface roughness was measured within 60µm x 20µm selection area with a 150x magnification. Thickness and surface roughness measurements of the unmodified electrodes (for reference), as well as the modified electrodes, were recorded. A comparative study of the thickness and RMS surface roughness of the sample electrodes is shown in Table 3.2.

Table 3.2: Measured thickness and RMS surface roughness of the electrodes prepared on Cr/Au, Ti/Au, and Ti/Pt MEAs

Sample Specification	Thickness, µm	Surface roughness RMS, µm
Cr/Au	1.460	0.023
Cr/Au/Pt black	2.667 (top layer, Ptb ~1.207)	0.154
Cr/Au/Pt	1.640 (top layer, Pt ~0.18)	0.045
Ti/Au	1.877	0.022
Ti/Au/Pt black	3.813 (top layer, Ptb ~1.936)	0.466
Ti/Au/Pt	2.059 (top layer, Pt ~0.182)	0.096
Ti/Pt	1.472	0.031
Ti/Pt/Pt black	2.214 (top layer, Ptb ~0.742)	0.239
Ti/Pt/Pt	1.534 (top layer, Pt ~0.062)	0.035

From Table 3.2, it is evident that Ti/Au/Pt_b had the maximum thickness and RMS surface roughness of all the samples. Taken the value of unmodified Ti/Au thickness as a reference, then the thickness of the deposited Pt black was (3.813-1.877=1.936 µm) almost 2 µm thick. This magnitude of Pt_b loading was only observed in Ti/Au MEA samples. The Cr/Au and Ti/Pt MEAs had a thinner coating of Pt_b, 1.458 µm, and 0.742 µm respectively. Following the same trend, the thickness of the Pt coating was also maximized on Ti/Au construction. It has been reported earlier that in multilayer systems, the performance of the top layer depends greatly on the underlying

layers and the interaction between them.[38, 44, 49-51] Under the same conditions and process parameters, the maximum thickness of Pt_b or Pt deposition was obtained on the Ti/Au construction rather than the other two electrode underlayers. This can be attributed to the interaction and interfacial compound formation between the adhesion and the conduction layer.[39] The continuous diffusion and oxidation of Ti in the Au conduction layer and formation of intermetallic compounds made the electrode surface favorable for the electrodeposition of an additional metal layer whereas for the Ti/Pt metallization, the limited diffusion of Ti near the Ti-Pt interface may be responsible why less Pt black and Pt deposition was observed. The SEM images of the Ti/Au, Ti/Au/Pt_b, and Ti/Au/Pt (Figure 3.10) showed grainy cluster-like deposition of Pt_b whereas Pt deposition had a smooth texture.

3.8 Conclusion

The application of microfabricated devices to in vivo sensing[52], as well as a multiplexed evaluation of extracellular potentials for the determination of neurotoxicity of toxic substances[53], are just two examples of how MEAs have impacted electroanalysis. MEAs are finding more and more in vivo applications recording multiple electrical responses in tissues from chemical stimuli.[15-19] Electrode arrays have also been used to stimulate engineered muscle tissues and were found to perform better than individual electrodes.[54] An electrode array composed of indium tin oxide (ITO) band electrodes have been fabricated and used as a bioreactor to stimulate cell proliferation.[55] Neurological electrical stimulation continues to be an active area of research.[56] A significant effort has been directed toward the biocompatibility of metal implants. Works on metallic corrosion under physiological conditions with electrical stimulation are also extensive. This report focuses instead on the ruggedness of not bulk materials as in the case of a prosthesis or needles, but on thin-layered metals found in microfabricated electrodes. The microbands with a Ti adhesion layer

performed better than Cr. Rapid loss of the Cr/Au MEA electrodes upon OER potential exposure made the Cr/Au system unsuitable for use at OER potentials. MEAs constructed on Ti/Au platforms, especially when coated with Pt and Pt_b are sustainable at positive potentials for short-term operation. The Ti/Pt constructed electrodes were considered the best candidates for long-term operational life. It leaves possibilities with further studies on this project by focusing on optimizing the coating thicknesses to observe if different coating thicknesses have any effects on the morphology and surface studies of the electrodes.

3.9 Acknowledgments

This project was supported by the Arkansas Bioscience Institute. The authors would like to thank Errol V. Porter, Atanu Dutta, and staffs of the High Density Electronics Center (HiDEC) Thin Film Facility under the University of Arkansas' Department of Electrical Engineering for training and guidance with microfabrication, Dr. Ingrid Fritsch, and her research group for the microscope, thermal evaporator and guiding with lithography, Emily C. Anderson and Benjamin J. Jones of the Fritsch research group for the design of the electrode chip. Mourad Benemara and Betty Martin of Arkansas Nano and Biomaterials Characterization Facility at the University of Arkansas for the SEM/EDX. Dr. Gregory Salamo and his research group of the Institute of Nanoscience and Engineering, and Dr. Min Zou and her research group of Mechanical engineering at the University of Arkansas for the Keyence 3D LASER viewer and analyzer.

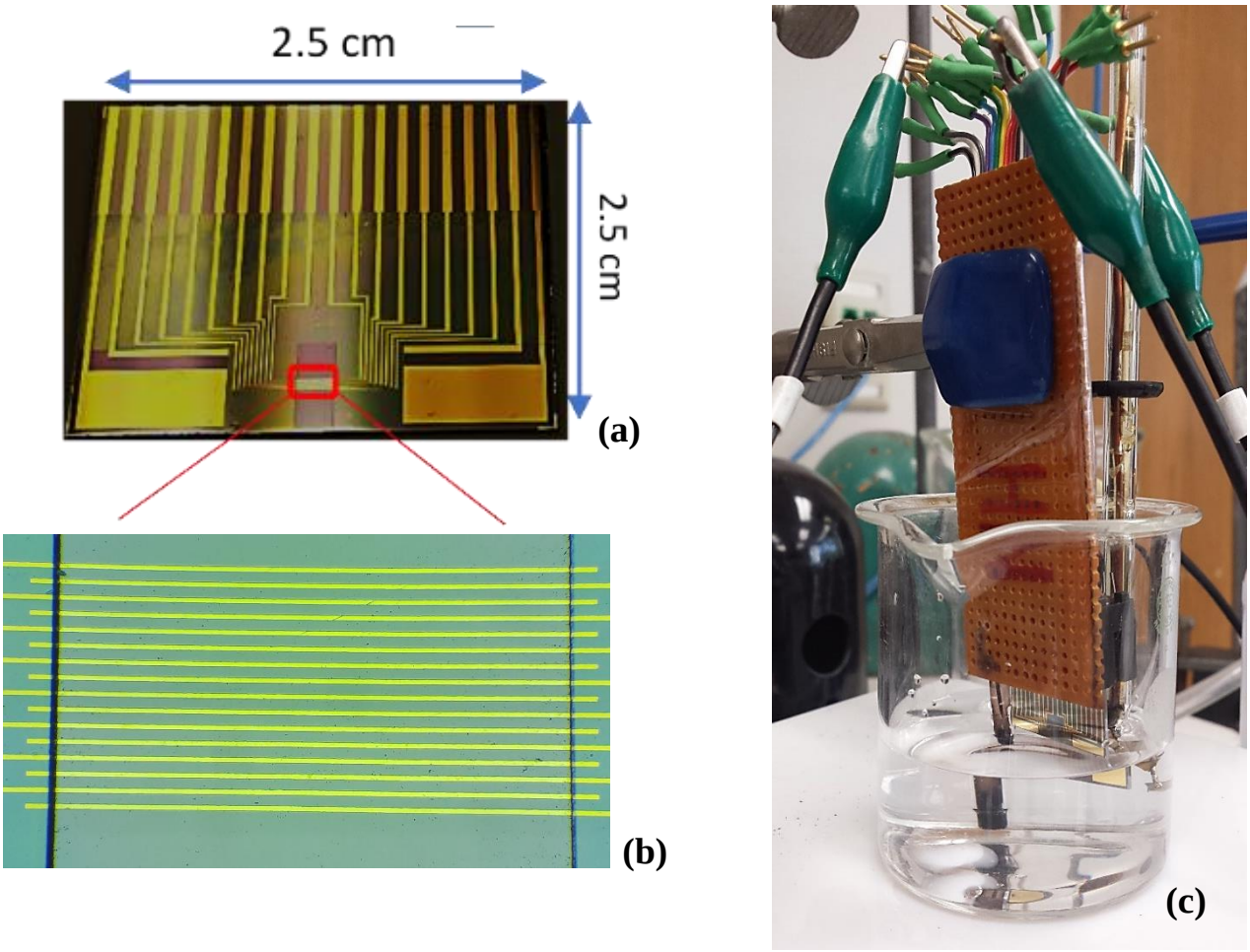

Figure 3.1 Fabricated (2.5cm x 2.5cm) Cr/Au MEA chip with edge connector leads (b) Enlarged view of sixteen interdigitated microelectrode array, each band with 25 µm width, 2 mm length and 25 µm band gap (c) An experimental set up with the MEA chip connected to the edge connector. Potentiostat applied voltages to the desired bands via electrode leads of the edge connector. Ag/AgCl in saturated KCl reference electrode and Pt counter electrode were applied in this set-up.

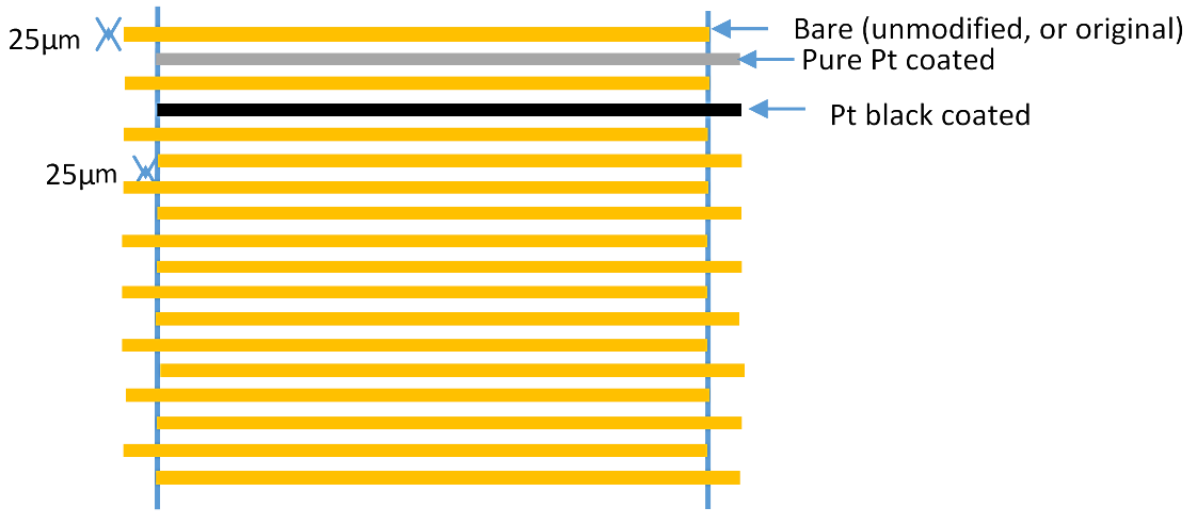

Figure 3.2 Schematic of a Cr/Au MEA samples for sustainability test. Samples on Ti/Au and Ti/Pt MEAs were prepared the similar way.

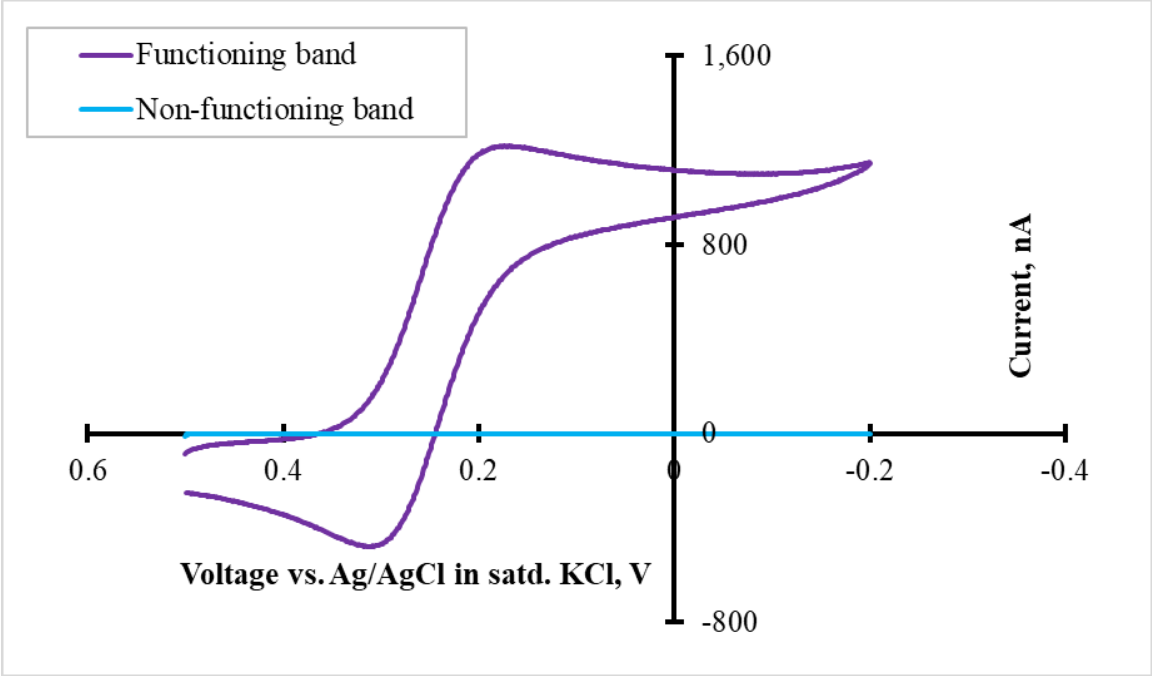

Figure 3.3 Comparison of the 5mM potassium ferricyanide signal in 0.1 M potassium chloride for the bare Ti/Au MEA bands: the functioning band (purple) CV showed reduction and oxidation peak at 0.22V and 0.33V respectively, where the non-functioning (blue) CV showed no reduction or oxidation response.

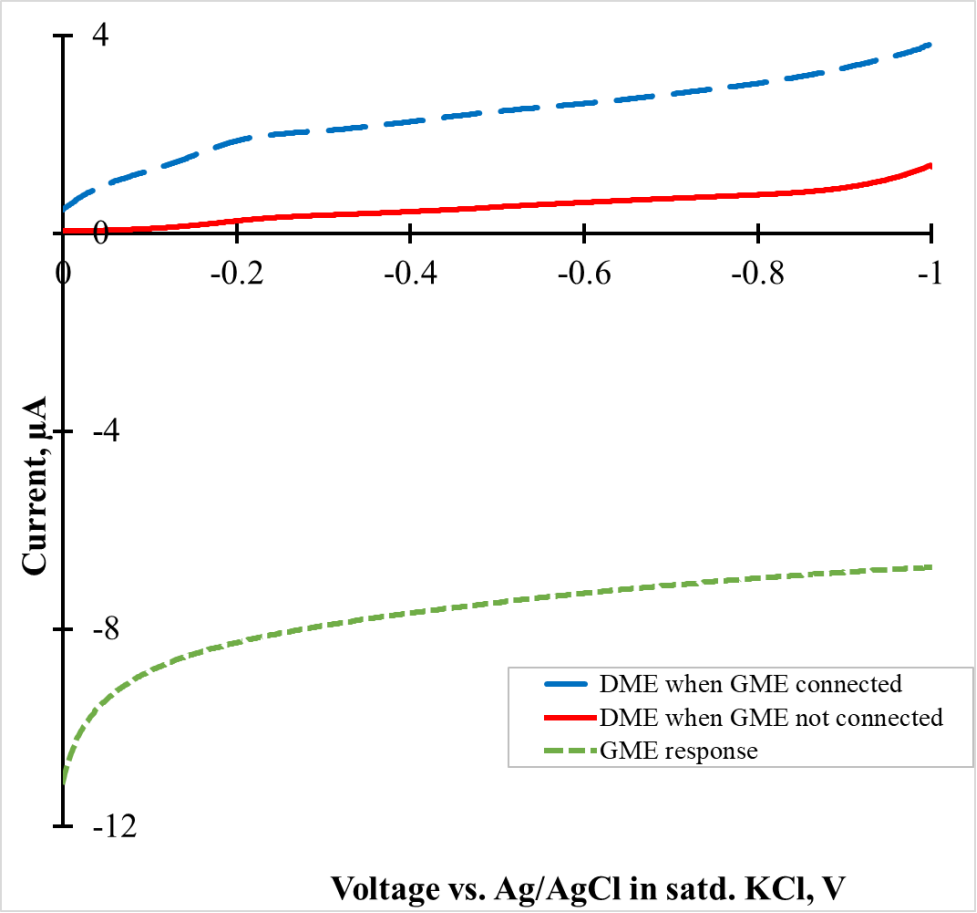

Figure 3.4 Linear sweep voltammetric responses of a Cr/Au DME in 10 mM PBS at room temperature when the 25 µm distant Cr/Au/Pt$_b$ GME was at open circuit (red solid line) and was connected at 1.4V (blue dashed line) showing the increased response at the detector due to collection of oxygen generated by the generator, the green square dotted line is the corresponding oxygen GME response at constant +1.4 V Vs. Ag/AgCl in satd. KCl.

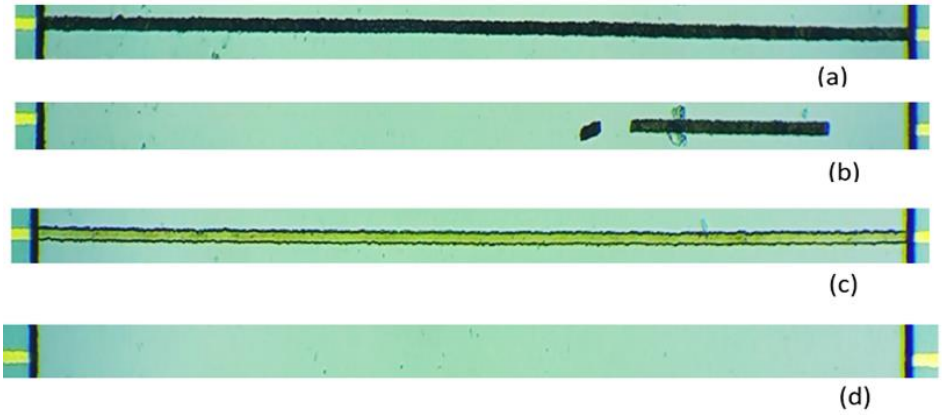

Figure 3.5 Microscopic view: Cr/Au/ Ptb GME (a) before and (b) after second oxygen generate-detect experiment. Cr/Au/Pt GME (c) before and (d) after third oxygen generate-detect experiment.

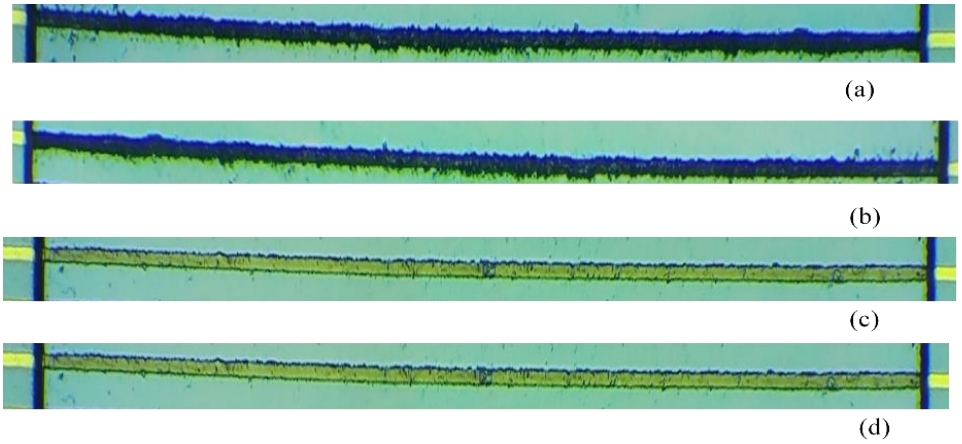

Figure 3.6 Microscopic view: Ti/Au/Pt$_b$ GME (a) before (b) after six scans of oxygen generate-detect test. Ti/Au/ Pt GME (c) before, and (d) after eight scans of oxygen generate-detect test.

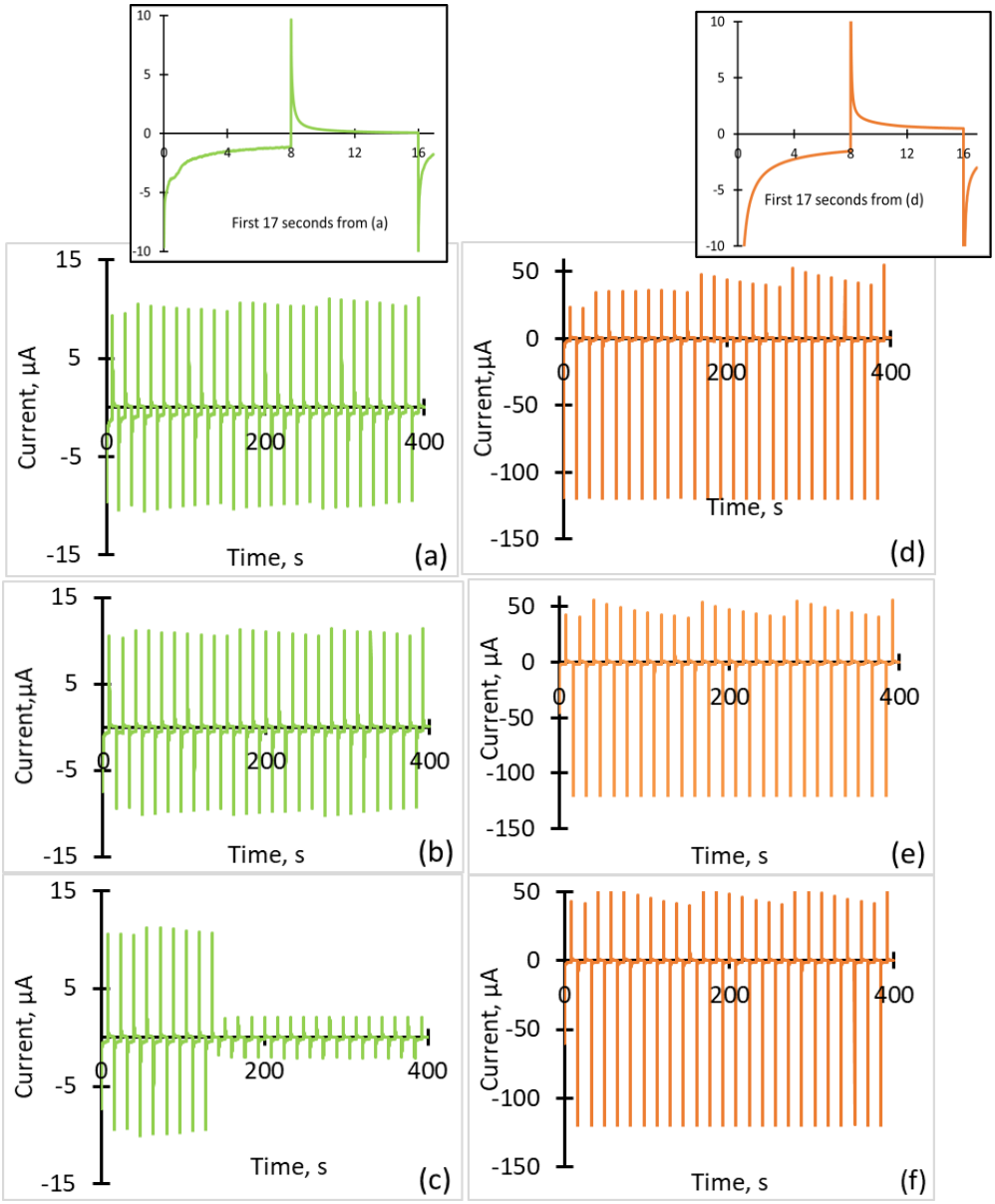

Figure 3.7 Chronoamperometric sustainability test from 0 V stepped to +1.4 V vs. Ag/AgCl in satd. KCl, pulse width= 7.992 s and sample interval= 0.012 s. Three consecutive rounds of fifty chronoamperometric steps: (a)- (c) Ti/Au/Pt$_b$ GME and (d)- (f) Ti/Au/Pt GME

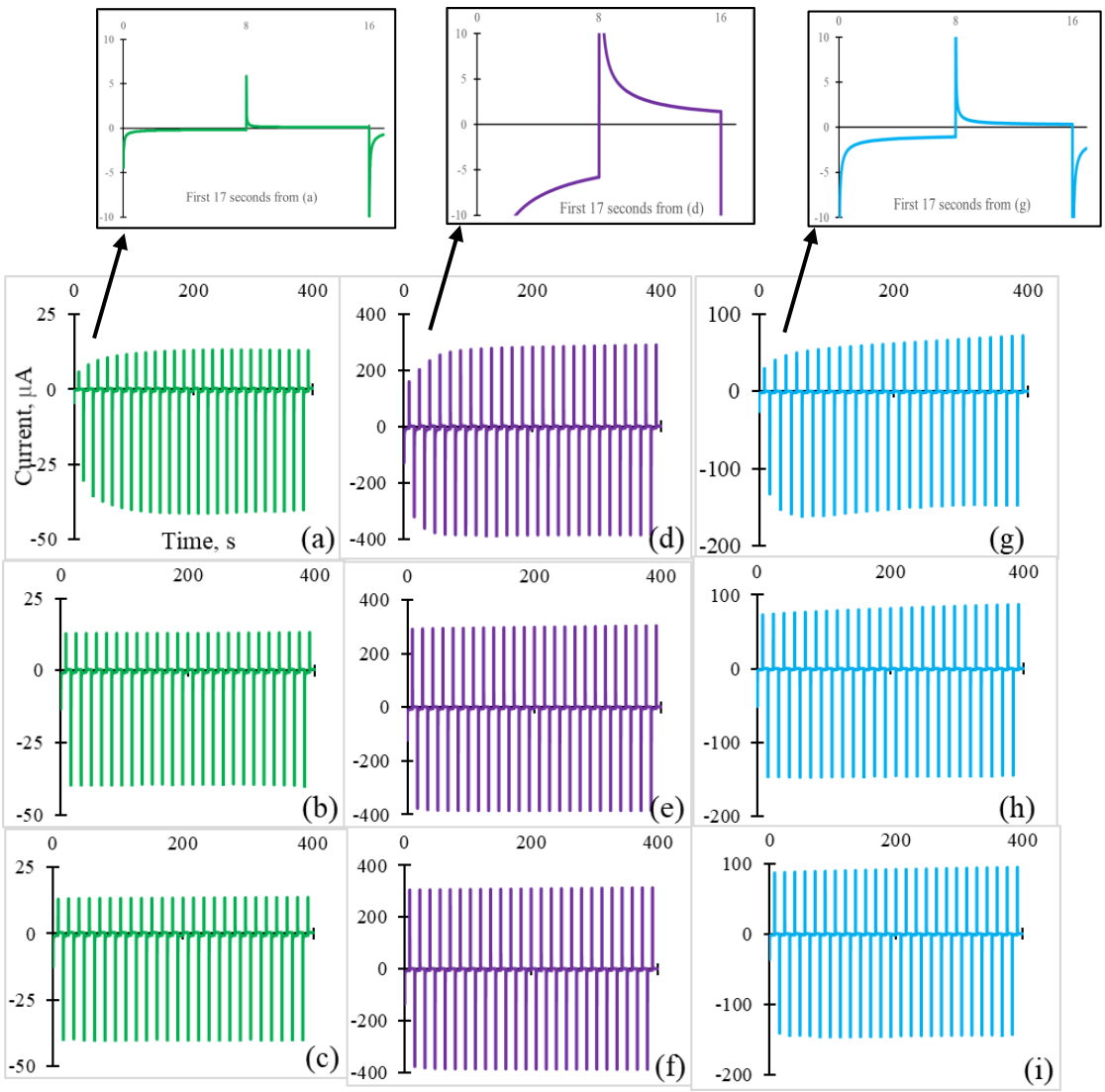

Figure 3.8 Potential step chronoamperometry on Ti/Pt GME samples between 0 V to 1.4 V vs. Ag/AgCl in KCl in 10 mM PBS solution for 150 steps; pulse width= 8 s; (a-c) unmodified Ti/Pt; (d-f) Ti/Pt/Pt$_b$; (g-i) Ti/Pt/Pt GMEs

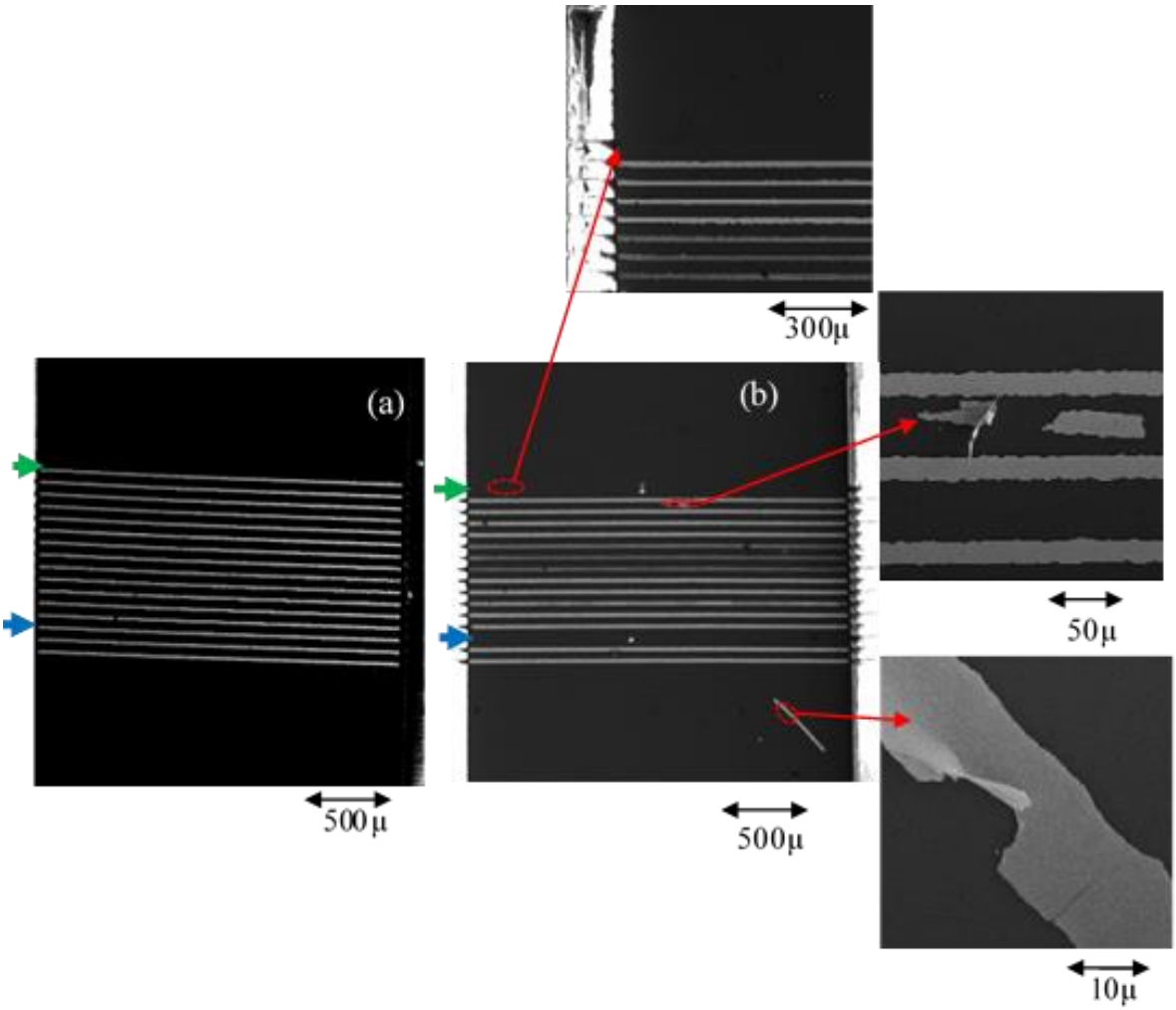

Figure 3.9 SEM images of coated OER generators over Cr/Au MEA: Pt-coated (green arrow) and Pt_b-coated (blue arrow), (a) before; (b) after subjected to OER potential with zoomed-in views of the missing Pt-coated band (top), fragmented and displaced remains of the failed generator bands (middle and bottom)

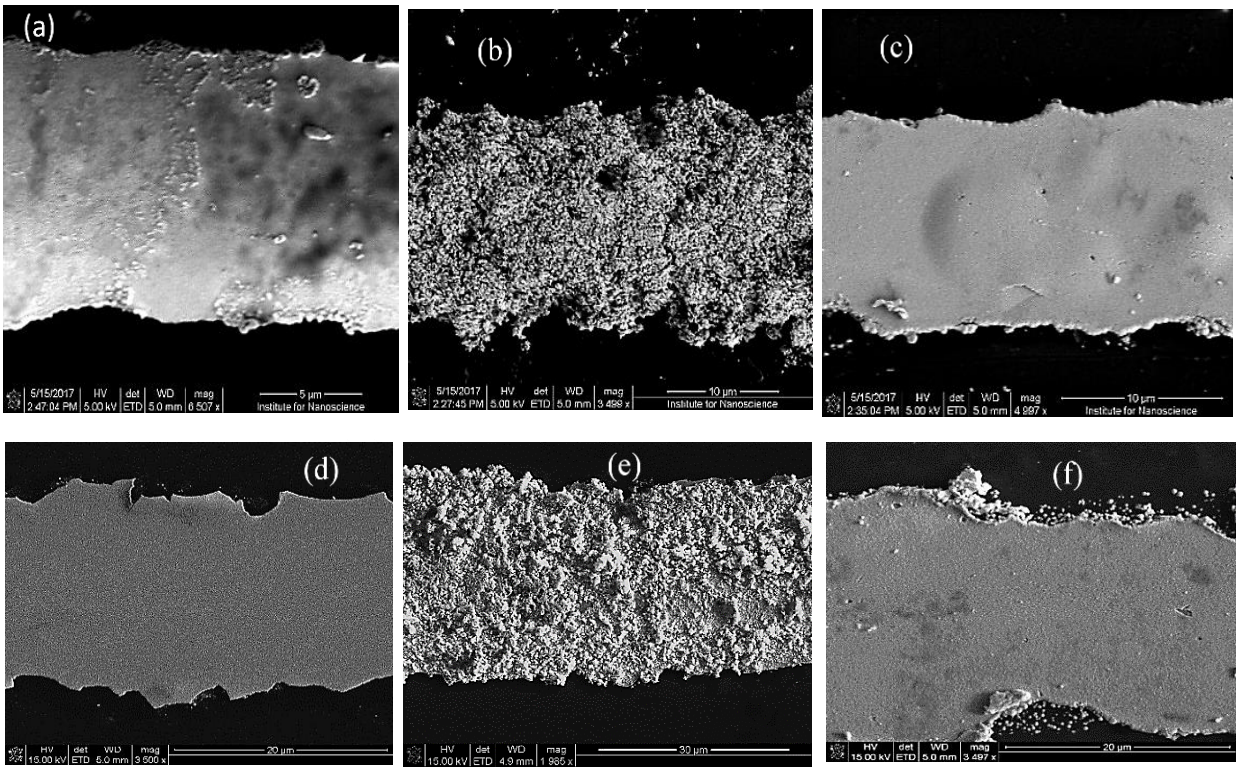

Figure 3.10 SEM images of (a) Ti/Au; (b) Ti/Au/Pt$_b$; (c) Ti/Au/Pt; (d) Ti/Pt (the torn edges were due to undercut caused by overetching); (e)Ti/Pt/Pt$_b$; and (f) Ti/Pt/Pt bands .

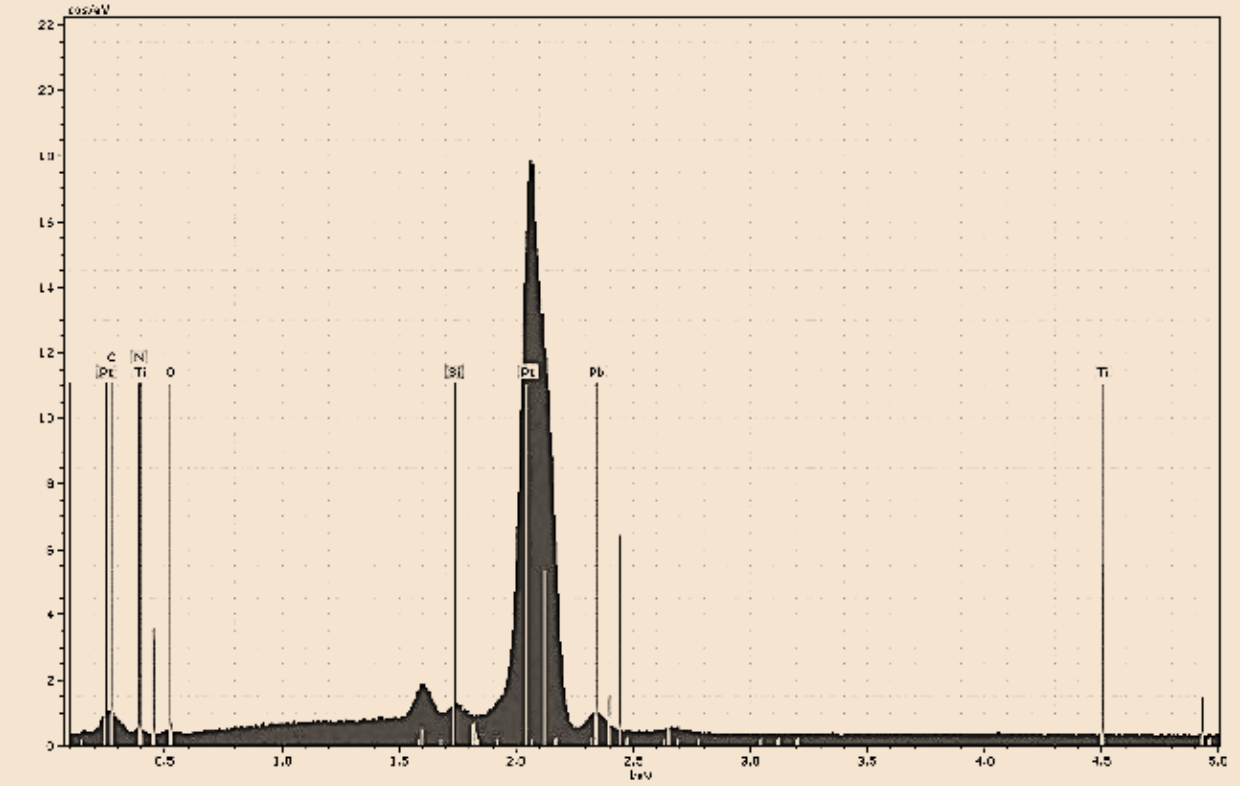

Spectrum: Acquisition

El	AN	Series	unn. C [wt.%]	norm. C [wt.%]	Atom. C [at.%]	Error [wt.%]
C	6	K-series	11.70	11.55	52.17	1.9
Pt	78	M-series	81.04	79.98	22.24	3.1
N	7	K-series	4.65	4.59	17.77	0.9
O	8	K-series	1.75	1.73	5.87	0.4
Si	14	K-series	0.79	0.78	1.51	0.1
Pb	82	M-series	1.29	1.28	0.33	0.1
Ti	22	K-series	0.10	0.09	0.11	0.0
		Total:	101.32	100.00	100.00	

Figure 3.11 EDX analysis at 5KeV; Ti/Pt/ Pt_b sample before sustainability test; similar EDX analysis were performed on each GME sample that underwent the sustainability test, once before and again after the test.

3.10 References

1. C. D. Johnson and D. W. Paul, *Sensors and Actuators B: Chemical*, 2005, **105**, 322-328.

2. F. B. Bolger and J. P. Lowry, *Sensors*, 2005, **5**, 473-487.

3. E. M. R. Doppenberg, A. Zauner, M. D. Ross Bullock, J. D. Ward, P. P. Fatouros and H. F. Young, *Surgical neurology*, 1998, **49**, 650-654.

4. E. M. R. Doppenberg, A. Zauner, J. C. Watson and R. Bullock, in *Intracranial Pressure and Neuromonitoring in Brain Injury*, Springer, 1998, pp. 166-169.

5. W. E. Hoffman, F. T. Charbel and G. Edelman, *Anesthesia & Analgesia*, 1996, **82**, 582-586.

6. K. L. Kiening, A. W. Unterberg, T. F. Bardt, G.-H. Schneider and W. R. Lanksch, *Journal of neurosurgery*, 1996, **85**, 751-757.

7. S. Rastogi, A. Kumar, N. K. Mehra, S. D. Makhijani, A. Manoharan, V. Gangal and R. Kumar, *Biosensors and Bioelectronics*, 2003, **18**, 23-29.

8. A. Kallel, T. Matsuto and N. Tanaka, *Waste management & research*, 2003, **21**, 346-355.

9. F. Adani, P. Lozzi and P. Genevini, *Compost Science & Utilization*, 2001, **9**, 163-178.

10. G. D. Zupančič and M. Roš, *Waste and Biomass Valorization*, 2012, **3**, 89-98.

11. D. W. Paul, I. Prajapati and M. L. Reed, *Sensors and Actuators B: Chemical*, 2013, **183**, 129-135.

12. X. J. Huang, A. M. O'Mahony and R. G. Compton, *Small*, 2009, **5**, 776-788.

13. R. G. Compton, G. G. Wildgoose, N. V. Rees, I. Streeter and R. Baron, *Chemical Physics Letters*, 2008, **459**, 1-17.

14. M. Fleischmann and S. Pons, *Analytical Chemistry*, 1987, **59**, 1391A-1399A.

15. A. F. M. Johnstone, G. W. Gross, D. G. Weiss, O. H. U. Schroeder, A. Gramowski and T. J. Shafer, *Neurotoxicology*, 2010, **31**, 331-350.

16. R. Polsky, J. C. Harper, D. R. Wheeler and S. M. Brozik, *Electroanalysis: An International Journal Devoted to Fundamental and Practical Aspects of Electroanalysis*, 2008, **20**, 671-679.

17. M. Seidel and R. Niessner, *Analytical and bioanalytical chemistry*, 2008, **391**, 1521.

18. H. Chen, C. Jiang, C. Yu, S. Zhang, B. Liu and J. Kong, *Biosensors and Bioelectronics*, 2009, **24**, 3399-3411.

19. J. Yan, V. A. Pedrosa, A. L. Simonian and A. Revzin, *ACS applied materials & interfaces*, 2010, **2**, 748-755.

20. C. C. L. McCrory, S. Jung, J. C. Peters and T. F. Jaramillo, *Journal of the American Chemical Society*, 2013, **135**, 16977-16987.

21. J. W. D. Ng, M. Tang and T. F. Jaramillo, *Energy & Environmental Science*, 2014, **7**, 2017-2024.

22. T. Reier, M. Oezaslan and P. Strasser, *Acs Catalysis*, 2012, **2**, 1765-1772.

23. A. Gencoglu and A. Minerick, *Lab on a Chip*, 2009, **9**, 1866-1873.

24. J. Ghilane, M. Guilloux-Viry, C. Lagrost, J. Simonet and P. Hapiot, *Journal of the American Chemical Society*, 2007, **129**, 6654-6661.

25. S. Mailley, M. Hyland, P. Mailley, J. A. McLaughlin and E. T. McAdams, *Bioelectrochemistry*, 2004, **63**, 359-364.

26. G. Xiao, Y. Song, Y. Zhang, Y. Xing, H. Zhao, J. Xie, S. Xu, F. Gao, M. Wang and G. Xing, *ACS sensors*, 2019, **4**, 1992-2000.

27. A. P. Markusse, B. F. M. Kuster and J. C. Schouten, *Catalysis today*, 2001, **66**, 191-197.

28. J.-H. Han, H. Boo, S. Park and T. D. Chung, *Electrochimica acta*, 2006, **52**, 1788-1791.

29. S. B. Hall, E. A. Khudaish and A. L. Hart, *Electrochimica Acta*, 2000, **45**, 3573-3579.

30. R. W. Bartlett, *Journal of the Electrochemical Society*, 1967, **114**, 547.

31. M. Peuckert and H. P. Bonzel, *Surface Science*, 1984, **145**, 239-259.

32. J. L. Wang, R. L. Liu, T. Majumdar, S. A. Mantri, V. A. Ravi, R. Banerjee and N. Birbilis, *Acta Biomaterialia*, 2017, **54**, 469-478.

33. E. Patrick, M. E. Orazem, J. C. Sanchez and T. Nishida, *Journal of neuroscience methods*, 2011, **198**, 158-171.

34. P. Vadgama, *Sensors*, 2020, **20**, 3149.

35. D. W. Hatchett, R. Wijeratne and J. M. Kinyanjui, *Journal of Electroanalytical Chemistry*, 2006, **593**, 203-210.

36. S. Cherevko, A. A. Topalov, A. R. Zeradjanin, I. Katsounaros and K. J. J. Mayrhofer, *Rsc Advances*, 2013, **3**, 16516-16527.

37. S. Cherevko, A. R. Zeradjanin, G. P. Keeley and K. J. J. Mayrhofer, *Journal of The Electrochemical Society*, 2014, **161**, H822.

38. S. Nilsson, O. Klett, M. Svedberg, A. Amirkhani and L. Nyholm, *Rapid communications in mass spectrometry*, 2003, **17**, 1535-1540.

39. M. A. Nicolet, *Thin Solid Films*, 1978, **52**, 415-443.

40. R. Bruchhaus, D. Pitzer, O. Eibl, U. Scheithauer and W. Hoesler, *MRS Online Proceedings Library Archive*, 1991, **243**.

41. A. M. Feltham and M. Spiro, *Chemical Reviews*, 1971, **71**, 177-193.

42. A. Barcz, A. Turos and L. Wieluński, in *Ion beam surface layer analysis*, Springer, 1976, pp. 407-414.

43. P. H. Holloway, D. E. Amos and G. C. Nelson, *Journal of Applied Physics*, 1976, **47**, 3769-3775.

44. J. C. Hoogvliet and W. P. Van Bennekom, *Electrochimica acta*, 2001, **47**, 599-611.

45. T. Maeder, L. Sagalowicz and P. Muralt, *Japanese journal of applied physics*, 1998, **37**, 2007.

46. J. M. Poate, *Gold Bulletin*, 1981, **14**, 2-11.

47. T. C. Tisone and J. Drobek, *Journal of Vacuum Science and Technology*, 1972, **9**, 271-275.

48. J. O. Olowolafe, R. E. Jones Jr, A. C. Campbell, R. I. Hegde, C. J. Mogab and R. B. Gregory, *Journal of applied physics*, 1993, **73**, 1764-1772.

49. F. Parmigiani, E. Kay and P. S. Bagus, *Journal of Electron Spectroscopy and Related Phenomena*, 1990, **50**, 39-46.

50. J. C. Vis, H. F. J. van't Blik, T. Huizinga, J. van Grondelle and R. Prins, *Journal of Molecular Catalysis*, 1984, **25**, 367-378.

51. M. El-Shabasy, *Periodica Polytechnica Electrical Engineering*, 1981, **25**, 123-134.

52. S. Sharma, Z. Huang, M. Rogers, M. Boutelle and A. E. G. Cass, *Analytical and bioanalytical chemistry*, 2016, **408**, 8427-8435.

53. J. P. Brown, B. S. Lynch, I. M. Curry-Chisolm, T. J. Shafer and J. D. Strickland, in *Cell Viability Assays*, Springer, 2017, pp. 153-170.

54. S. Ahadian, J. Ramón-Azcón, S. Ostrovidov, G. Camci-Unal, V. Hosseini, H. Kaji, K. Ino, H. Shiku, A. Khademhosseini and T. Matsue, *Lab on a Chip*, 2012, **12**, 3491-3503.

55. N. Tandon, A. Marsano, R. Maidhof, K. Numata, C. Montouri-Sorrentino, C. Cannizzaro, J. Voldman and G. Vunjak-Novakovic, *Lab on a Chip*, 2010, **10**, 692-700.

56. R. Guo and J. Liu, *Journal of Micromechanics and Microengineering*, 2017, **27**, 104002.

4. Transferring Sensor-construction Technology to Micro-electrodes and Investigation on the Effects of Oxygen Generated by Electrolysis on the Glucose Microsensor

4.1 Abstract

The glucose oxidase enzyme is the bio component of electrochemical glucose sensors. The enzyme is immobilized onto the surface of an electrode and the peroxide product of the enzymatic reaction with glucose is oxidized to develop an electrical signal that is proportional to the concentration of the glucose present. The reaction also depends on the presence of oxygen which must be constant and in excess to ensure that the sensor responds proportionately to glucose. Successful first-generation glucose sensors either limit the amount of glucose reaching the enzyme to ensure oxygen is in excess or use a synthetic mediator in place of oxygen. Here the construction of a first-generation glucose sensor has been reported that can function with high sensitivity and a larger dynamic range under oxygen-limited conditions. One member in a microband electrode array serves as the glucose sensor (DME) and a second band as an oxygen generator (GME) via water electrolysis. The sensor and generator electrodes are operated individually as expected, but the combined action of both sensor-generator electrodes did not work as expected, rather showing a decreased glucose signal. Ultimately peroxide diffusional 'cross-talk' to the generating electrode was established as the reason behind the decrease in signal and further experiments showed the method to be a valid approach to the oxygen limitation. Glucose sensitivities of sensors constructed on gold and platinum microbands were also examined and discussed.

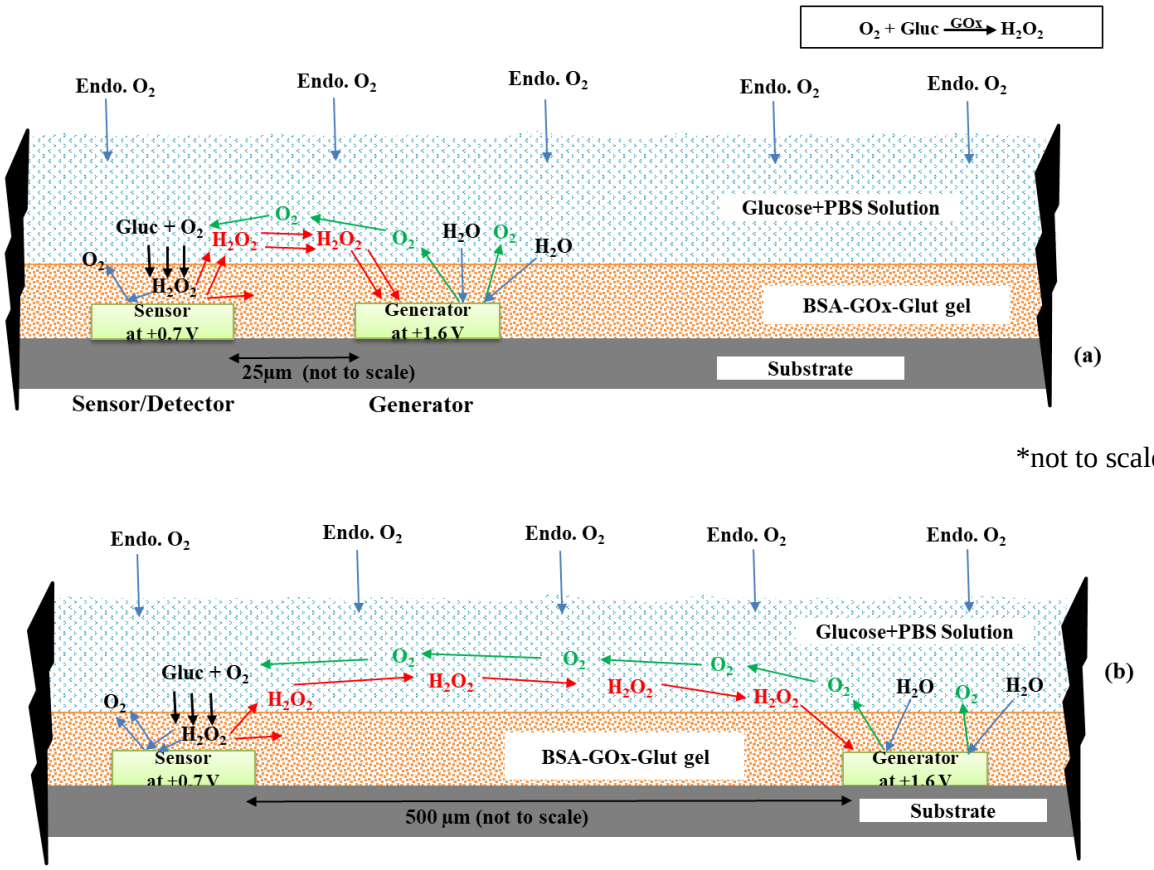

Graphical abstract: Schematic representation of peroxide diffusion cross-talk to the generator and the effect of distance between the oxygen generator and glucose sensor electrode when they are (a) 25 µm apart and (b) 500 µm apart (not to scale). The substrate here is Si substrate, sensor, and generator both are Ti/Pt microband electrodes (25 µm X 2000 µm each). Glucose enzymatic reactions are shown with black arrows, peroxide cross-talk with red arrows, oxygen generated by the generator electrode with green arrows, and all other sources of oxygen (oxygen generated from peroxide oxidation and endogenous oxygen) are shown with blue arrows. All the potentials mentioned in the diagram are for the reference electrode Ag/AgCl in saturated KCl.

4.2 Introduction

Oxidase enzyme-based first-generation biosensors require molecular oxygen as an electron acceptor, so they are oxygen-dependent. Examples of such oxidase-enzyme used in biosensors are glucose oxidase, glutamate oxidase, alcohol oxidase, lactate oxidase, ascorbate oxidase, galactose oxidase, cholesterol oxidase, choline oxidase, laccase, tyrosinase, etc.[1-35] The glucose oxidase enzyme (GOx) is the bio component of electrochemical glucose sensors.[32, 36] The enzyme is immobilized onto the surface of an electrode, and the products of the reaction with glucose are oxidized to develop an electrical signal proportional to the concentration of glucose present. In a glucose oxidase-based sensor the enzyme reacts with glucose, but the reaction also depends on the presence of oxygen. To ensure that the sensor responds proportionately to glucose, and not oxygen, the oxygen concentration must be equal to or above that of glucose, making glucose the limiting reagent.[37] The sensor's oxygen demand has been avoided by two clever approaches, one for external glucose measurements in blood, and much later, a different approach for in vivo glucose measurements.[38, 39] Both constructions provided a working sensor for each application, but at a loss in sensitivity and limit of detection.

For in-vivo applications, intercellular oxygen is variable and limited compaired to glucose. For example, oxygen content in brain extracellular fluid (in rodents) is reported by microdialysis to be 0.03 – 0.08 mM,[40] and varies throughout the brain[41]. Glucose brain ECF levels also determined by microdialysis are 1.57±0.76 mM but levels can vary up to about 2 mM. Implantable continuous glucose monitors currently available (for humans) in the market are being implanted into subcutaneous tissue area where it measures the interstitial fluid (ISF) glucose. To construct an implantable sensor that is glucose-limited at the electrode surface, the sensor is coated with several additional layers that limit the amount of glucose (and any interferences to the analyte) reaching

the enzyme but allow oxygen to pass freely.[42-44] The glucose reaching the enzyme is reduced and this, in turn, lowers the oxygen demand. Unfortunately, this construction raises the detection-limit and lowers the sensitivity of the sensor.[45]

For external glucose measurements, particularly for levels in the blood, the oxygen limitation was by-passed by using artificial mediators in place of oxygen. Commercial grade blood glucose sensors have used this non-oxygen-mediator technology to great success. The most common application of this technology is the blood glucose test strip, widely sold to diabetics for monitoring blood sugar, but using a blood sample outside the body. Non-oxygen-mediators are toxic, only safe to use outside the body.[39] If placed in vivo, the concern is that the mediators could leach out. Leaching prevents their use for in-vivo continuous glucose monitoring.

In this chapter, we present evidence for an alternative method of providing the needed oxygen in areas where there is insufficient oxygen concentration compared to glucose. The action of the glucose-sensing electrode is the same: in the presence of glucose, oxygen, and the enzyme, the glucose substrate is oxidized, and hydrogen peroxide is produced. The peroxide is electrochemically oxidized at the same electrode, and the current is measured. This current will be proportional to the amount of glucose present with oxygen in excess. If a modest amount of oxygen is available, the response will be set by both glucose and oxygen, and if the oxygen can be held constant there will be a linear response to glucose. Unfortunately in vivo oxygen is variable leading to a current response that will result in a false glucose value.[45] In the extreme case, where there is insufficient oxygen at the enzymatic reaction site, the reaction becomes oxygen-limited.

The proposed scheme overcomes the limitations of inadequate oxygen by generating oxygen by water electrolysis at a generator electrode, supplying the generated oxygen to the reaction site at the sensor. Microelectrode arrays (MEAs) are perfect for this application as one member of the

electrode array can serve as a GOx enzyme sensor and a second member as the oxygen generating electrode. The MEA chosen for this application was an array of sixteen (25 µm x 2 mm) microbands.

The initial premise was that oxygen diffuses out from the generator over to the area of the sensor, supplying the needed oxygen, resulting in an increase in signal. When practically implemented, however, the scheme initially failed to work as proposed. When the generator was connected at OER potential, the sensor's peroxide oxidation signal was observed to decrease instead of the expected increase, resulting in 'reductive offsets'. After several failed attempts using trial and error experiments to identify the possible reasons for the reductive offset when generating oxygen, a version of diffusional cross-talk was hypothesized. Schemes were reported here to maximize the oxygen at the DME band while minimizing the consumption of peroxide at the GME band. In addition, details as to the immobilization of GOx onto microbands is given along with the stability of the glucose response using gold and platinum microband electrodes.

4.3 Materials and Methods

4.3.1 Instruments and reagents

O-phenylenediamine (oPD) monomer (Sigma, St. Louis, MO), bovine serum albumin (Amresco, Solon, OH), phosphate buffered saline tablets (PBS) (EMD Millipore, Billerica, MA) were obtained. Solutions of oPD monomer (300 mM) were prepared in 10 mM PBS. CH Instruments 1030A or an 830A potentiostat, using an Ag/AgCl in saturated KCl reference electrode, a platinum flag counter electrode, in 10 mM pH 7.4 PBS solution (140 mM NaCl, 10 mM phosphate buffer, 3 mM KCl), with a 0.8 M glucose stock (in 10 mM PBS solution) were used in all experiments performed in this chapter unless otherwise mentioned. Sloan DekTak 3030 profilometer was used for thickness measurement

4.3.2 Working microelectrode preparation

4.3.2.1 Platinization of the gold microelectrodes

Before the fabrication of Ti/Pt MEAs, microelectrode experiments were performed with gold microband electrodes using Cr/Au and Ti/Au MEAs. Since gold oxidizes at the positive potentials needed for peroxide detection or oxygen generation, the microelectrodes were electroplated with platinum. Initially, platinization was performed using a commercially available YSI 3140 platinizing solution that resulted in a Pt_b coating on the microbands. This coating was formed by applying -1.0 V (vs Ag/AgCl in satd. KCl) on the desired gold microband for 60 seconds. This procedure was repeated twice so that a uniform and even black coating was verified by microscopic examination.

After MEA fabrication, profilometry indicated a gold layer thickness of 0.2 µm. Electrodeposition with single-platinization and double-platinization resulted in about 1.9 µm and 6 µm thick platinum coatings respectively over the gold. Double platinization provided a Pt-black thickness three times that of single platinization over gold microelectrode.

Later in the project, a platinizing solution was prepared that resulted in the electrodeposition of a pure Pt coating over the gold microbands. Pt was electrodeposited from a chloroplatinic acid solution by applying −0.1V vs. Ag/AgCl for 5 seconds, repeating two additional times. The chloroplatinic acid solution was prepared from 20 mM potassium tetrachloroplatinate(II) (Sigma Aldrich, USA) in 1M perchloric acid.[40] The Pt coating appeared light gray color under the microscope.

4.3.2.2 Glucose sensing membrane construction

First-generation GOx enzyme sensors were constructed on the Ti/Au/Pt (electroplated) or fabricated Ti/Pt MEAs. The GOx enzyme was immobilized by either electropolymerization with

oPD or drop cast using a glutaraldehyde crosslinking solution. The direct transfer of the sensor construction by electropolymerization from macroelectrodes (discussed in chapter 2) to the microbands of MEAs was unsuccessful, showing little or no sensitivity to glucose. After several failed attempts a modified version of electropolymerization entrapment of GOx did show a successful response to glucose. Sensors constructed on platinized Ti/Au MEAs via this technique were used during initial experiments to determine the response to glucose. The glucose sensors on both Ti/Au/Pt_b and Ti/Au/Pt microbands provided glucose sensitivity over seven days. Although glucose sensor on Ti/Au/Pt_b showed much higher sensitivity compared to the sensor on Ti/Au/Pt microbands, instability and existence of Pb in the Pt_b electroplated layer discontinued its further use as both GME and DME. Ti/Au/Pt survived longer at the high positive potential when applied as GMEs but their possible degradation and highest amount of oxygen generation by Ti/Pt based GMEs led the future experiments to switch to Ti/Pt MEAs. However, sensors constructed over unmodified Ti/Pt microbands by electropolymerization entrapment of GOx proved to have unstable sensitivity; with an operational life of fewer than three days. GOx immobilization by glutaraldehyde cross-linking using a drop-casting technique on to Ti/Pt microband provided a longer operational life of up to ten days.

Electropolymerization technique on to microbands

This construction method was modified from the technique described by Malitesta et. al. [46], Zhang [47], De Corcuera et. al. [48], and Sardesai et. al. [49]. The electropolymerizing solution consisted of 30 mM oPD, 10g/L GOx in acetate buffer (pH 5.2, I= 0.2M); construction of the GOx sensor electrode occurred by applying +0.9V vs. Ag/AgCl in satd. KCl for 30 minutes.

The thickness of the constructed GOx/PoPD membrane was estimated using charge-density data. According to Holdcroft and Funt, 45 mC/cm^2 charge density provides 0.1 µm film thickness [50]. Charge density from the successful electropolymerization was calculated to be 655 mC/cm^2, which should provide a film thickness of 1.46 µm. The profilometer measured the thickness of the GOx/PoPD membrane to be about 1µm. The possible reason behind the mismatch could be the hard stylus tip made from the milled or etched diamond that can scratch through the softer PoPD layer [51]. The responses to the microband GOx sensor to glucose confirmed the presence of the enzyme in the film. The sensor was stored in 10 mM PBS in the refrigerator at ~4^{o}C overnight before its first application and when not in use.

Drop cast technique

3 mL of 100 mM PBS with 0.08 g of BSA and 0.01 g of GOx was stirred until dissolved. 300 µL of glutaraldehyde was added while stirring. When the BSA-GOx-Glut mixture became thick but still fluid enough to be drawn into a micropipette, 5 µL of the thick solution was micro pipetted onto the electrode array. After 5 minutes the droplet became gel-like and adhered to the array. The GOx enzyme was thus entrapped in a BSA-Glut gel over the entire array. The coating must remain hydrated to stay permeable. In common with other practices, the sensor was allowed to "cure" overnight in the refrigerator before use. The amount of BSA used is ten times that of typical constructions,[4] but using less BSA did not provide good adhesion to the microbands. The coating could be removed by soaking for a few minutes in 0.1 M NaOH, and another sensing layer rebuilt. The sensor was stored in 10 mM PBS in the refrigerator when not in use. A comparative graphic representation of the two construction methods mentioned above is shown in Figure 4.1. Note that electropolymerization builds a selective GOx sensor membrane on a single microband, whereas drop-casting builds a GOx sensor membrane all over the array.

4.4 Experimental

4.4.1 Glucose calibration and sensitivity over time

The response to 0-15 mM glucose on GOx biosensors built on either the platinized Ti/Au microbands or Ti/Pt microbands using electropolymerization technique were recorded by applying cyclic voltammetry between 0 and +1.0 V vs. Ag/AgCl in satd. KCl to the glucose-sensing electrode. The peroxide oxidation signals at +0.7 V vs. Ag/AgCl in satd. KCl were plotted against the glucose concentrations to give glucose calibration curves. The sensitivities from the respective glucose calibration curves were calculated and plotted over time. Glucose responses and respective calibration curves were repeated until the sensor's sensitivity to glucose became very low. When not in use, the sensors were stored in 10 mM PBS at 4^{o}C.

4.4.2 Effects of oxygen from electrolysis on the glucose responses of the GOx sensor

The glucose response of the microband-electrode sensor in presence of electro-generated oxygen was compared to the response without the action of the generator i.e. using only ambient oxygen. This was done to outline the reduction in glucose signal (peroxide oxidation) due to the action of the generator. A series of CV were recorded with glucose concentrations between 0 and 10 mM with only ambient oxygen present and the generator open circuit. The second set of CVs were taken with the generator energized at +1.4 V vs satd. Ag/AgCl during the scan for each glucose concentration. The solution was stirred for five minutes between scans. Calibration curves for each case were constructed and the results were compared.

To investigate the "reductive-offset" or the lowering of the glucose signal seen when the generator is energized, a control experiment was initiated with oxygen being supplied from an external bottle and not the generator electrode. A series of glucose response signals between 0 mM and 30 mM glucose were recorded using cyclic voltammetry between 0 V and +1 V (vs satd. Ag/AgCl) at the

sensor microband-electrode. For each concentration, one CV was recorded at ambient conditions and the other after flooding the solution with oxygen. The solution was stirred for five minutes between any two cyclic voltammograms. Taking the signal response for peroxide at +0.7 V (vs satd. Ag/AgCl), two sets of glucose calibration curves were obtained by recording the glucose responses of the GOx sensor at +0.7 V (vs satd. Ag/AgCl): one without added oxygen and one with added oxygen. the CV experiments were performed with the sensor and generator electrodes being 25μm apart, and both electrodes were platinized.

As the unstable generator microband-electrode issue was partially resolved by applying Pt coating on Ti/Au MEAs (Ti/Au/Pt), the generator could be polarized for longer periods, as would be the case for chronoamperometry with the sequential addition of glucose. Glucose concentrations ranging between 0-60 mM each with a separate i-t amperometric response for each concentration were recorded with the generator at the open circuit for the first 60 seconds, then at +1.4 V for next about 20 seconds, then again at open circuit potential, while the sensor was all-time held +0.7 V. After each addition of glucose, the solution was stirred for about 1.5-2 minutes, the stirring was turned off and then the amperometry began.

4.4.3 Verification of the 'Diffusional Cross-talk' of the Peroxide

As the action of the generator was suspected to take peroxide away from the sensor, a scheme was developed to verify this using a temporal method. The sensor microband and the oxygen generator microband are never energized at the same time. These experiments were performed using Ti/Pt microband arrays with the GOx enzyme immobilized in a gel formed by crosslinking with BSA/glutaraldehyde as described in section 4.3.2. One electrode band was used as the glucose sensor and one band was used as the generator. The generator was energized producing oxygen to saturate the immediate area of the sensor with oxygen. The generator was then left open-circuit

and the sensor was activated to +0.7 V (vs satd. Ag/AgCl) to measure the current from peroxide. The experiment consisted of the following three sequential steps:

Pre-flood glucose reading: To determine the additional glucose signal due to electrogenerated oxygen, a baseline amperometric i-t was first recorded for the microband GOx sensor at +0.7 V vs. (Ag/AgCl in satd. KCl) while the generator microelectrode was at open circuit potential.

Flooding: The oxygen generator microband electrode was held at +1.6 V (vs satd. Ag/AgCl) for 5-60s to flood the sensor microelectrode with the electro-generated oxygen while the sensor was at open circuit potential.

Post-flood glucose reading: The sensor microelectrode was activated at +0.7 V (vs. Ag/AgCl in satd. KCl) while the generator was at open circuit and an amperometric i-t signal was recorded to measure the current from peroxide. A schematic of the sequences of this three-step flooding experiment is shown in Figure 4.2.

Experiments were performed for near (25 μm apart) and far (500 μm apart) generator-detector electrodes to investigate the effect of generator microelectrode's distance on the peroxide cross-talk. The experiment was performed for a single glucose concentration of 1mM for both far and near electrode condition.

4.4.4 Effect of the age of enzyme on post-flood calibration linearity

The GOx sensor microelectrode was prepared on the Ti/Pt MEA by drop cast technique described in section 4.3.2. To determine the aging of the sensor, a set of pre-flood/ post-flood glucose response tests (described in section 4.4.2) for varying glucose concentrations between 0-7 mM were performed for a GOx-BSA-Glut sensor electrode on the Ti/Pt microbands over ten days.

4.5 Results and Discussion

4.5.1 Glucose calibration and sensitivity over time

The first experiments were used to verify the response of the GOx microband to glucose. Comparative results of the glucose calibration curves for 0-15 mM glucose for GOx immobilized by electropolymerizatrion on Ti/Au/ Pt and Ti/Pt MEAs and respective sensitivities to glucose are shown in Figure 4.3. To determine the sensitivity per unit area, the sensitivity values were divided by the surface area of the microband electrode (2000 µm x 25 µm). The uncertainty values were determined using the LINEST function of Excel. Although sensor on the Ti/Au/Pt_b band showed highest glucose sensitivity among all the glucose sensors constructed in the lab (44.2±0.02 µA/mM-cm^2), it was discontinued due to instability, rapid loss of Pt_b layer and presence of Pb. The Ti/Au microbands were electroplated with pure Pt platinization before GOx immobilization on a single MEAs band by electropolymerization as discussed in section 4.3.2.2. It was observed that the sensors constructed by electropolymerization over Ti/Pt microbands experienced rapid loss in glucose sensitivity compared to the sensors constructed over platinized Ti/Au/Pt microbands. The glucose calibration curves for the sensor on Ti/Au/Pt microband for 0 to 15 mM glucose on day 1 showed a sensitivity of (24.73±3.25) µA/mM-cm^2. On day 4, the sensor's sensitivity towards glucose ~2.5x decreased to (9.71±2.23) µA/mM-cm^2, and by day 8 the sensitivity lowered to (2.67±0.96) µA/mM-cm^2. For the sensor built on the Ti/Pt microband the calibration curve on day 1 was (16.01±0.89) µA/mM-cm^2, on day 2, the sensitivity had ~7x lowered to (2.31±0.86) µA/mM-cm^2 with reduced linearity. The reason behind the very short operational life of the sensors on the Ti/Pt MEAs was possibly due to the poor adhesion quality of the sensor film to the Ti/Pt band surface. The platinization effect on the Ti/Au band created more

surface area and made the surface rougher at the same time. This resulted in better adhesion, higher loading of the enzyme, and longer operational life.

4.5.2 Effects of oxygen from electrolysis on the glucose responses of the GOx sensor

The experiments were conducted to investigate if the production of oxygen from the generator electrode can effectively compensate for the need for oxygen by the GOx electrode. Several experiments were performed by CV from 0 to +1.0 Volts (vs Ag/AgCl sat. KCl) to follow the oxidation of enzyme generated peroxide for 0-10 mM glucose concentrations. One CV was taken with the generator at +1.4 V during the scan at the sensor— 'generator on', and a second scan taken with the generator at the open circuit—'generator off'. Representative CVs were shown in Figure 4.4(a) for 0 and 5 mM glucose. What was observed was that when the generator was on and generating oxygen, the waves shifted in the reductive direction compared to the generator off. Not knowing the reason for this at the time effect was labeled the "reductive offset" caused by the action of the generator. This was the opposite of the glucose signal expected if the enzyme was given extra oxygen, i.e. the anodic current should increase. The anodic current at +0.7V vs. satd. Ag/AgCl for glucose concentrations between 0-10 mM from the same experiment was shown in Figure 4.4(b). The magnitude of the anodic current was less with the generator on compared to the generator off. Numerous of these experiments were performed with similar results. The additional oxygen provided by the generator was having the opposite result of what was hoped for. A series of trial and error experiments were performed over three years period in order to discover the reason for the anomalous "reductive offset" to glucose responses at +0.7 V(vs. Ag/AgCl in saturated KCl) when the generator was on at +1.4 V. Initially, some possible explanations for these unexpected results include: the generator was not making oxygen, or in some way, the immobilization of the enzyme was such that the additional oxygen was not reaching the enzyme.

Studies with rotating ring-disc electrodes (data not shown) proved that at +1.4 V (vs Ag/AgCl in satd. KCl) oxygen was being produced and observed reducing at the ring. To verify if the buffer type affected the action of the enzyme[52-56], various buffers were used with the glucose solution. In attempts to find out if the presence of chloride ions, phosphate ions, or sulfate ions had any effect on the "reductive offset", CVs similar to Figure 4.4(a) with the generator off for one scan and on for a second with chloride and sulfate ion free solutions (10 mM $NaHPO_4$ solution), chloride and phosphate-free solution (10 mM Na_2SO_4 solution), but the reductive offset still existed. Moreover, altering other parameters of the experiment, such as varying the generator voltages between +1.1 V and +1.9 V, and the detector voltages between +0.5 V and +0.9 V could not elucidate the problem.

To determine whether or not additional oxygen was reaching the enzyme, CV experiments were performed with glucose solutions in the presence and absence of additional oxygen supplied from an external cylinder. Figure 4.5(a) shows a CV performed in ambient conditions for 0 and 5 mM glucose. The solution was then saturated with oxygen from the cylinder just before the repeat of the CV experiment. With the additional oxygen available in the solution there was a marked increase in the anodic current over just endogenous oxygen from the air.

A calibration curve was constructed with and without oxygen preflood using all the concentrations (Figure 4.5(b)). The improvement in linear dynamic range and sensitivity with additional oxygen is clear. The externally supplied oxygen provided a linear dynamic range up to 10 mM and with a sensitivity of 60 μA/mM-cm^2 glucose. The same sensor without the additional oxygen has a sensitivity of only 2.2 μA/mM-cm^2 glucose. The response without additional oxygen was linear but more likely is responding to oxygen-limited conditions under ambient conditions, resulting in low sensitivity.

Combining the results from Figure 4.4and Figure 4.5, it was then realized that the action of the generator reduces the peroxide oxidation signal at the sensor micro band. To determine if the reductive offset was dependent upon glucose concentration, chronoamperometric experiments were performed on a single microband electrode at +0.7 V (vs. Ag/AgCl) using glucose concentrations between 0-60 mM (Figure 4.6(a) and (b)). The reductive offset was seen to increase non liearly with increasing glucose concentration.

An investigation was done on the hypothesis of peroxide cross-talk that was reported by Quinto et al[57] as a possible reason for a reductive offset which will be discussed in the following section.

4.5.3 Verification of the 'Diffusional Cross-talk' of the Peroxide

Diffusional cross-talk between micro bands occurs when the product from one micro band diffuses over to an adjacent band where it could undergo an electrode reaction, or serve as an interference to the chemistry occurring at the adjacent band. The hiatus came after reading a recent paper published by M. Quinto.[57] One of the potential advantages of individually addressable microelectrode arrays is the possibility of sensing multiple analytes. The Quinto paper dealt with a scenario of electrode array members each microband coated with a different oxidase enzyme. Each electrode derives its signal from peroxide oxidation coming from the immobilized enzyme allowing for simultaneous detection of glucose, lactose, glutamine using a single array. The complication would be that the enzyme-generated peroxide would have to stay in the local of a single microband to be oxidized. Otherwise, peroxide signals from each microband would be mixed with each other, foiling the multi-analyte advantage of the area. What Quinto reported was the reality that the peroxide does not remain local to the GOx microband but, diffuses to neighboring bands, aka diffusional cross-talk of peroxide. The microband electrode arrays used in the Quinto paper were of similar dimensions to the ones used here. The point of this paper was

to develop schemes to minimize diffusional cross-talk of peroxide between GOx electrode. To examine the peroxide diffusional cross-talk complication, Quinto modified one band of the array with the GOx leaving three adjacent bands unmodified. Glucose calibration curve was constructed by applying H_2O_2 oxidation voltage at the microband of interest (Figure 4.7). It was verified that the enzymatically generated peroxide spills out over the array to adjacent unmodified bands where its oxidation signals record the extent of 'cross-talk' of the peroxide.

The peroxide cross-talk reported by Quinto et.al. [57] indicated that the action of the generator could be "stealing" the peroxide produced from the glucose sensor band. The three-step oxygen flood experiment (Figure 4.2) was performed to investigate this possibility. The results of these experiments are shown in Figure 4.8and Figure 4.9. These experiments were conducted using cross-linked glutaraldehyde to immobilize GOx and applied by drop-casting. The idea is to use the generator to load the vicinity of the glucose sensor band with oxygen, but only measure the peroxide signal when the generator is off. Also, note that there is endogenous oxygen was available in the glucose solution solubilizing from the air. Additional oxygen produced by the generator electrode diffuses into the solution/gel so that it was available to the enzyme. The sensor electrode in the array detects the peroxide produced from the action of the enzyme; the current being proportional to the concentration of glucose as long as oxygen is in excess or a stable concentration. The issue with the "reductive offset" can be simply explained. The sensor microelectrode at +0.7 V vs. satd. Ag/AgCl only oxidizes peroxide, but the generator microelectrode at +1.6 V vs. satd. Ag/AgCl not only oxidizes water but also oxidizes any peroxide crossing over from the sensor electrode. The reactions at the generators are:

$H_2O \leftrightarrow 4H^+ + 4e^- + O_2 \quad E^o = +1.23$ V vs N.H.E.

$H_2O_2 \leftrightarrow 2H^+ + 2e^- + O_2 \quad E^o = +0.69$ V vs N.H.E.

The result is that the generator competes with the sensor for peroxide acting as a peroxide sink.

4.5.3.1 Effect of near vs. far generator electrodes on the peroxide diffusion

Experiments were conducted to determine the effect of proximal and distal generator site locations on the glucose signals recorded at the sensor. The hope was to find a suitable distance where less peroxide is consumed by the generator electrode, yet at the same time providing excess oxygen for the glucose reaction. In Figure 4.8, the ordinate shows the change in the absolute value of glucose signals between pre-flood and post-flood reading, with flood time plotted along the abscissa. The line demarked by red × and green ● on the plot shows the change in the absolute value of glucose signals recorded at the sensor due to the action of the generator with a 25μm separation and a 500 μm separation. Referring to Figure 4.8 with the generator and sensor on adjacent bands (25 μm apart), shows a decreasing trend in the post-flood peroxide signal with increasing the flood time. For 500 μm apart electrodes, the post-flood peroxide signal increased up to 30 seconds of flood time exposure, then gradually decreased with longer flooding times. The data indicates for the distal electrode configuration, 30 seconds of flooding optimizes the increase in post-flood glucose signal due to additional oxygen. It might be considered counterintuitive that moving the generator site away from the sensor should cause an increase in signal as oxygen from the generator emitting at a solid angle should be more diluted by the time it reaches the enzyme on the sensing electrode. However, the results show that placing the generator electrode closer to the sensor electrode reduces the peroxide signal (red line with × in Figure 4.8).

Figure 4.9 (a and b) illustrates what might be going on. Peroxide diffusion from the sensor arrives at the generator almost immediately when the generator is 25 μm away. Hence, the generation of oxygen by water electrolysis and oxidation of the peroxide diffusing from the sensor electrode

began simultaneously at the generator electrode the moment it was connected to the OER potential. Using the equation[58]-

$$t = \frac{x^2}{2D}$$

where x is the distance traveled, and D is the diffusion coefficient for oxygen. According to Tacken,[59] the diffusion coefficient for oxygen and peroxide in the buffer is 1.93 X 10^{-5} cm^2/s and 1.43 X 10^{-5} cm^2/s respectively. In a hydrogel made of PVA, the diffusion coefficients of each are about 20% of these values. For the 500 μm separation, for the arrival times predicted in Table 4.1, to have any relevance to the data, the path between the sensor-to-generator would have to be through the solution. Peroxide and oxygen must leave the gel and travel through the buffer. The predicted arrival times to the generator for peroxide through the solution begins at about 87 s which is about twice what the data suggests.

Table 4.1: Estimated arrival times for O_2 and H_2O_2 between the DME and GME microbands

Buffer	Buffer	PVA Gel	Buffer	PVA Gel
Distance	25 μm	25 μm	500μm	500 μm
O_2 Travel Time(s)	0.16	0.82	64	328
H_2O_2 Travel Time(s)	0.21	1.1	87	437

Due to the almost instantaneous stealing of peroxide by the generator when in close proximity to the sensor, the glucose signals at the sensor electrode experienced a decrease in the post-flood value throughout the experiment. The values on the table indicate that oxygen has shorter travel times compared to peroxide, i.e. oxygen diffuses faster. Unlike the 25 μm apart electrodes case, the long separation would mean that oxygen from the generator arrives at the sensor before peroxide from the sensor arrives at the generator. There is then a small window of time when the

oxygen generated by the generator was able to arrive at the sensor electrode before any stealing of peroxide by the generator electrode begins. An enhancement of glucose signal at the sensor electrode was seen during this time. After 30 s flood time, the stealing of peroxide by the generator begins, i.e. indicating the arrival of peroxide at the generator, and a decrease in the post-flood glucose signal is seen. At longer generation times, greater than 50 s, the oxygen production, and peroxide consumption reach a steady state at the generator electrode. At this point, the generator electrode became a sink for the peroxide effectively "stealing" peroxide diffusing away from the sensing electrode. In addition, there is a concentration gradient for peroxide between the sensor band and the generator band which will be discussed in the next section.

4.5.3.2 Interpretation of i-t Data by the Diffusional 'Cross-talk'

The hypothesis of diffusional cross-talk by peroxide was able to successfully explain the anomalies observed while the generator was on. The data in Figure 4.6 was re-interpreted based on the peroxide cross-talk hypothesis. In Figure 4.6(a) unexpected "reductive offsets" at the detector (sensor) microelectrode were observed while the generator microelectrode was at OER potential. This anomaly can be interpreted by the near-electrodes explanation discussed in section 4.5.3.1. Since the sensor and generator microelectrodes were only 25 µm apart, hence peroxide stealing by the generator was more than that would have been if they were far apart. This stealing of peroxide dominated the oxygen diffusion from the generator. Therefore, the detector's signal was reduced every time the generator was on, and as soon as the generator was off, the glucose signal turned back to the same trend as it had before the generator was turned on. Secondly, it was observed that as the glucose molarity became higher, the magnitude of the "reductive offest" observed at the sensor became higher when the generator was on. For example, in Figure 4.6(b) the increase in the reductive offsets for 10 mM glucose (red line) vs 60 mM glucose (brown line) was more than

double when the generator is on between 60 and 80 seconds. The explanation is that with the generator on, less glucose exists at the sensor. Higher glucose values will result in the enzyme producing peroxide at a higher rate (albeit not at the glucose-limited rate). The peroxide is either oxidized at the sensor or the generator the rates of which depend upon the diffusion gradients in either direction. The rate at which peroxide leaves the sensor to the generator depends upon the peroxide gradient between the two electrodes. Figure 4.10 shows that at +1.4 V at the generator the peroxide value is zero at the generator surface. The value of peroxide at the sensor varies with glucose concentration, so the higher glucose concentration the larger the peroxide gradient between the two electrodes. The increase in current at the generator due to the dual oxidation of peroxide and water cannot be observed. However, the loss of peroxide at the sensor is observed as an increase in the "reductive offset", which can now be seen as less peroxide at the sensor due to the action of the generator. Another way to say this is that the action of the generator increases peroxide diffusion away from the sensor at higher glucose concentrations.

4.5.4 Effect of the age of enzyme on post-flood calibration linearity

The experimental data in Figure 4.11 shows that glucose sensitivity decreases as the sensor ages. Each curve has two parts, one at a low concentration of glucose when oxygen is in excess and the sensitivity is high. As the concentration of glucose increases, the response develops an oxygen concentration component in it as well, and the sensitivity decreases, but the sensor still responds in the increase in glucose concentration. When extra oxygen is provided by the generator the sensitivity increases and there is a slight increase in the linear dynamic range. This is marked in Figure 4.11 as the projected straight lines. Note also that when extra oxygen is provided the current increase, as would be predicted with additional oxygen provided. As the enzyme ages, its activity diminishes, and so does the oxygen demand, hence the calibration curves become

gradually more linear connecting a wide range of data points and much less steep (red and blue lines corresponding to day 5 and day 10 old sensor in the diagram). For day 1 with fresh enzyme with high activity, it was found that the oxygen term dominates between 0 and 0.5 mM glucose. By day 5, the activity of the enzyme has decreased some, and the linear range has now moved to between 1.0 and 1.5 mM glucose, but the sensitivity has decreased and the 0.5 mM glucose is now below the detection limits. By day 10, the enzyme activity has diminished so that the linear range is between 2 and 4 mM, but at the expense of glucose sensitivity.

Kinetic Analysis of 1-day old sensor response

The treatment of 1-day old GOx sensor current for pre and post-flood followed the expected first-generation glucose kinetics for enzymatic reaction mechanisms.[60]

In the presence of glucose oxidase, the reaction sequence with glucose is:

$$E_{ox} + glu \xrightarrow{k_1} E_{red} + P1 \qquad (1)$$

$$E_{red} + O_2 \xrightarrow{k_3} E_{ox} + H_2O_2 \qquad (2)$$

The enzyme oxidizes β-D-glucose to glucono-δ-lactone (P1), and O_2 re-oxidizes the enzyme, producing H_2O_2.

Kinetic details are-

Reaction rates have two factors, concentration and rate constant.

At a steady-state, the rates of all steps are equal, so

$R = k_1[E_{ox}][glu]$

$R = k_3[E_{red}][O_2]$ (3)

The rates will be equal, but the magnitude of the rate will depend upon the slowest step or smallest term: which will partially dependent on the k_1 or k_3 term. k_1 is estimated to be 32 $(mM\text{-}s)^{-1}$, k_3

ranges from 440 to 2400 $(mM\text{-}s)^{-1}$. The magnitude of the slowest step is key and depends upon the relative values of glucose and oxygen.

The total concentration of the enzyme is given by:

$$C = [E_{Ox}] + [E_{red}] \qquad (5)$$

If at steady state the value of the rate can be expressed by equating the values in (3)

$$[E_{Ox}] = \frac{R}{k_1[glu]}$$

$$[E_{red}] = \frac{R}{k_3[O_2]}$$

Substituting into equation 5:

$$C = \frac{R}{k_1[glu]} + \frac{R}{k_3[O_2]} \qquad (6)$$

C is the GOx concentration (really activity), and if it is assumed that the activity does not change over the life-time of one experiment, C is a constant. Note that an increase in either glucose or oxygen will increase the rate so that C remains constant. The rate of peroxide production, R, is proportional to current :

$$C = \beta i \left(\frac{1}{k_1[glu]} + \frac{1}{k_3[O_2]}\right) \qquad (7)$$

Where β is an empirical conversion factor converting reaction rate to current i.

Solving for i:

$$i = \frac{C}{\beta} \frac{k_1[Glu]k_3[O_2]}{k_1[Glu] + k_3[O_2]} \qquad (8)$$

Note the if the oxygen term dominates the current will be:

$$i = \frac{C}{\beta} k_1[Glu]$$

With excess oxygen, the current will be directly proportional to glucose concentration and this basis of the electrochemical sensor for glucose.

If the glucose term dominates then:

$$i = \frac{C}{\beta} k_3 [O_2]$$

And the sensor measures oxygen instead, which is the issue with first-generation glucose sensors. If the oxygen and glucose terms are similar in magnitude then equation 8 including both oxygen and glucose provides the model.

We were not able to measure the oxygen at the sensor surface, but we could estimate the oxygen with the generator open circuit by assuming it was that of air saturation. Oxygen saturation is 7.6 mg O_2 per liter. Conversion to mM oxygen would be.

$$\frac{0.0076\ g\ O_2}{L} \frac{1000\ mM\ O_2}{32\ g\ O_2} = 0.237\ mM$$

As reported by Goodisman the glucose values are known the values for k_1 and k_3 vary over a range: $23<k_1<32$ and $800<k_3<2400$, For this case, the current was plotted against the term $k_1[Glu]k_3[O_2]$ in equation 8 and shown in Figure 4.12. With the ambient case ($[O_2]$ = 0.237 mM), and with glucose values known, a model curve for current i, was plotted using equation 8, and the values of k_1 and k_3, adjusted to the best fit of the data, Figure 4.12. These values were: k_1=60; k_3=600. The k_1 is outside the range of values reported in the literature, but the literature values were estimated in homogenous solutions and not enzyme sequestered on an electrode. There could also be a diffusional component to the current but that aspect was not investigated.

With the generator on there is an increase in current due to added oxygen. It is possible to predict what oxygen level would have to be to increase the pre-flood current to the post-flood current data.

Figure 4.12 b is a plot of the current for post-oxygen flood (orange dots). The dashed line is the predicted line from the above equation (8). The oxygen value that makes the fit is 0.35 mM oxygen. If the oxygen level of the preflood is assumed to be that of air saturation, or 0.237 mM, the action of the generator increases the oxygen by more than a factor of 1.5 or a 50% increase in oxygen in the local of the sensor.

The question then becomes: is enough oxygen is generated to achieve glucose-limited current? The answer is that it depends on the activity level of the enzyme. The action of the oxygen generator increases the linear dynamic range for glucose. By looking at the tabulated values for k_1[Gul] and $k_3[O_2]$ only the lower levels of glucose in this experiment will achieve the glucose limit rate. The range is variable depending on the activity of the enzyme.

4.6 Conclusion

The practical implementation of the oxygen-generation scheme showed initial promise, but the inability to reproduce the experiment led to numerous experiments that extended the project for three years. One of the most difficult obstacles to overcome was to recognize that the action of the generator removes the peroxide produced from the action of the enzyme at the sensors local. The most sensitive and stable glucose response was found with a gold sensing electrode, and a Ti/Pt generating electrode. These could be fashioned by gold plating one of the microbands of a Ti/Pt array. The peroxide signal from the enzyme could be maximized by placing the generator at one end of the array and the sensor at the other.

Indications are that the scheme will works best when glucose concentrations are below 1 mM for this particular configuration used in the experiment. At greater concentration, the micro-sized generating electrode can not produce enough oxygen.

4.7 Acknowledgments

The authors acknowledge financial support from the Arkansas Biosciences Institute, the major research component of the Arkansas Tobacco Settlement Proceeds Act of 2000. The authors are also grateful to Error Porter, and Dr. Ang research group from HiDEC facility at the University of Arkansas for the guidance with Ti/Pt MEAs fabrication used in the experiments, Emily C. Anderson and Benjamin J. Jones from the Fritsch research group for the design of the electrode chip. The authors are thankful to Aisha Soliman, and Jansen Reidler from Dr. Paul's research group for participating in some of the experiments mentioned in this chapter.

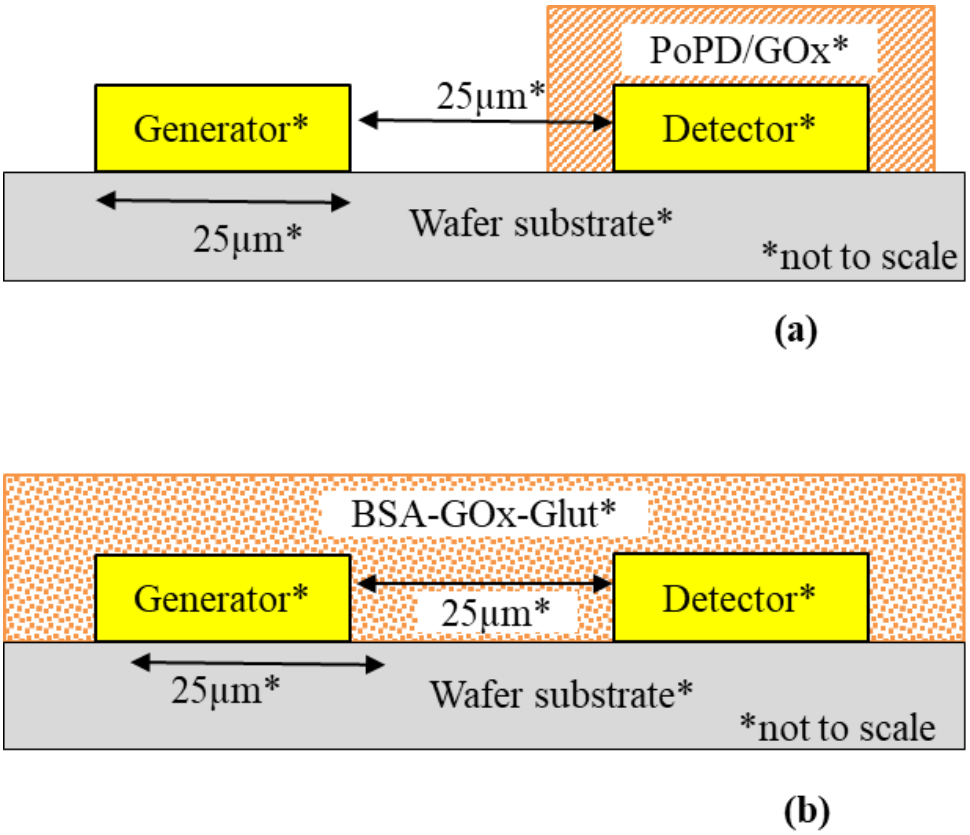

Figure 4.1 Schematic of sensor microelectrode preparation: (a) sensor construction on selective microband by applying electropolymerization technique; (b) sensor construction covering the whole array by applying the drop-cast technique

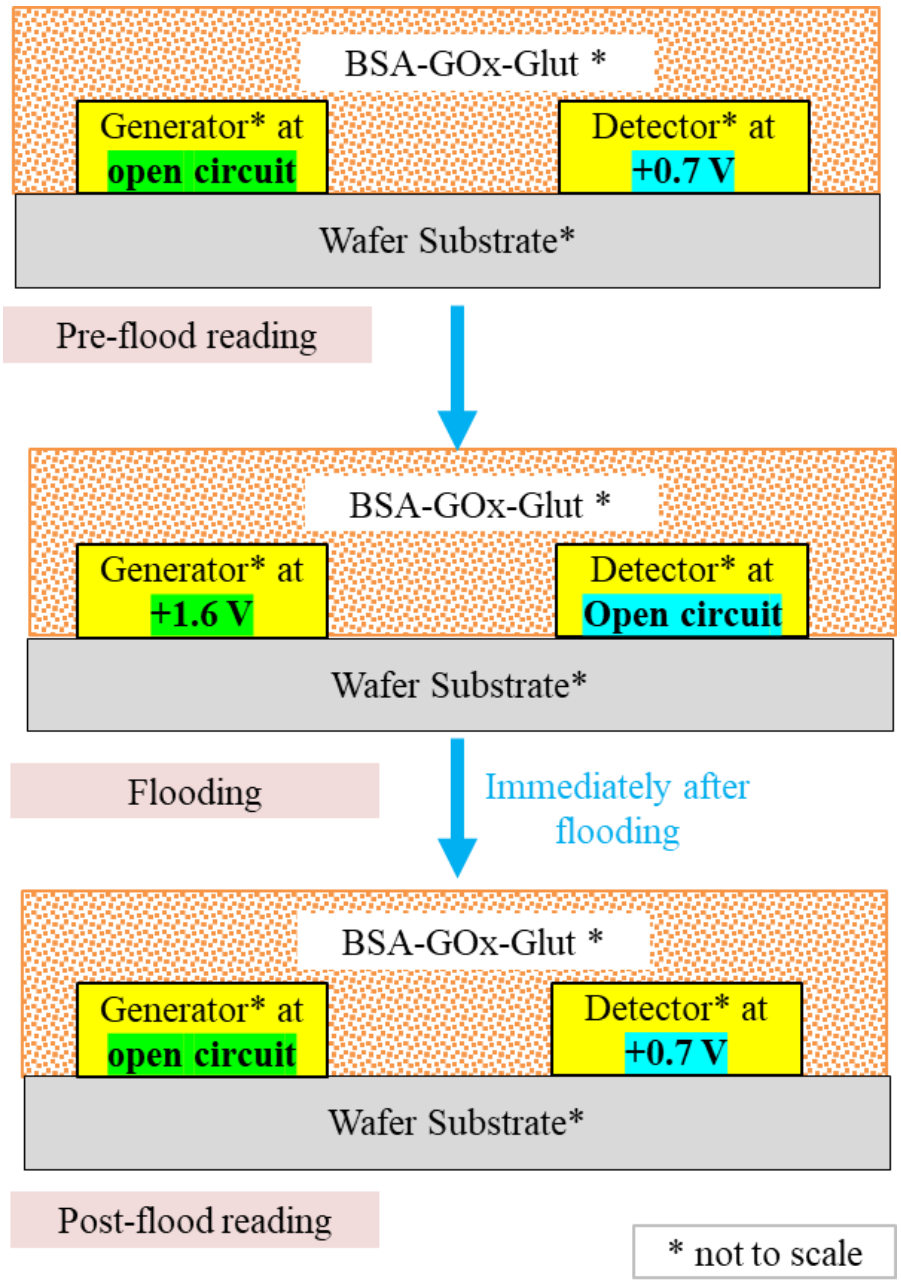

Figure 4.2 Schematic representation of the three-step oxygen flooding experiment to verify the cross-talk hypothesis of peroxide. BSA-GOx-Glut sensor drop cast on the Ti/Pt MEA was used for this experiment. All the potentials mentioned here are with respect to Ag/AgCl in saturated KCl.

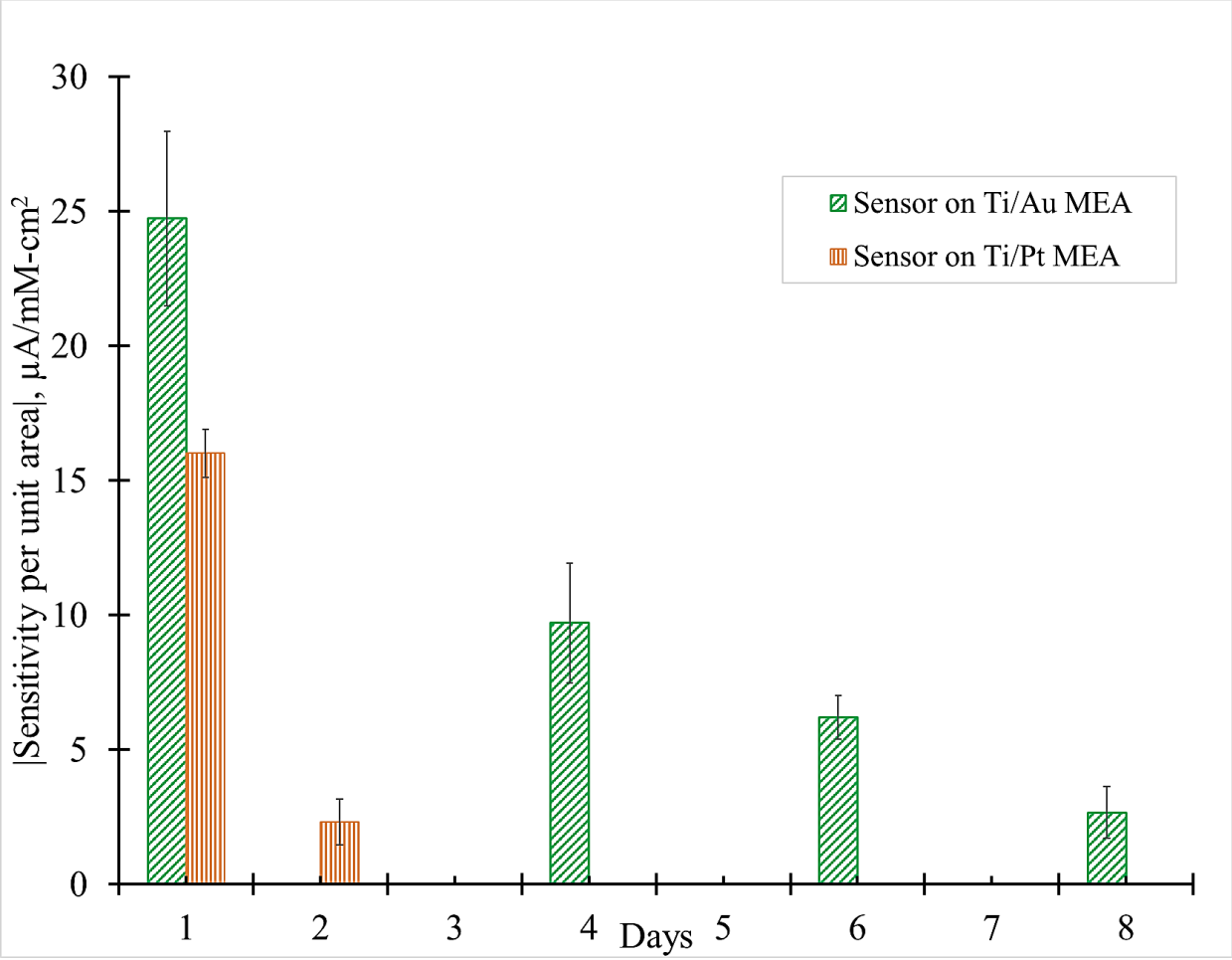

Figure 4.3 Sensitivities over time for the GOx electropolymerized on pure Pt platinized Ti/ Au (green) and Ti/Pt (orange) microband; Green column showing sensitivities on day 1, 4, 6, 8 were (24.73±3.25) µA/mM-cm^2 (R^2= 0.92), (9.71±2.23) µA/mM-cm^2 (R^2= 0.79), (6.20±0.81) µA/mM-cm^2 (R^2= 0.92), and (2.67±0.96) µA/mM-cm^2 (R^2= 0.61) respectively, orange column showing sensitivity on day 1 was (16.01±0.89) µA/mM-cm^2 (R^2= 0.99), on day 2 lowered by 1.3 times to (2.31±0.86) µA/mM-cm^2 with reduced linearity (R^2= 0.71).

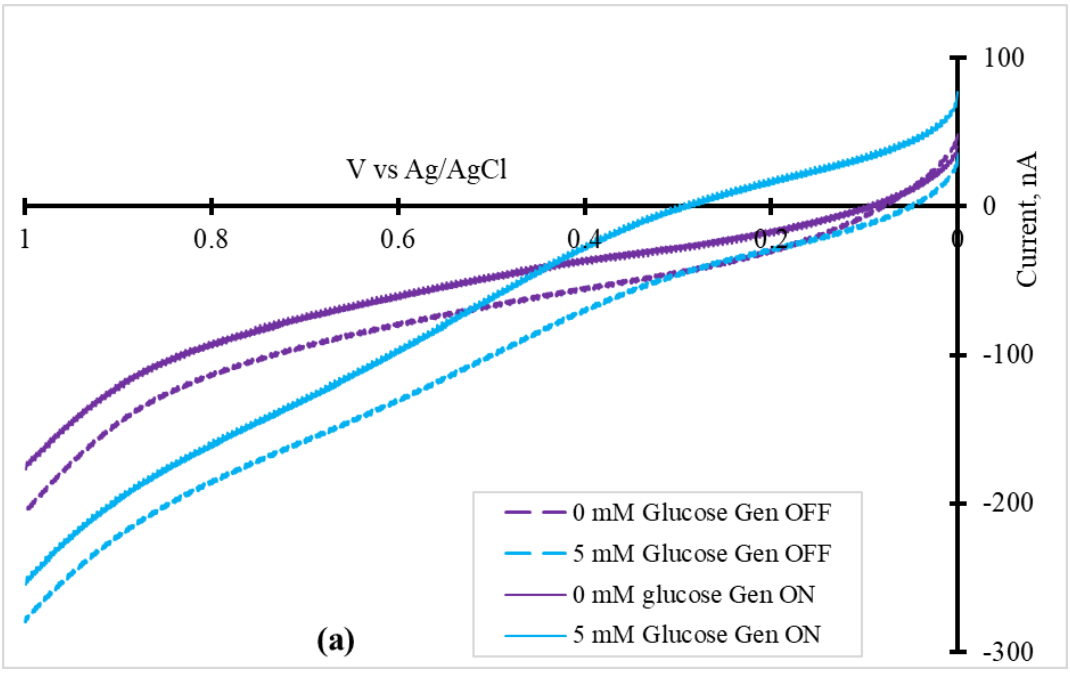

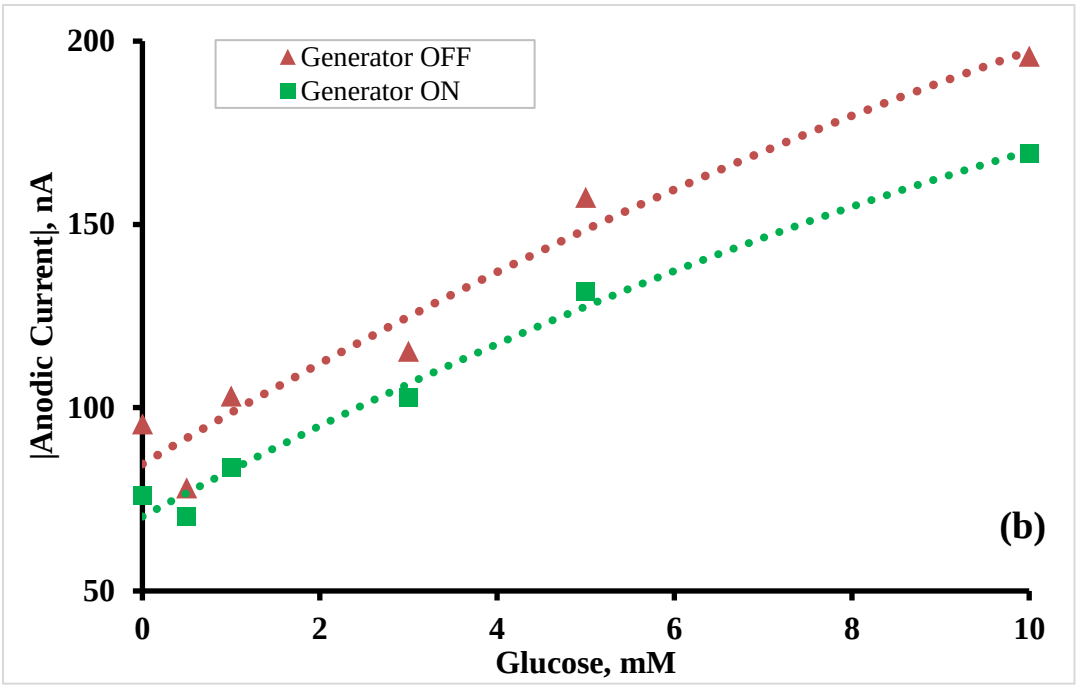

Figure 4.4 (a) 0-1 V CV for 0 mM (blue) and 5 mM (purple) glucose at the GOx sensor on the pure Pt platinized Ti/ Au band in ambient condition (dashed line) vs additional oxygen condition by oxygen generation by the 25 µm distant generator electrode (solid line) (b) Glucose calibration curves with added oxygen from generator on (green line) vs. generator off (red line). The 'generator on' curve was opposite of what might be expected with addition oxygen provided.

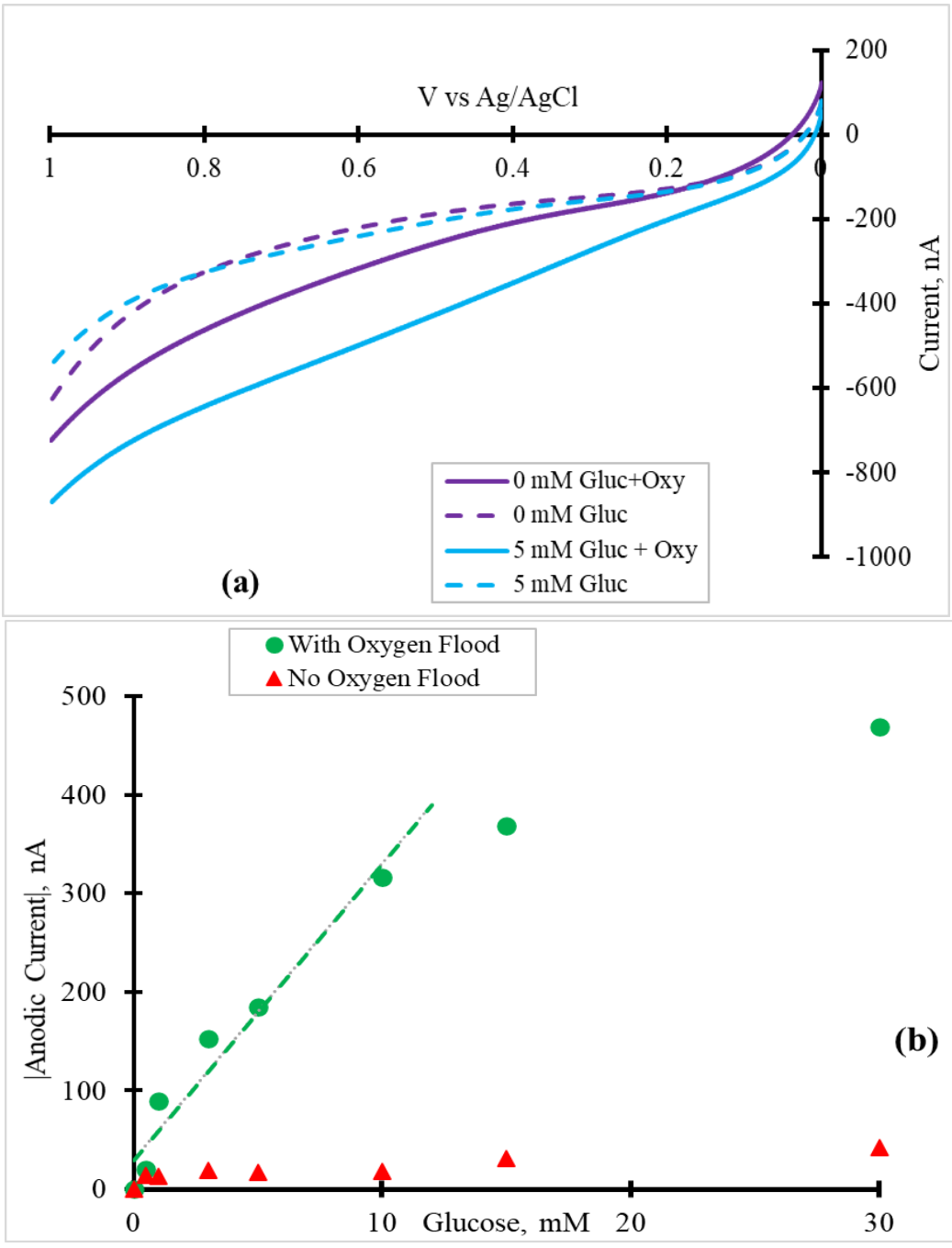

Figure 4.5 (a) 0-1 V CV for 5 mM Glucose at the GOx sensor on the pure Pt platinized Ti/ Au band for ambient condition (in blue) vs additional oxygen condition by oxygen generation by the 25 µm distant generator electrode (purple), the generator response at +1.4 V is shown in green; (b) Glucose calibration curve comparison with added oxygen (green) vs. ambient oxygen (red). Current values are taken as the difference between current a 0.0 V and +0.7V vs satd. Ag/AgCl. The dashed green line brings out the point that the calibration curve becomes nonlinear with added oxygen. But the sensitivity dramatically increases to about 30 nA/ mM.

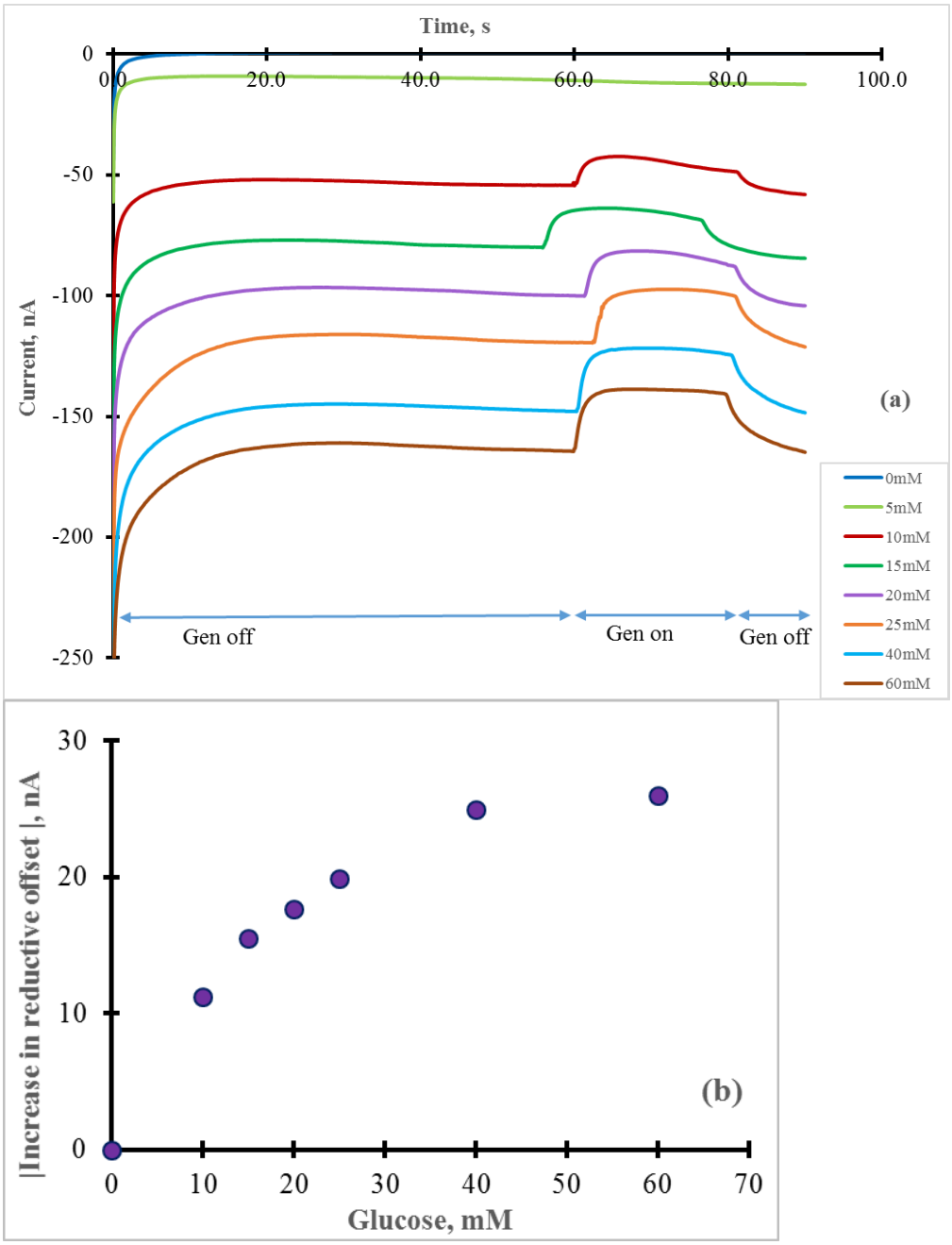

Figure 4.6 (a)Individual amperometric i-t responses at the sensor with no stirring for various glucose concentrations between 0-60 mM. As expected, an increase in oxidative response was observed for increasing glucose concentrations when the generator was off, but when the generator was on a reductive offset was seen (b) corresponding increase in reductive offsets between initial gen off and gen on (between 55 to 65 seconds); the Ti/Pt/PoPD/GOx sensor was at +0.7 V and the Ti/Pt generator at connected +1.4 V. Each time the generator was on, the reduction current at the detector was evident and there was a nonlinear increase in reductive offsets with increase in glucose.

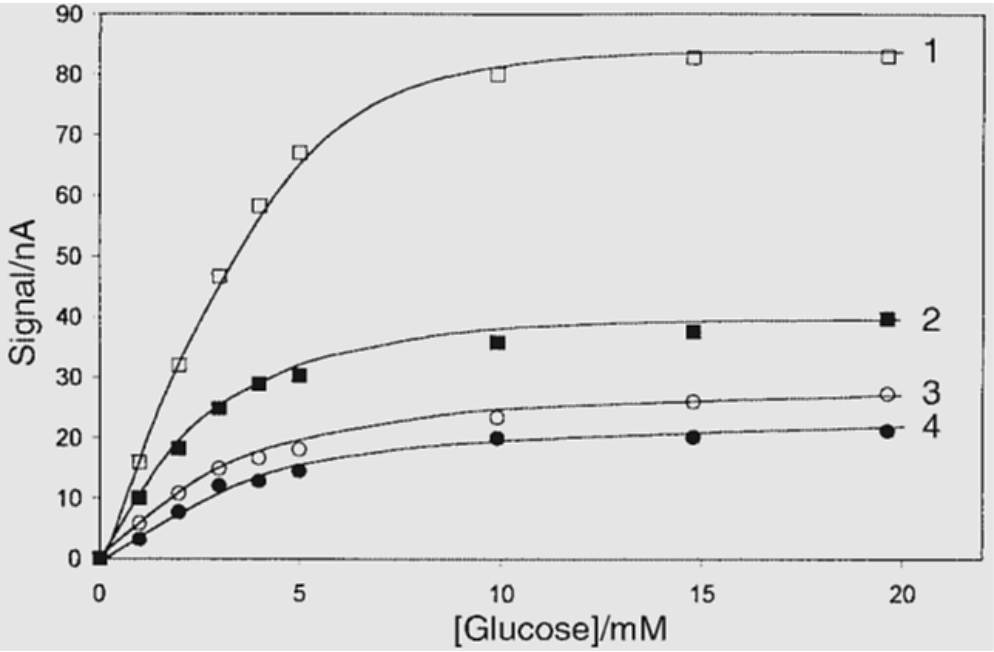

Figure 4.7 Calibration curves relevant to the four microbands. 1, GOx modified microband; 2-4 the second, third, and fourth unmodified microbands, respectively. The measurements were performed applying the H2O2 oxidation potential (E = 650 mV vs. SCE) only at the microband of interest. The figure was taken from Quinto, M.; Palmisano, F.; Koudelka-Hep, M., Enzyme modified microband electrodes: cross-talk effects and their elimination. Analyst (Cambridge, U. K.) 2001, 126 (7), 1068-1072

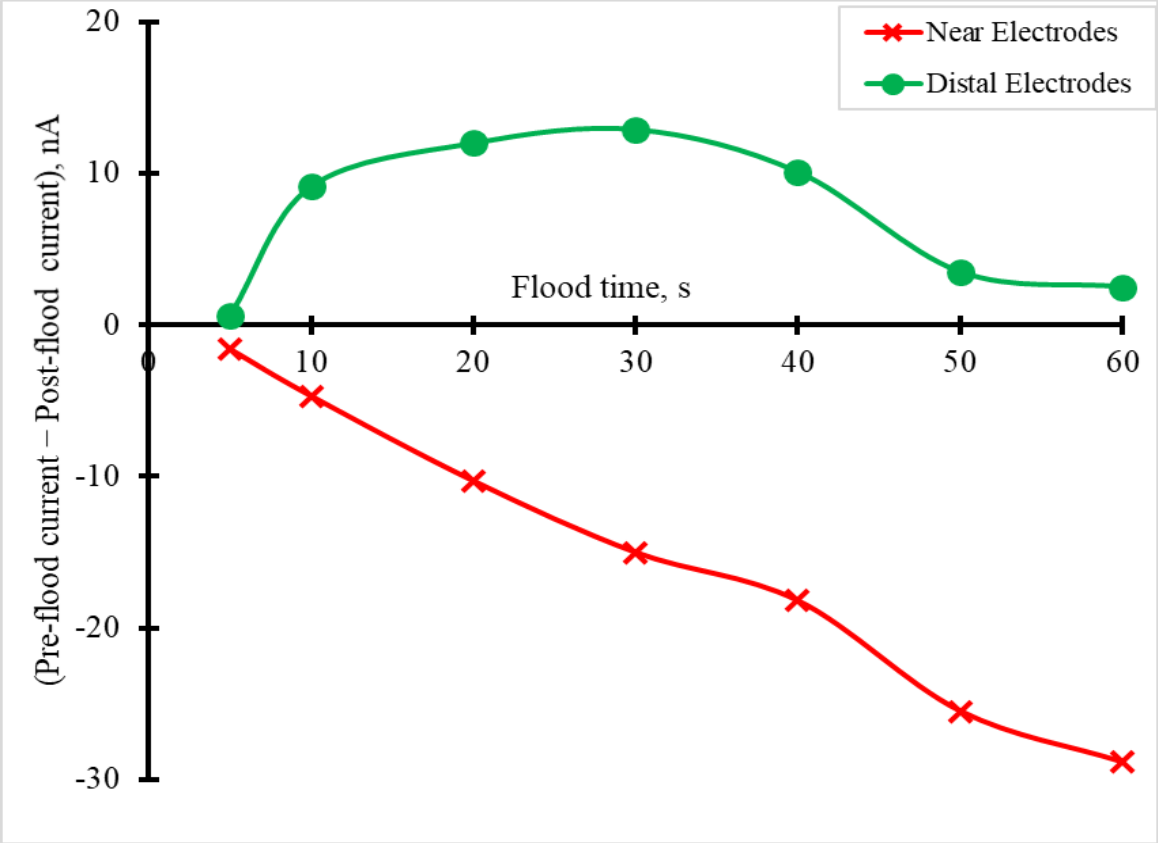

Figure 4.8 The effect of distance between the oxygen generation and the glucose detecting electrodes on the Ti/Pt MEA. Line demarked by red × = generator and detector electrode separated by 25 µm; line demarked by green ● = generator and detector separated by 500 µm. The line only serves as an aid to the eye.

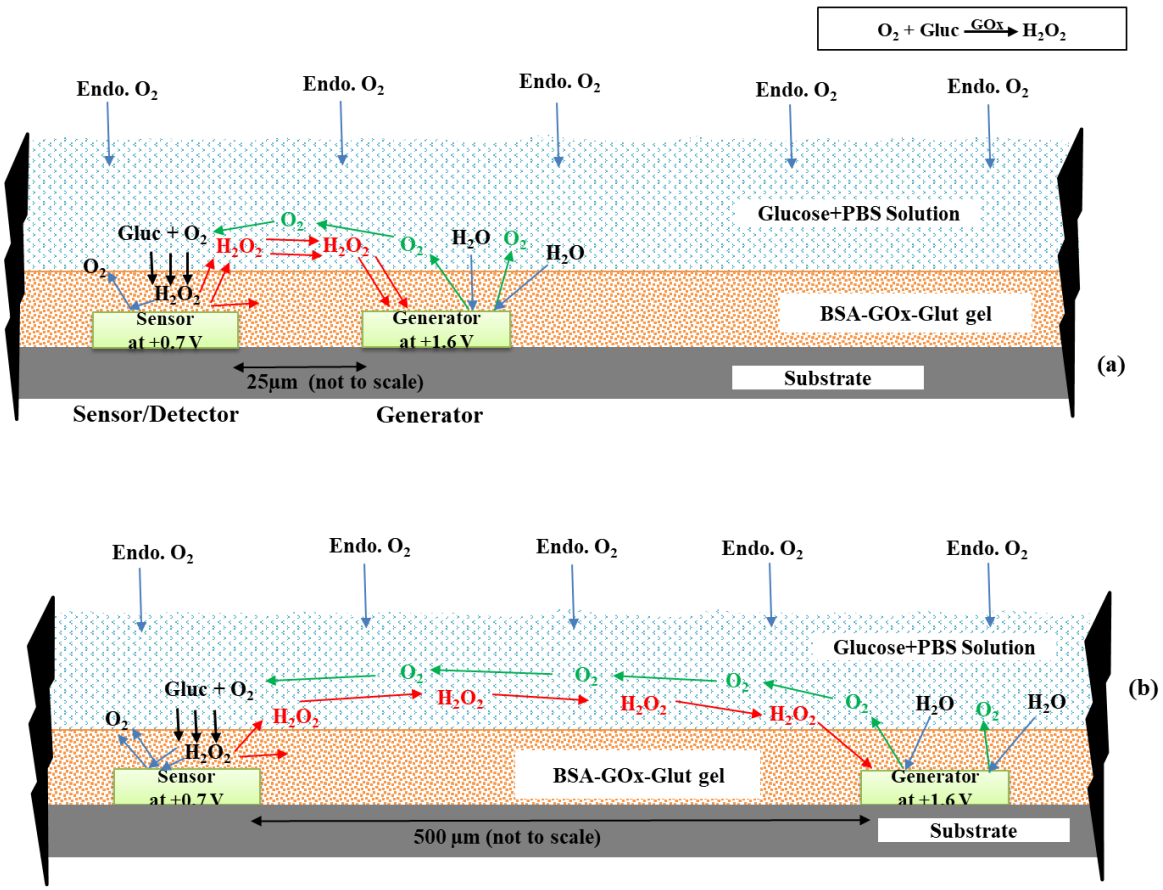

Figure 4.9 Schematic representation of the hypothesis of hyperoxide stealing by the generator and the effect of distance between the oxygen generator and glucose sensor electrode when they are (a) 25 µm apart and (b) 500 µm apart (not to scale). The substrate here is Si substrate, sensor, and generator both are Ti/Pt microband electrodes (25 µm X 2000 µm). Glucose enzymatic reactions are shown with black arrows, peroxide stealing with red arrows, oxygen generated by the generator electrode with green arrows, and all other sources of oxygen (oxygen generated from peroxide oxidation and endogenous oxygen) are shown with blue arrows. All the potentials mentioned in the diagram are with respect to the reference electrode Ag/AgCl in saturated KCl.

(b)

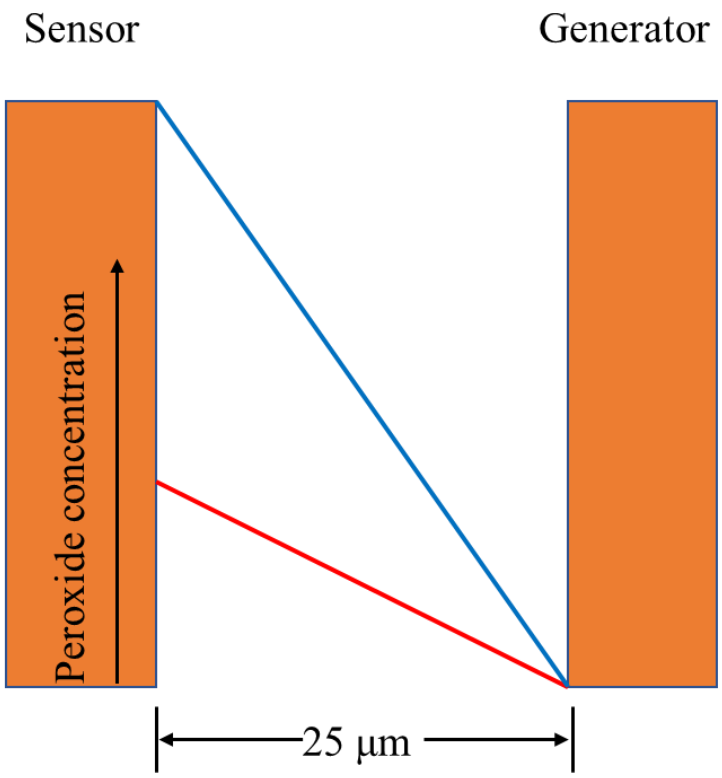

Figure 4.10 Peroxide diffusion gradients between sensor and generator: Red- low peroxide concentration gradient with lower glucose concentration; blue - high peroxide concentration gradient with higher glucose concentrations. Higher concentrations of glucose increases diffusion of peroxide away from the sensor.

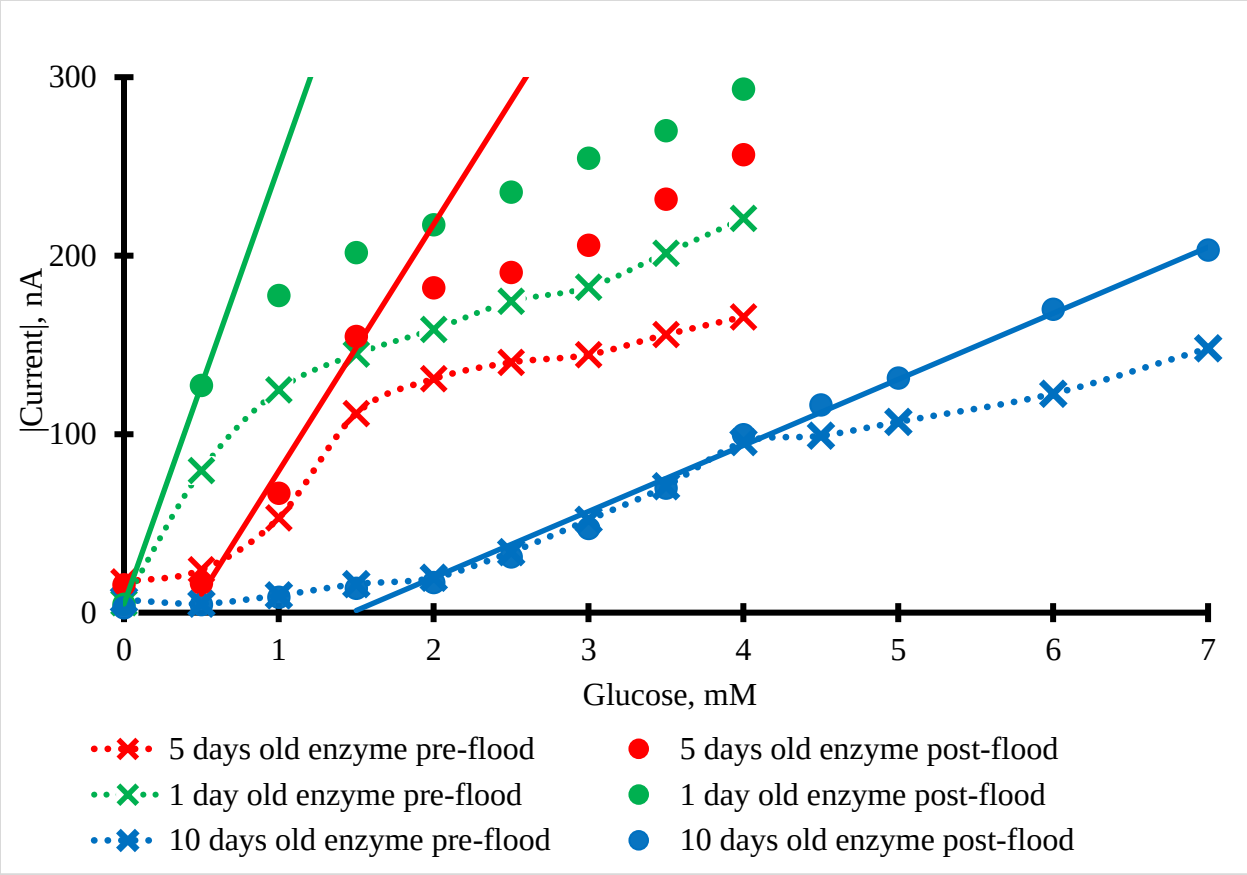

Figure 4.11 Effect of the age of GOx enzyme on the GOx sensor's post-flood linearity. Age of Enzyme: green- 1 Day old sensor, red: 5 days old, blue: 10 days old. With time from day 1 to day 10, the enzyme activity gradually diminishes resulting in decreased glucose sensitivity and oxygen demand, hence the calibration curves become less steep, and linear trendlines connect wider range of data points over time.

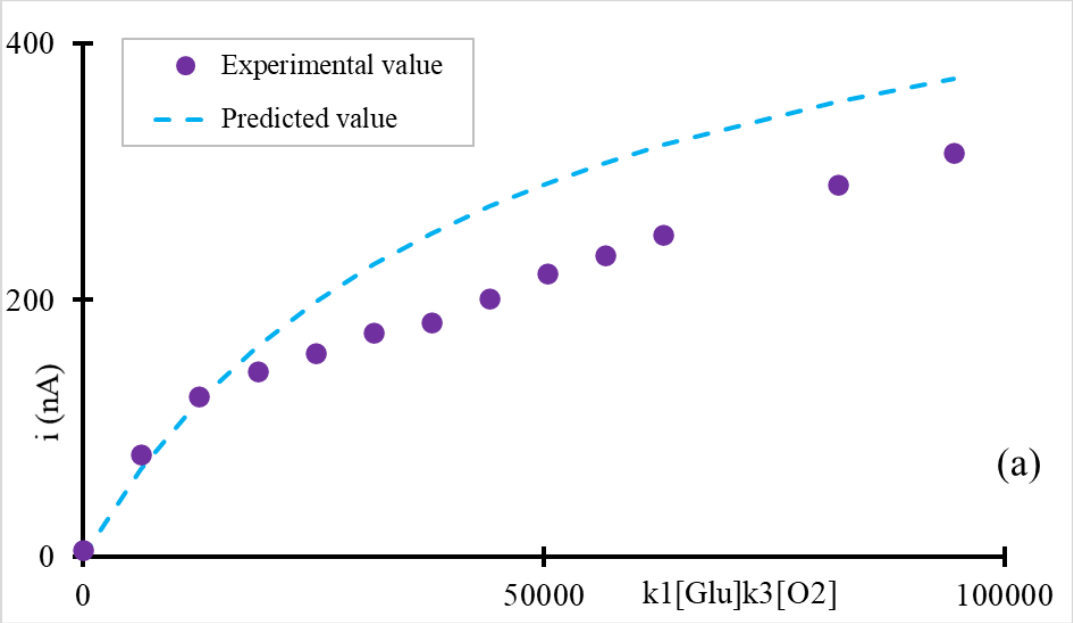

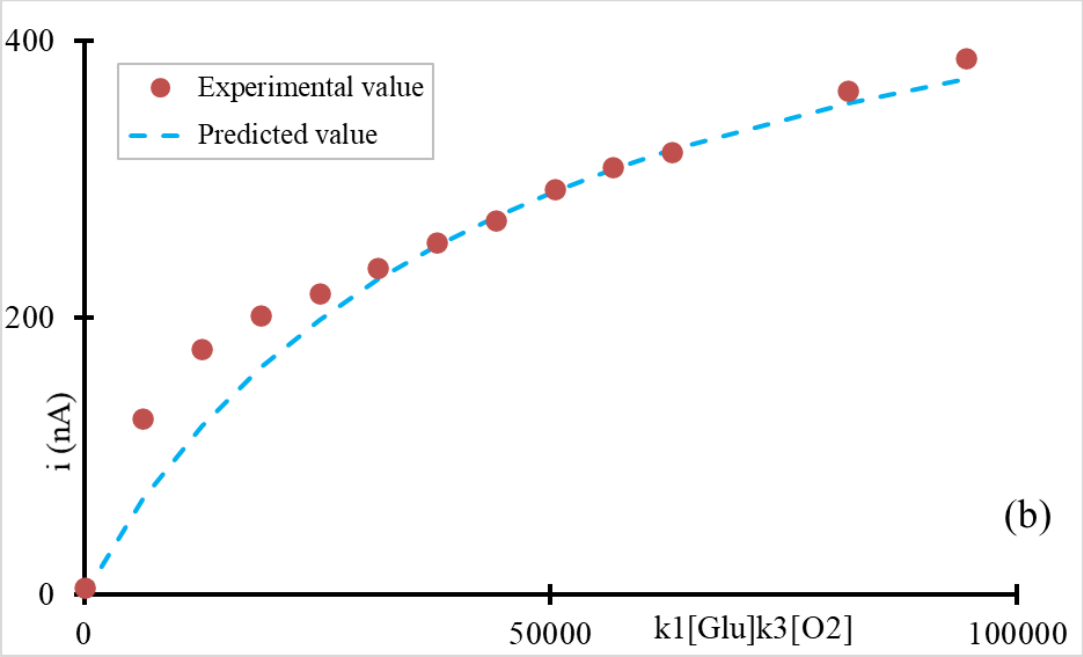

Figure 4.12 (a) Purple dots - preflood current; dashed line - predicted current using equation 8 with fitted values for k1 and k3 (b) post-flood current (orange dots); dashed line - predicted current using equation (8) with an oxygen value of 0.35 mM that makes the fit.

4.8 References

1. P. Jin, A. Yamaguchi, F. A. Oi, S. Matsuo, J. Tan and H. Misawa, *Analytical sciences*, 2001, **17**, 841-846.

2. N. Radhakrishnan, J. Park and C.-S. Kim, *Sensors*, 2012, **12**, 8955-8965.

3. G. Rocchitta, O. Secchi, M. D. Alvau, D. Farina, G. Bazzu, G. Calia, R. Migheli, M. S. Desole, R. D. O'Neill and P. A. Serra, *Analytical chemistry*, 2013, **85**, 10282-10288.

4. R. Devasenathipathy, V. Mani, S.-M. Chen, S.-T. Huang, T.-T. Huang, C.-M. Lin, K.-Y. Hwa, T.-Y. Chen and B.-J. Chen, *Enzyme and microbial technology*, 2015, **78**, 40-45.

5. N. Hernández-Ibáñez, L. García-Cruz, V. Montiel, C. W. Foster, C. E. Banks and J. Iniesta, *Biosensors and bioelectronics*, 2016, **77**, 1168-1174.

6. L. P. Andrus, R. Unruh, N. A. Wisniewski and M. J. McShane, *Biosensors*, 2015, **5**, 398-416.

7. M. Marrakchi, S. V. Dzyadevych, F. Lagarde, C. Martelet and N. Jaffrezic-Renault, *Materials Science and Engineering: C*, 2008, **28**, 872-875.

8. C. P. McMahon, G. Rocchitta, P. A. Serra, S. M. Kirwan, J. P. Lowry and R. D. O'Neill, *Analytical Chemistry*, 2006, **78**, 2352-2359.

9. C. P. McMahon, G. Rocchitta, P. A. Serra, S. M. Kirwan, J. P. Lowry and R. D. O'Neill, *Analyst*, 2006, **131**, 68-72.

10. S. K. Hamdan, *The Malaysian Journal of Medical Sciences: MJMS*, 2014, **21**, 12.

11. G. Hughes, R. M. Pemberton, P. R. Fielden and J. P. Hart, *TrAC Trends in Analytical Chemistry*, 2016, **79**, 106-113.

12. Y. Deng, W. Wang, L. Zhang, Z. Lu, S. Li and L. Xu, *Journal of biomedical nanotechnology*, 2013, **9**, 318-321.

13. C. González-Gaitán, R. Ruiz-Rosas, E. Morallón and D. Cazorla-Amorós, *RSC advances*, 2017, **7**, 26867-26878.

14. A. M. Azevedo, D. M. F. Prazeres, J. M. S. Cabral and L. P. Fonseca, *Biosensors and Bioelectronics*, 2005, **21**, 235-247.

15. M. Pohanka and P. Skládal, *Journal of applied biomedicine*, 2008, **6**.

16. O. Secchi, M. Zinellu, Y. Spissu, M. Pirisinu, G. Bazzu, R. Migheli, M. S. Desole, R. D. O'Neill, P. A. Serra and G. Rocchitta, *Sensors*, 2013, **13**, 9522-9535.

17. H. B. Yildiz and L. Toppare, *Biosensors and Bioelectronics*, 2006, **21**, 2306-2310.

18. Y. P. Wen, L. M. Lu, D. Li, M. Liu, H. H. He and J. K. Xu, *Chinese Chemical Letters*, 2012, **23**, 221-224.

19. Y. Wen, J. Xu, M. Liu, D. Li and H. He, *Applied biochemistry and biotechnology*, 2012, **167**, 2023-2038.

20. M. Liu, Y. Wen, J. Xu, H. He, D. Li, R. Yue and G. Liu, *Analytical Sciences*, 2011, **27**, 477-477.

21. R. Monošík, M. Stred'anský and E. Šturdík, *Journal of clinical laboratory analysis*, 2012, **26**, 22-34.

22. L. Kumari and S. S. Kanwar, 2012.

23. X. Lin, Y. Ni and S. Kokot, *Sensors and Actuators B: Chemical*, 2016, **233**, 100-106.

24. M. Trojanowicz and M. L. Hitchman, *TrAC Trends in Analytical Chemistry*, 1996, **15**, 38-45.

25. R. M. Santos, J. Laranjinha, R. M. Barbosa and A. Sirota, *Biosensors and Bioelectronics*, 2015, **69**, 83-94.

26. M. M. Rodríguez-Delgado, G. S. Alemán-Nava, J. M. Rodríguez-Delgado, G. Dieck-Assad, S. O. Martínez-Chapa, D. Barceló and R. Parra, *TrAC Trends in Analytical Chemistry*, 2015, **74**, 21-45.

27. G. Favero, G. Fusco, F. Mazzei, F. Tasca and R. Antiochia, *Nanomaterials*, 2015, **5**, 1995-2006.

28. C. Lete, S. Lupu, B. Lakard, J.-Y. Hihn and F. J. del Campo, *Journal of Electroanalytical Chemistry*, 2015, **744**, 53-61.

29. P. A. Raymundo-Pereira, T. A. Silva, F. R. Caetano, L. Riboviski, E. Zapp, D. Brondani, M. F. Bergamini, L. H. M. Junior, C. E. Banks and O. N. Oliveira Jr, *Analytica Chimica Acta*, 2020.

30. M. Sýs and K. Vytřas, *Current medicinal chemistry*, 2018, **25**, 3988-4006.

31. S. Tembe, S. Inamdar, S. Haram, M. Karve and S. F. D'Souza, *Journal of biotechnology*, 2007, **128**, 80-85.

32. G. Rocchitta, A. Spanu, S. Babudieri, G. Latte, G. Madeddu, G. Galleri, S. Nuvoli, P. Bagella, M. I. Demartis and V. Fiore, *Sensors*, 2016, **16**, 780.

33. H. H. Nguyen, S. H. Lee, U. J. Lee, C. D. Fermin and M. Kim, *Materials*, 2019, **12**, 121.

34. A. Economou, S. K. Karapetis, G.-P. Nikoleli, D. P. Nikolelis, S. Bratakou and T. H. Varzakas, *Advances in Food Diagnostics; Toldrá, F., Nollet, LML, Eds*, 2017, 231-250.

35. C. A. Cordeiro, M. G. de Vries, W. Ngabi, P. E. Oomen, T. Cremers and B. H. C. Westerink, *Biosensors and Bioelectronics*, 2015, **67**, 677-686.

36. R. Wilson and A. P. F. Turner, *Biosensors and Bioelectronics*, 1992, **7**, 165-185.

37. J. Wang, *Chemical reviews*, 2008, **108**, 814-825.

38. B. M. Dixon, J. P. Lowry and R. D O'Neill, *Journal of Neuroscience Methods*, 2002, **119**, 135-142.

39. Q. Liu and P. Wang, *Cell-based biosensors: principles and applications*, Artech House, 2009.

40. P. K. Nair, D. G. Buerk and J. H. Halsey, Jr., *Stroke*, 1987, **18**, 616-622.

41. L. Wang, Y. Li, H. Han, G. Liu and P. G. Osborne, *Neurosci. Lett.*, 2003, **344**, 91-94.

42. Y. Hu and G. S. Wilson, *Journal of neurochemistry*, 1997, **69**, 1484-1490.

43. R. Tipnis, S. Vaddiraju, F. Jain, D. J. Burgess and F. Papadimitrakopoulos, *Journal of diabetes science and technology*, 2007, **1**, 193-200.

44. R. A. Croce, S. Vaddiraju, F. Papadimitrakopoulos and F. C. Jain, *Sensors*, 2012, **12**, 13402-13416.

45. Y. Zhang and G. S. Wilson, *Analytica chimica acta*, 1993, **281**, 513-520.

46. C. Malitesta, F. Palmisano, L. Torsi and P. G. Zambonin, *Analytical chemistry*, 1990, **62**, 2735-2740.

47. L. Zhang and J. Lian, *Journal of Solid State Electrochemistry*, 2008, **12**, 757-763.

48. J. I. R. De Corcuera, R. P. Cavalieri and J. R. Powers, *Journal of Electroanalytical Chemistry*, 2005, **575**, 229-241.

49. N. P. Sardesai, M. Ganesana, A. Karimi, J. C. Leiter and S. Andreescu, *Analytical chemistry*, 2015, **87**, 2996-3003.

50. S. Holdcroft and B. L. Funt, *Journal of electroanalytical chemistry and interfacial electrochemistry*, 1988, **240**, 89-103.

51. M. Zecchino, *Journal*, 2005.

52. R. K. Scopes, *e LS*, 2001.

53. I. Losito, E. De Giglio, N. Cioffi and C. Malitesta, *Journal of Materials Chemistry*, 2001, **11**, 1812-1817.

54. J. W. Long, C. P. Rhodes, A. L. Young and D. R. Rolison, *Nano Letters*, 2003, **3**, 1155-1161.

55. G. A. El-Sherbeny, A. A. Shindia and Y. Sheriff, *Int J Agric Biol*, 2005, **7**, 953-958.

56. N. W. Barton, V. Lipovac and A. Rosenberg, *Journal of Biological Chemistry*, 1975, **250**, 8462-8466.

57. M. Quinto, M. Koudelka-Hep and F. Palmisano, *Analyst*, 2001, **126**, 1068-1072.

58. J. B. Allen and R. F. Larry, *Electrochemical methods fundamentals and applications*, John Wiley & Sons, 2001.

59. S. A. M. van Stroe-Biezen, F. M. Everaerts, L. J. J. Janssen and R. A. Tacken, *Analytica chimica acta*, 1993, **273**, 553-560.

60. Z. Tao, R. A. Raffel, A.-K. Souid and J. Goodisman, *Biophysical journal*, 2009, **96**, 2977-2988.

5. Conclusions and future work

5.1 Conclusions

This research work investigated the practicality of electrochemically generating additional oxygen for first-generation glucose sensors. The results are expected to make an important contribution to the development of in vivo glucose sensors functioning in hypoxic conditions. The proposed scheme was proven for glucose sensing but should be applicable to other oxidase sensors requiring additional oxygen. Sensor construction over microelectrode arrays benefits it from the advantages microelectrode arrays offer for in-vivo applications. Although the straight transfer of glucose sensor construction methods from macroelectrodes to microelectrodes was unsuccessful, successful GOx immobilization and glucose sensing on the microband electrodes was unique. Because of enzyme-generated peroxide cross-talk, it may not be possible to densely populate individual oxidase biosensors onto a single chip. However, the successful construction of a glucose sensor onto a microband electrode opens the possibility of use with other non-oxidase based sensors constructed on other members of the array. To the author's knowledge, no investigations on the optimization and stability of the glucose sensors, and oxygen electro-generation on micro band electrode arrays have been reported. The operational life of both the microband glucose sensor and the generating electrode was found to depend upon the adhesion/conducting metal couples that were incorporated into the fabrication of the MEA. Ti/Pt metal layer microbands showed superior sustainability towards OER potential, while glucose sensors constructed on the platinized Au microbands showed higher glucose sensitivity and longer stability than on unmodified Pt microbands.

To the author's knowledge, no previous work has been published on the implementation of oxygen generation coupled with glucose-sensing incorporated onto a microband electrode array. The

proposed scheme of using electrogenerated oxygen to travel to the neighboring bands was verified. The discovery of unanticipated reductive responses at the glucose sensor during oxygen production led to the emphasis on investigating the causes behind such a response. The investigation successfully detected the peroxide "stealing" by diffusional cross-talk of the enzyme-generated peroxide and was verified through several experiments. The rate of diffusional cross-talk of peroxide was found to depend on the rate of peroxide production which is proportional to the concentration of the glucose present at the enzymatic reaction site. For this reason, the glucose signal is decreased further at higher glucose concentrations. After the discovery of the peroxide cross-talk to the generator, the research was focused on how to minimize the effects of peroxide diffusing to adjacent bands. Preliminary experiments showed an increase of the micro-range distance between the sensing band and the oxygen-generating band from 25 μm to 500 μm with temporal separation of oxygen-generating and glucose-sensing proved that the concept was viable.

5.2 Future work

A number of prospective solutions to minimize/eliminate the effects of peroxide diffusing to oxygen generating band can be suggested as future investigative studies. First, a diffusion barrier for peroxide between the sensor and the generator can be created. In this method, the barrier is created between the detector and generator electrodes by applying peroxide oxidizing potentials at the unmodified microbands adjacent to the GOx modified band. Peroxide consumption occurring at these adjacent microbands limits the diffusion of the peroxide generated. This is shown schematically in Figure 5.1. The idea is to use bands adjacent to the enzyme-modified band (poised at +0.7V vs satd. Ag/AgCl) to oxidize and therefore consume the peroxide as it is making its way to the oxygen-generating band. The additional bands collect more of the peroxide signal leading to improved limits of detection and glucose sensitivity. Oxygen, due to its slow electron

transfer, does not reduce at the potentials set at the intermediate electrodes, which allows it to proceed to the sensor band providing the necessary oxygen.

The second possibility would be to modify the bands between the sensor and the generator with catalase enzyme to consume the peroxide on its way to the oxygen-generating band.[1, 2] Quinto showed that the deposition of a catalase layer on the microbands adjacent to the GOx modified band resulted in superior efficacy in peroxide cross-talk elimination over other approaches.[1] The disadvantage might be that some of the peroxide signals from the reaction with glucose is destroyed, raising detection limits and reducing sensitivity.

A third potential solution would be a bi-enzyme approach to construct the glucose sensor microband proposed by Kulys.[3-5] In this method, a microband electrode is constructed coupling the oxidase enzyme with a peroxidase enzyme. The peroxide generated by the reaction of the oxidase enzyme with glucose is then reduced by the action of the peroxidase enzyme to water; thus reducing the possibility of peroxide cross-talk. At the same time, the coupled enzyme electrode results in a significant drop in the working potential of the enzyme electrode compared to the enzyme electrode based on glucose oxidase only. Studies show that the coupling of glucose oxidase with the peroxidase enzyme lowers the glucose detection potential from 0.65V to -0.1V.[4]

Other possibilities: The enhanced performance of glucose sensing by the action of the generator is modest. One approach might be to increase the enzyme sensor's glucose sensitivity but with more efficient use of the oxygen available. Studies conducted by McMahon discovered that a first-generation GOx sensor with enzyme deposited over a PoPD polymer showed ~20 times higher sensitivity to glucose than a sensor configuration with enzyme immobilized under PoPD polymer.[6] This feature allows precise glucose monitoring independent of small fluctuations in oxygen

concentration.[6, 7] If this GOx immobilization method were coupled with the oxygen generation scheme, there should be a significant increase in the linear dynamic range for glucose sensing.

It was evident from chapter 3 that the Pt_b coated Ti/Pt band generated the highest amount of oxygen among all the GMEs tested for OER potential sustainability. Also, from discussions in chapter 4, glucose-sensing DME constructed on the Pt_b coated Ti/Au band had the maximum glucose sensitivity among all the glucose sensors fabricated in the lab for this project. Upon fixing the instability issues of the Pt_b electroplated layer, such configurations of GME or DME or both can be applied in order to achieve enhanced glucose sensitivity and greater oxygen generation. The remaining issue is that when the enzyme is directly exposed in vivo, fouling is likely to follow.

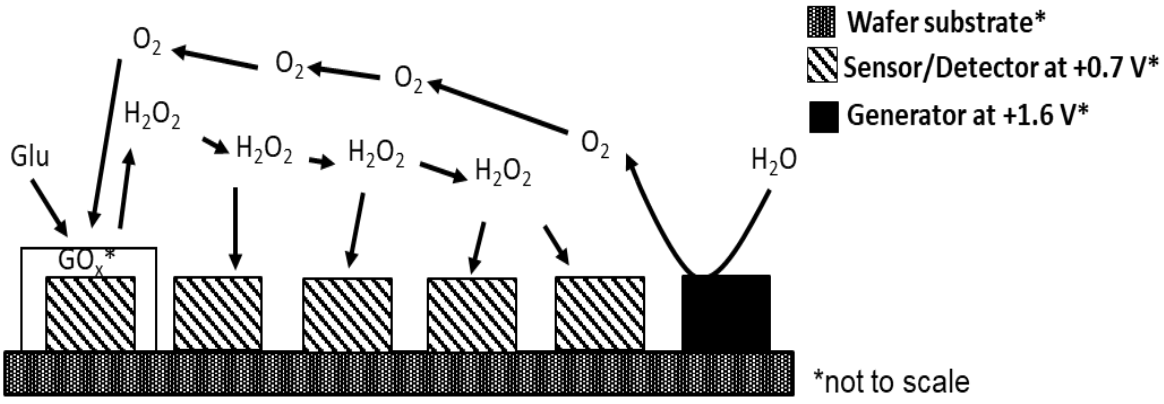

Figure 5.1 Proposed electrochemical barrier between the generator and sensor microelectrode; from left: GOx enzyme sensor poised at +0.7 V, next four microbands poised at the same potential act as the electrochemical barriers where the peroxide diffused from the sensor get oxidized before approaching the generator band, the sixth band is the generator poised at +1.4 V for oxygen electro-generation. All the voltage are presented vs. satd. Ag/AgCl reference electrode.The combined effect of distant sensor-generator and creating an electrochemical barrier in between the two bands enable reduction of peroxide stealing by the generator

5.3 References

1. M. Quinto, M. Koudelka-Hep and F. Palmisano, Analyst, 2001, 126, 1068-1072.

2. E. Dempsey, D. Diamond, M. R. Smyth, G. Urban, G. Jobst, I. Moser, E. M. J. Verpoorte, A. Manz, H. M. Widmer and K. Rabenstein, Analytica chimica acta, 1997, 346, 341-349.

3. J. J. Kulys, A. S. Samalius and G. J. Švirmickas, FEBS letters, 1980, 114, 7-10.

4. J. J. Kulys, M. V. Pesliakiene and A. S. Samalius, Journal of Electroanalytical Chemistry and Interfacial Electrochemistry, 1981, 128, 81-88.

5. E. Mikeladze, A. Schulte, M. Mosbach, A. Blöchl, E. Csöregi, R. Solomonia and W. Schuhmann, Electroanalysis: An International Journal Devoted to Fundamental and Practical Aspects of Electroanalysis, 2002, 14, 393-399.

6. C. P. McMahon, S. J. Killoran and R. D. O'Neill, Journal of Electroanalytical Chemistry, 2005, 580, 193-202.

7. J. P. Lowry, R. D. O'Neill, M. G. Boutelle and M. Fillenz, Journal of neurochemistry, 1998, 70, 391-396

Appendix

Chapter 3

A1. Fabrication of Cr/Au MEAs

The silicon wafers were cleaned by immersion in a stirred solution of NH_4OH (30%): H_2O_2 (30%): distilled (DI)H_2O (5:1:1 by volume) at 75^oC for 10 minutes to remove any organic residues. Wafers were coated with 10 nm chromium followed by 200 nm gold metal by vapor deposition in a nitrogen atmosphere using the thermal evaporator. Photolithography for the wafer included the following sequence of steps: dehydration at 110^oC for 90 seconds, followed by spin coating of an HMDS (hexamethyldisilazane) adhesion promotor at a rate of 2500 rpm. Next, a positive photoresist (AZ 4330) was spin-coated at 6000 rpm creating a 2.8 µm thick photoresist layer. The photoresist layer was then soft-baked at 90 ^oC for 2 minutes, then at 45 ^oC for 30 seconds to remove any residual solvent. Alignment of the mask over the top of the wafer was accomplished using a contact aligner. The UV light energy and exposure time were calculated to be 126 mJ/cm^2 and 19.6 seconds according to the formulae:

Light energy= 45mJ/cm^2-µm x thickness of the resist

Exposure time= (Light energy/ Intensity) x 1.1

The exposed wafer was developed in AZ 300 MIF developer for 2 minutes revealing the pattern of the electrodes. Pattern inspection was done under a microscope to verify completeness, and clean, sharp edges. If the pattern was of high quality, the wafer was etched, otherwise, the polymer image was removed, recoated with photoresist, exposed, and developed again. The wafer was wet etched first in gold etchant solution for 45 seconds exposing the underlying chromium layer then placed in chromium etchant solution (CEP 200), for about 15 seconds after which the underlying

silicon layer was visible. After the etch, the wafer was exposed to a blank mask and developed with the developer again to remove any residual photoresist.

In order to expose only the band electrodes and the edge connector for electrical contact, an insulating layer, benzocyclobutene (BCB) was used to coat the remainder of the pattern. This step used a negative photoresist adhesion promoter either AP 3000 or VM 652 before BCB was spin-coated over the electrode pattern to a thickness of 7.4 μm. The BCB UV exposure time 25.5 seconds was calculated using the following formulae:

Light Energy = 25 mJ/cm^2/μm X Thickness of the resist

Exposure time= (Light energy/ Intensity) x 1.1

The BCB layer was then oven-cured in a nitrogen atmosphere for 12 hours using the temperature program provided by the manufacturer. A dry-etch procedure was used to develop the insulating layer by RIE, using CF_4, or Ar ion plasma. The major steps of Cr/Au microphotolithography are illustrated in Figure A-1.

A2. Fabrication of Ti/Au MEAs

Ti-Au MEAs were fabricated using the same technique as the Cr-Au MEAs except that for thicknesses: 10 nm Ti and 500 nm Au were deposited using an E-beam Evaporator.

A3. Fabrication of Ti/ Pt MEAs

The Cr/Au and Ti/Au MEAs were fabricated using an etch-back technique: a subtractive process (Figure 1). Unlike Au, Pt is difficult to wet etch precisely with small electrode features, hence a lift-off technique was used for Ti-Pt MEAs fabrication. Lift-off is an additive process that avoids Pt metal etching altogether (Figure A-2). The blank silicon wafer was dehydrated at 160 ^{o}C for 30 minutes. Adhesion promoter HMDS (hexamethyldisiloxane) was spin-coated onto the wafer at 2500 rpm, followed by dehydration, and the spin coating of negative photoresist AZ 5214E at 4000

rpm. The photoresist coated wafer was then subjected to soft baking at 88 ^{o}C for 45 seconds using an EMS hotplate. The contact aligner was then used to align the wafer with the mask, then exposing to UV light for a minimum of 3s depending upon the energy and intensity of the light. Following post-exposure baking at 106 ^{o}C for 30 seconds, the wafer was again exposed to UV light for about 36 seconds depending on the energy and intensity of the light. The result is a reverse image on the wafer that exposes the areas where metal was desired. The reverse pattern was then developed using AZ 300 MIF positive developing solution, followed by a spin-rinse-dry (SRD) procedure. 10 nm Ti followed by 100 nm of Pt was then deposited on the photoresist-patterned wafer by E beam evaporation. The resist was removed by sonication in acetone. The image-reversal technique was also used for the application of the insulating silicon dioxide layer. The result was the silicon dioxide insulating all of the metal traces save for the MEA and the edge connector. The resulting twelve microarrays were diced, and plasma cleaned before use.

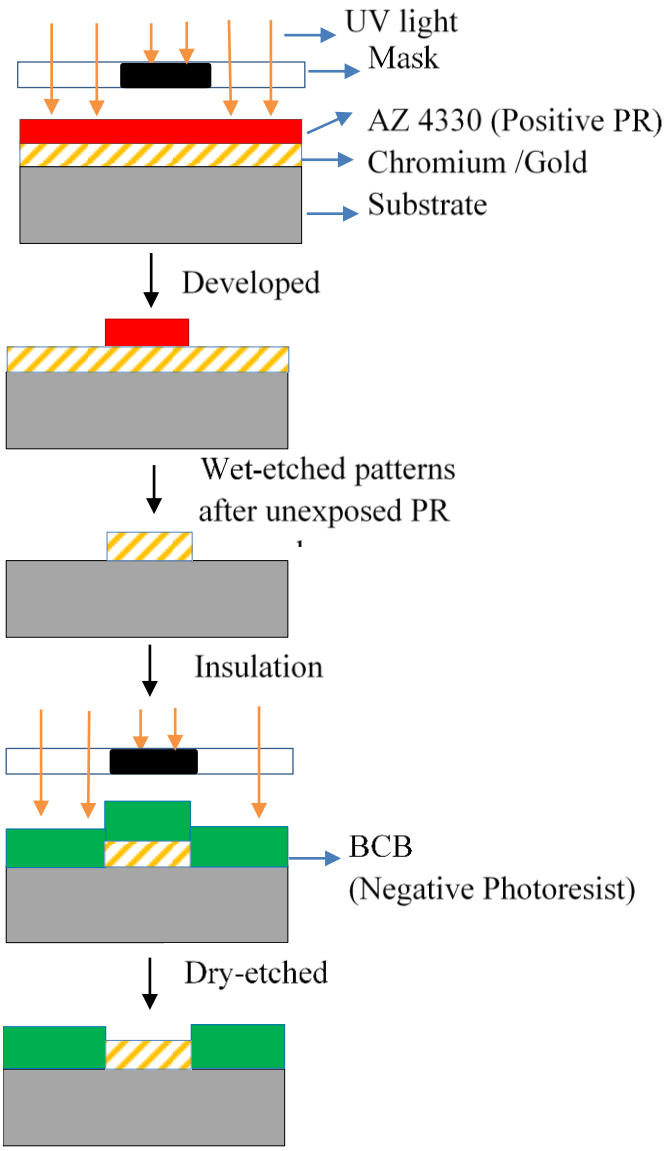

Figure A-1 Schematic of a sequence of photolithographic steps during Cr/Au MEAs microfabrication (Drawing is not to scale). The exposed areas of the positive photoresist and the unexposed areas of the negative photoresist become more soluble after UV exposure and washed away during development. PR= Photoresist.

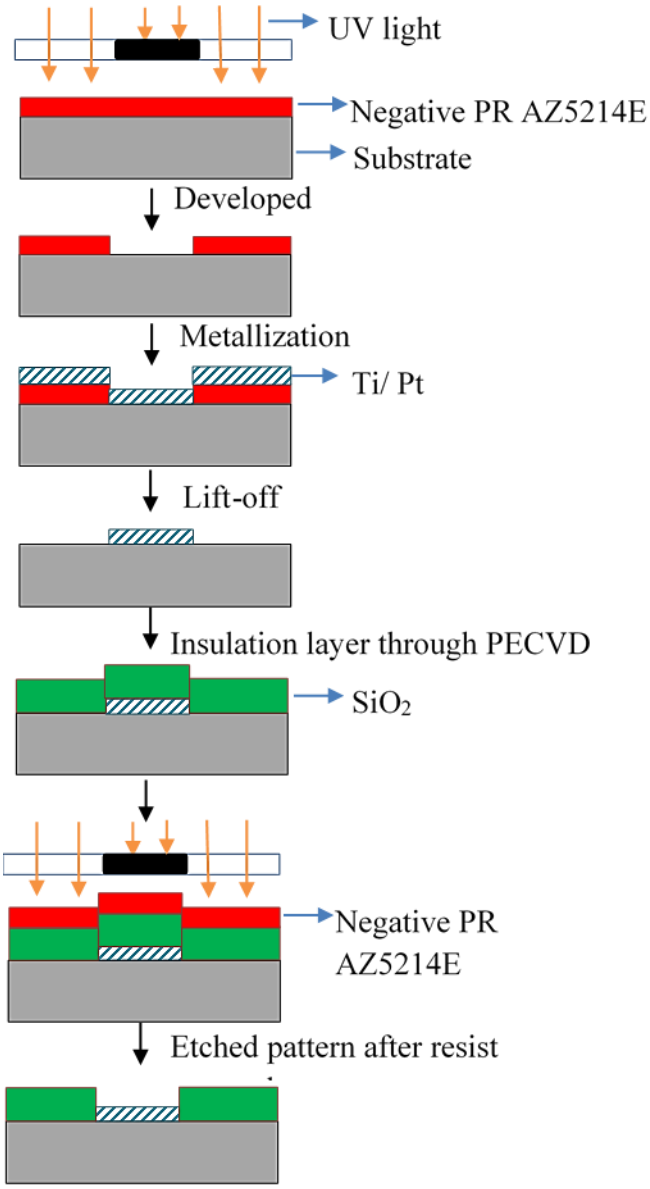

Figure A-2 Schematic of a sequence of photolithographic steps during Ti/Pt MEAs microfabrication (Drawing is not to scale). PR= Photoresist.